

MICROCOPY RESOLUTION TEST CHART
NATIONAL BUREAU OF STANDARDS-1963-A

12

DTNSRDC/SPD 1076-01

DAVID W. TAYLOR NAVAL SHIP RESEARCH AND DEVELOPMENT CENTER



Bethesda, Maryland 20884

ADA 130516

VERTICAL PLANE MOTIONS OF SWATH SHIPS IN REGULAR WAVES

By

K.K. McCreight
and
Ralph Stahl

Approved for Public Release: Distribution Unlimited

Ship Performance Department

DTIC
ELECTE
JUL 20 1983

B

June 1983

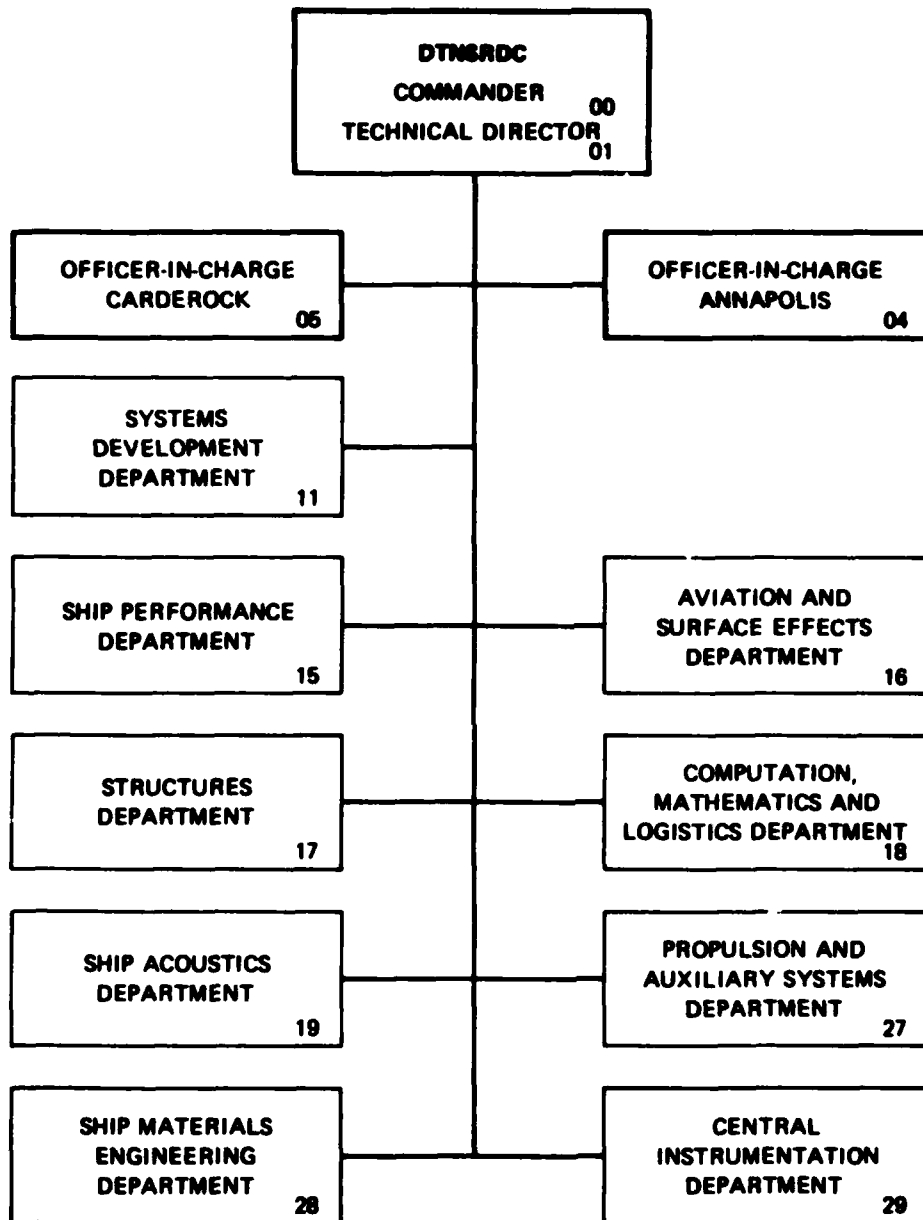
DTNSRDC/SPD - 1076-01

DTIC FILE COPY

VERTICAL PLANE MOTIONS OF SWATH SHIPS IN REGULAR WAVES

83 07 19 117

MAJOR DTNSRDC ORGANIZATIONAL COMPONENTS



UNCLASSIFIED

SECURITY CLASSIFICATION OF THIS PAGE (When Data Entered)

REPORT DOCUMENTATION PAGE		READ INSTRUCTIONS BEFORE COMPLETING FORM
1. REPORT NUMBER DTNSRDC/SPD - 1076-01	2. GOVT ACCESSION NO. AD-A130 516	3. RECIPIENT'S CATALOG NUMBER
4. TITLE (and Subtitle) Vertical Plane Motions of SWATH Ships in Regular Waves		5. TYPE OF REPORT & PERIOD COVERED
7. AUTHOR(s) K.K. McCREIGHT and RALPH STAHL		6. PERFORMING ORG. REPORT NUMBER
9. PERFORMING ORGANIZATION NAME AND ADDRESS David Taylor Naval Ship R&D Center Ship Performance Department Bethesda, Maryland 20084		8. CONTRACT OR GRANT NUMBER(s)
11. CONTROLLING OFFICE NAME AND ADDRESS		10. PROGRAM ELEMENT, PROJECT, TASK AREA & WORK UNIT NUMBERS
14. MONITORING AGENCY NAME & ADDRESS (if different from Controlling Office)		12. REPORT DATE June 1983
		13. NUMBER OF PAGES 108
		15. SECURITY CLASS. (of this report) UNCLASSIFIED
		15a. DECLASSIFICATION/DOWNGRADING SCHEDULE
16. DISTRIBUTION STATEMENT (of this Report) Approved for Public Release: Distribution Unlimited		
17. DISTRIBUTION STATEMENT (of the abstract entered in Block 20, if different from Report)		
18. SUPPLEMENTARY NOTES		
19. KEY WORDS (Continue on reverse side if necessary and identify by block number) Small - Waterplane - Area, Twin Hull Ships, Ship Motion in Waves		
20. ABSTRACT (Continue on reverse side if necessary and identify by block number) The vertical plane motions of SWATH ships are theoretically modeled. Strip theory is used to evaluate hydrodynamic forces. Contributions due to body lift, cross flow drag, and fin lift dominate the damping coefficients. Consequently, their accurate modeling is vital to the accuracy of motion predictions. Semiempirical methods developed for evaluating these components are described. Data for oscillating two-dimensional cylinders, flat plates, and pairs of fins, as well as semiempirical expressions for submarine hydrodynamic coefficients		

DD FORM 1473
1 JAN 73

EDITION OF 1 NOV 68 IS OBSOLETE
S/N 0102-LF-014-6601

UNCLASSIFIED

SECURITY CLASSIFICATION OF THIS PAGE (When Data Entered)

UNCLASSIFIED

SECURITY CLASSIFICATION OF THIS PAGE (When Data Entered)

have been utilized in this development. Correlation between predicted and experimental results are presented for hydrodynamic coefficients, exciting force and moment, and responses to regular waves. The expressions developed result in correlation which is good and which is notably better than results reported previously.

Accession For	
NTIS GRA&I	<input checked="" type="checkbox"/>
DTIC TAB	<input type="checkbox"/>
Unannounced	<input type="checkbox"/>
Justification	
By _____	
Distribution/	
Availability Codes	
Dist	Avail and/or Special
A	



UNCLASSIFIED

SECURITY CLASSIFICATION OF THIS PAGE (When Data Entered)

TABLE OF CONTENTS

	Page
LIST OF FIGURES	1
LIST OF TABLES	11
NOTATION	111
ABSTRACT	1
ADMINISTRATIVE INFORMATION	1
INTRODUCTION	1
EQUATIONS OF MOTION	2
HYDRODYNAMIC COEFFICIENTS AND EXCITING FORCES AND MOMENT	3
COMPARISON BETWEEN RESULTS FROM EXPERIMENT AND PREDICTION	4
ADDED MASS AND DAMPING	5
WAVE EXCITING HEAVE FORCE AND PITCH MOMENT	6
RESPONSES TO REGULAR WAVES	6
DISCUSSION	6
CONCLUSIONS AND RECOMMENDATIONS	9
ACKNOWLEDGEMENTS	9
REFERENCES	11
APPENDIX A - FREQUENCY DEPENDENT HYDRODYNAMIC COEFFICIENTS, FORCES AND MOMENTS	74
APPENDIX B - POTENTIAL FLOW COMPONENTS	83
APPENDIX C - VISCOUS COMPONENTS	87

LIST OF FIGURES

1 - Comparison between Experiment and Prediction for Added Mass and Damping Coefficients of the SWATH 6A (Bare Hull) for Various Speeds	17
2 - Comparison between Experiment and Prediction of Added Mass and Damping Coefficients for the SWATH 6A	21

3 - Comparison between Experiment and Prediction of Heave Exciting Force and Pitch Exciting Moment for the SWATH 6D	33
4 - Comparison between Experiment and Prediction of Heave Exciting Force and Pitch Exciting Moment for the SSP KAIMALINO in Head Waves	45
5 - Comparison between Experiment and Prediction of Regular Wave Transfer Functions for the SWATH 6A	51
6 - Comparison between Experiment and Prediction of Regular Wave Transfer Functions for the SWATH 6B	56
7 - Comparison between Experiment and Prediction of Regular Wave Transfer Functions for the SWATH 6C	61
8 - Comparison between Experiment and Prediction of Regular Wave Transfer Functions for the SWATH 6D	66
9 - Drag and Inertia Coefficients versus Keulegan-Carpenter Number for Constant Values of the Frequency Parameter (From Reference 5). .	80
10 - The Drag Coefficient of Flat Plate (+), Diamond (◇) and Circular (○) Cylinders at Low KC (From Reference 6)	81
11 - Experiment-Prediction Comparison for Damping Coefficient with No Correction for C_D	96
12 - Experiment-Prediction Comparison for Damping Coefficient for Two-Dimensional Cylinders	97

LIST OF TABLES

1 - Full-Scale Particulars of SWATH Configurations	14
2 - Particulars of Stabilizing Fins	15
3 - Nondimensionalization Factors for Added Mass, Damping, Wave Exciting Force, and Wave Exciting Moment	16
4 - Ratio of Lift on Aft Fin to Lift on Forward Fin for Various Fin Separations and Oscillation Frequency to Speed Ratios	82

NOTATION

A	Amplitude of incident wave
AR	Effective aspect ratio of stabilizing fin
A_{ij}	Added mass coefficient for the i^{th} mode due to motion in the j^{th} mode ($j = 1$ for surge, $j = 3$ for heave, $j = 5$ for pitch)
A_n	Projected area of stabilizing fin
A_o	Characteristic body area
A_p	Projected area of body
A_w	Waterplane area
a	Horizontal axis of a two-dimensional section
a_o	Viscous lift coefficient
a_{33}	Sectional heave added mass coefficient due to heave motion
B	Sectional beam
B_{ij}	Damping coefficient for the i^{th} mode due to motion in the j^{th} mode
b	Vertical axis of a two-dimensional section
b_{33}	Sectional heave damping coefficient due to heave motion
C_D	Cross flow drag coefficient
$C_{D\text{SARPKAYA}}$	Values of C_D obtained by Sarpkaya
C_{ij}	Restoring coefficient for the i^{th} mode due to motion in the j^{th} mode
$C_{L\alpha_n}$	Lift curve slope with respect to angle of attack for n^{th} stabilizing fin
C_{Lz_n}	Correction to $C_{L\alpha_n}$
C_m	Inertia coefficient

c_n	Chord of n^{th} stabilizing fin
d	Transverse dimension
d_e	Center of surge force
d_s	Average depth
d_l	Distance between the mean waterline and the center of the lower hull
F_n	Froude number $U/(gL)^{1/2}$
$F_i^{(e)}$	Wave exciting force in the i^{th} mode
F_v	Vertical force on a slender moderately inclined body
GM_L	Longitudinal metacentric height
g	Acceleration due to gravity
i	Imaginary unit $((-1)^{1/2})$
K_c	Keulegan-Carpenter number $(U_m T/d)$
k	Wave number $(= \omega_o^2/g)$
k_1, k_2	Lamb's hydrodynamic coefficients
L	Overall ship length
l_n	x coordinate of quarter chord of stabilizing fin
M	Mass of displaced volume
M'_w, M'_q	Coefficients of pitch moment due to heave velocity and pitch velocity
n_2, n_3	Unit normals
r	Hull radius
S	Area of ellipse of two-dimensional section
S_D	Distance between the centerline of the ship and the centerline of a hull

S_{D_n}	Horizontal distance between ship's plane of symmetry and centroid of stabilizing fin
s_n	Span of n^{th} stabilizing fin
T	Period of oscillation
t_n	Thickness of n^{th} stabilizing fin
t_s	Draft of strut
U	Forward speed of ship
U_m	Amplitude of harmonically varying velocity
w	Vertical velocity of body relative to the velocity of the fluid
$\dot{z}_{po} (\dot{z}_{so})$	Vertical velocity of port (starboard) lifting surface relative to the velocity of the fluid
Z'_w, Z'_q	Coefficients of vertical force due to heave velocity and pitch velocity
\dot{z}_{10}	$ \dot{z}_{1s} + \dot{z}_{1p} $
$\dot{z}_{1p} (\dot{z}_{1s})$	Vertical velocity of port (starboard) hull relative to the velocity of the fluid
α	Angle of incidence of flow
α_o	Used in evaluating k_1
β	Heading of the ship relative to the incident wave ($\beta = 180$ for head waves)
β_k	Period parameter ($d^2/\nu T$)
β_o	Used in evaluating k_2
ϵ	Used in evaluating α_o and β_o
$\dot{\zeta}_v$	Vertical velocity of water
ν	Kinematic viscosity of water

$\xi_j, \dot{\xi}_j, \ddot{\xi}_j$ Displacement (velocity, acceleration) of ship from its mean position in the j^{th} mode

ρ Mass density of water

ψ_3 Velocity potential

ω Wave encounter frequency

ω_0 Wave frequency

ABSTRACT

The vertical plane motions of SWATH ships are theoretically modeled. Strip theory is used to evaluate hydrodynamic forces. Contributions due to body lift, cross flow drag, and fin lift dominate the damping coefficients. Consequently, their accurate modeling is vital to the accuracy of motion predictions. Semiempirical methods developed for evaluating these components are described. Data for oscillating two-dimensional cylinders, flat plates, and pairs of fins as well as semiempirical expressions for submarine hydrodynamic coefficients have been utilized in this development. Correlation between predicted and experimental results are presented for hydrodynamic coefficients, exciting force and moment, and responses to regular waves. The expressions developed result in correlation which is good and which is notably better than results reported previously.

ADMINISTRATIVE INFORMATION

This work was funded under the Ships, Subs and Boats Program Task Area SF 421-350-200, N62345. The funding was administered by the Exploratory Development Programs Office, Code 1506, Ship Performance Department, David Taylor Naval Ship Research and Development Center (DTNSRDC).

INTRODUCTION

The Small Waterplane Area Twin Hull (SWATH) ship is composed of two hulls, each of which has one or two surface piercing struts connecting them to the above-waterline deck. Typically the lower hull is composed of circular or elliptical cross-sections. Some hulls are submarine-like in shape and others are composed of a series of cylinders and conic frustums.

The motions of SWATH ships are greatly determined by the ship's unique geometry. Since a large portion of the ship's buoyancy is located in the lower hulls, the wave exciting forces are relatively small. The waterplane area (A_w) and longitudinal metacentric height (GM_L) are small in comparison with those of conventional displacement ships. Since the heave and pitch natural periods are inversely proportional to the square root of A_w and GM_L , respectively, relatively long natural periods result. Low responses for operation at moderate speeds in seaways occur in part because most of the energy of a seaway typically occurs at short wave periods. Thus, the small waterplane area can result in a highly seaworthy ship.

Two-dimensional theory has been used to predict the motions in a seaway of conventional ships^{1*} and SWATH ships.² Two-dimensional theory assumes that there is no longitudinal hydrodynamic interaction so that hydrodynamic forces can be evaluated by integrating the hydrodynamic contributions of two-dimensional sections along the ship's length.

For conventional displacement ships and for catamarans, as well, vertical plane motions can be predicted accurately using potential flow theory. However, Lee² recognized that for SWATH ships viscous contributions to the hydrodynamic damping coefficients are important. They can be dominant, making their accurate modeling important. In a theoretical development Lee² introduced contributions due to lift and cross flow drag of the body and stabilizing fins. Hong³ introduced pitch due to surge and demonstrated its importance in modeling low speed motions. This approach was generally successful in predicting the vertical plane responses of SWATH ships. However, discrepancies between predicted and experimental magnitudes and uncertainty over the appropriate values of cross flow drag and lift coefficients motivated the present study. The goal of this investigation is to improve the quality of predictions and to predict vertical plane responses of a SWATH ship to waves given only the ship geometry, the location of the center of gravity, and the longitudinal radius of gyration (gyradius).

EQUATIONS OF MOTION

For the purpose of this derivation, a SWATH ship is assumed to be moving at a constant speed at a fixed angle relative to a sinusoidal wave train in infinitely deep water. The wave amplitude is assumed to be small so that the rigid body motions can be described using a linear model. The ship is defined in a right-handed coordinate system having its origin at the mean waterline at the ship's longitudinal center of gravity and centerline. The z-ordinate is positive upward.

The equations of motion of the ship for the vertical plane are:

$$M\ddot{\xi}_1 = F_1^{(e)} e^{-i\omega t}$$

*References appear on page 11.

$$(M + A_{33})\ddot{\xi}_3 + B_{33}\dot{\xi}_3 + C_{33}\xi_3 + A_{35}\ddot{\xi}_5 + B_{35}\dot{\xi}_5 + C_{35}\xi_5 = F_3^{(e)}e^{-i\omega t}$$

$$(I_5 + A_{55})\ddot{\xi}_5 + B_{55}\dot{\xi}_5 + C_{55}\xi_5 + A_{53}\ddot{\xi}_3 + B_{53}\dot{\xi}_3 + C_{53}\xi_3 = F_5^{(e)}e^{-i\omega t}$$

where M is the mass of the displaced volume and I_5 is the pitch mass moment of inertia. A_{ij} , B_{ij} , and C_{ij} are the added mass, damping, and restoring coefficients in the i^{th} mode due to a sinusoidal motion of unit amplitude in the j^{th} mode. The subscript 1 denotes surge, 3 heave, and 5 pitch. $F_i^{(e)}$ is the complex exciting force or moment and ω is the wave frequency of encounter.

In evaluating the coefficients, forces, and moments, strip theory is employed. This is a reasonable assumption for the SWATH ship with its slender and gradually changing geometry over its length.

HYDRODYNAMIC COEFFICIENTS AND EXCITING FORCES AND MOMENT

The hydrodynamic coefficients and exciting forces and moment are composed of potential flow, cross flow drag, and lift terms. Lee's² development included cross flow drag and lift terms for the body and the stabilizing fins. These components affect the damping and restoring coefficients and the exciting forces and consequently the motions at all speeds since the cross flow drag terms are independent of speed and the lift terms are proportional to some power of speed. In this investigation, new expressions evolved for the cross flow drag coefficients, the body lift terms, and the fin cross flow drag and lift curve slope coefficients. Final expressions for the hydrodynamic coefficients and the exciting forces and moments are given in Appendix A. Details of the development of these expressions are given in Appendices B and C. It is useful to briefly summarize the results.

Currently, the potential flow components of the added mass and damping can be evaluated utilizing either the Frank Close Fit Technique⁴ or the Dalzell Approximation Technique.* When the Dalzell Approximation Technique is utilized, as it is in the results in this report, the distribution of the potential on the two-dimensional section is unavailable and evaluation of the exciting force and

*As described by Dalzell in Stevens Institute of Technology reports with limited distribution.

moment requires further approximation. In Appendix B expressions for the surge and heave exciting forces and the pitch exciting moment are developed. This development includes an expression for an approximate depth used in the heave exciting force and pitch exciting moment and an expression for the center of surge which facilitates inclusion of surge in the exciting moment.

In Appendix C a development of the cross flow drag and lift terms and the corresponding coefficients is given. The cross flow drag coefficients for the body are evaluated using experimental values for oscillating circular cylinders.⁵ A factor to reflect the effect of a strut on the cross flow drag coefficient is developed from oscillation data for two-dimensional SWATH sections.* The cross flow drag coefficient for the stabilizing fins is evaluated using experimental data for oscillating plates.⁶ Semiempirical expressions for the vertical plane hydrodynamic coefficients of submarines** serve as a basis for the development of the SWATH body lift components. The lift curve slope of the fins⁷ is given and a correction is made for the frequency dependent interference effect of the forward fin on the lift of the aft fin.^{8,9} For appropriate configurations, an additional correction is made for the effect of the hull wake on the lift of the aft fin.¹⁰

COMPARISON BETWEEN RESULTS FROM EXPERIMENT AND PREDICTION

Oscillation, excitation, and regular wave data are available for SWATH configurations denoted 6A, 6B, 6C, 6D, and SSP KAIMALINO. These results were used to guide the development of the expressions in this report. The four configurations in the SWATH 6 series employ the same lower hull which is a body of revolution. The struts are designed so that the GM_L differs for each strut design. Configurations 6A and 6B are single strut designs, whereas 6C and 6D are twin strut designs. Particulars of the configurations and of the lifting surfaces are given in Tables 1 and 2.

Correlation between experiment and prediction are given in Figures 1 through 8. Nondimensionalization factors for added mass, damping, exciting force, and

* As described by Stahl in a DTNSRDC report with limited distribution.

** As described by Dempsey in a DTNSRDC report of higher classification.

exciting moment are given in Table 3. Open symbols are used for experimental results and solid symbols are used for predicted results using the expressions given in Appendix A. Predicted results using Lee's² expressions are given in solid lines on some of the added mass and damping and all of the regular wave figures. Hong's³ modifications are included in the regular wave results.

In solving the cross flow drag contributions, it is necessary to know the motion of the model relative to the incoming wave. For regular wave motion predictions, this component must be solved iteratively, until the responses of the craft converge; that is, the difference between the estimated and computed responses diminish to acceptable values. However, in the case of forced oscillation experiments, the motion of the body is known and there is no incident wave. Conversely, for wave exciting experiments, the body is held rigid and the motion of the wave is known. Therefore, calculation of these components is straightforward.

ADDED MASS AND DAMPING

Two sets of data for heave and pitch forced oscillation tests are available for the SWATH 6A. Results from a 1:51.2 scale bare hull model for speeds corresponding to full-scale speeds of 10, 20, and 35 knots¹¹ are presented in Figure 1 along with predicted results. Results from a 1:22.5 scale model with and without stabilizing fins for speeds corresponding to full-scale speeds of 0, 20, and 28 knots¹² are presented in Figure 2. Included are predicted results based on the expressions in Appendix A and Lee's predicted results which were presented in Reference 12. These latter predicted results do not include the cross flow drag contributions. Inclusion of these terms would increase the magnitudes of the damping terms, most significantly at zero speed.

It is useful to compare experimental results given in Figure 1a ($F_n = 0.384$) with those in Figure 2e (bare hull). It is expected that these results should be close in value since they are for identical conditions. Only the model scales differ. However, the results for A'_{33} given in Figure 1a are smaller than those given in Figure 2e. The difference in results for A'_{53} is particularly important at higher speeds as can be seen in Figures 1a and 2i. The predicted results agree well with the measured results in Figure 1a; however, no explanation of the difference in experimental results is proposed in this presentation.

WAVE EXCITING HEAVE FORCE AND PITCH MOMENT

Fein and Stahl¹³ carried out experiments to measure the surge and heave wave exciting forces and the pitch exciting moment. They investigated five speeds in head and following seas for a 1:22.5 scale model of the SWATH 6D and five speeds in head waves for a 1:7.8 scale model of the SSP KAIMALINO. The data given in this report are presented in a different format from that of Reference 13. To elucidate the data in following seas, all data have been presented as a function of wavelength to ship length, rather than encounter frequency. Since the theory is developed with the pitch moment about the LCG at the mean waterline, the measured pitch exciting moment and surge exciting force were used to transform the moment to be about the LCG at the mean waterline, so that the predicted and experimental results were comparable. These results are given in Figures 3 and 4.

RESPONSES TO REGULAR WAVES

Kallio^{14,15} carried out regular wave experiments for the SWATH 6 series. Heave, pitch, and relative bow motion responses as a function of wavelength to ship length are given for five relative wave headings for the 6A, 6B, and 6C and for head and following waves for the 6D. Results are given in Figures 5 through 8. Note that two sets of predicted results are given for all conditions. One set results from the development in this report and one results from Lee's² work with Hong's³ modifications included.

DISCUSSION

Initial work by Lee indicated that correlation between experimental and predicted results at zero speed for long wavelengths was not satisfactory. Hong's³ results demonstrated the importance of introducing the effects of surge and of using the proper wave amplitude in evaluating the nonlinear terms. The improved correlation that results from the incorporation of the expressions developed in this report is evidently due to the method of evaluating C_D . Previously, it had been assumed to be constant, whereas, for two-dimensional sections (or stabilizing fins) it is here considered to be a function of the major and minor axis of the lower hull and the strut thickness (or fin span), the wave frequency and the amplitude of the relative vertical velocity at each two-dimensional section (or fin).

High speed responses for all configurations utilizing the expressions derived in this report result in excellent correlation with experimental data. The

responses predicted through the present methodology are notably closer to the experimentally determined responses than results found with any of the previous methods.

Responses of SWATH configurations traveling at high speed in following waves has been a topic of interest. One problem in correlation for this condition is that it is difficult experimentally. As noted by Kallio,¹⁴ in quartering and following waves there was considerable surge and consequently the model safety restraint lines became taut. Lee² reported extremely large predicted heave responses for the 6A at the wavelength corresponding to zero encounter frequency.* Since the potential flow two-dimensional approach is not valid at small encounter frequencies, theoretical work was undertaken to overcome this limitation. Hong^{16,17} applied to SWATH ships unified slender body theory developed by Newman and Sclavounos.¹⁸ Results from Hong's implementation did not improve correlation and did not remove the spike in the 6A heave predictions. However, the results developed here which focused on the viscous components but retained the two-dimensional potential flow approach utilized by Lee,² do not include the spiked response. Although pitch is overpredicted for the 6A and 6B, these results show generally good correlation and support the hypothesis that the aberrant predictions for the 6A are not related to the two-dimensional potential flow theory.

Since the predicted heave response spike occurs near zero encounter frequency, it has been assumed that the problems with the predictions were due to two-dimensional theory. However, Figure 5e suggests an alternative explanation. The large heave response reported by Lee² occurs near the wavelength which corresponds to zero encounter frequency; however, this also occurs in the region where the pitch response peaks. Since heave and pitch are coupled, errors in modeling one

* The regular wave predictions which are attributed to Lee include a modification which was an attempt to remove the spiked behavior. In the modification when ω is less than 0.07 the potential flow added mass and damping coefficients for each section have been assumed to be equal to those for $\omega = 0.07$. Generally this will alter predictions only at high speeds in following or stern seas. This approximation merely suppressed the response. (See Figure 5e.)

response will affect the other. That is, the spike in the predicted heave for the 6A may be due to inadequacies in the pitch predictions.

Analysis of the relative importance of various terms in the pitch equation of motion indicates that the term C_{55} may be dominant. For simplicity, consider the uncoupled pitch equation of motion:

$$(I_5 + A_{55})\ddot{\xi}_5 + B_{55}\dot{\xi}_5 + C_{55}\xi_5 = F_5 e^{-i\omega t}$$

Utilizing the relationship $\xi_5 = (\xi_{5R} + i\xi_{5I})e^{-i\omega t}$, this becomes

$$[-\omega^2(I_5 + A_{55}) + C_{55}]\xi_5 + B_{55}\dot{\xi}_5 = F_5 e^{-i\omega t}$$

Two-dimensional theory is not valid at small encounter frequencies and A_{55} becomes very large in this region. However, the presence of ω^2 results in a very fortunate situation for small ω . That is, when ω approaches zero, $\omega^2 A_{55}$ will be small. The important term is C_{55} . Whereas A_{55} and B_{55} are calculated using two-dimensional theory, C_{55} is not. C_{55} is composed of a fin lift term, a body lift term, and a term which is essentially GM_L . Since the fin lift term will be approximately equal for all configurations in the SWATH 6 series, it can be neglected in this discussion. In addition, as configured in this report, the body lift term is dependent on mass and particulars of the lower hull and will be equal for the 6A, 6B, and 6C configurations. However, GM_L increases significantly from the first model in the SWATH 6 series to the last with the 6A having the smallest and the 6D the largest GM_L . For small GM_L the lift terms, and the body lift term in particular, will be relatively more important than for a large GM_L configuration. This argument is consistent with the correlation which indicates that the predicted heave spike in earlier work occurred for the 6A only. Consequently, good correlation between experimental and predicted results for configurations with small GM_L 's will be strongly dependent on accurate modeling of C_{55} .

The body lift component used for the C_{55} development is based on experimental work on the 6A. This is an unfortunately slim data base. It is expected that this term is important for other low GM_L configurations. Better correlation for pitch for the 6A and 6B probably would result from better modeling of C_{55} .

CONCLUSIONS AND RECOMMENDATIONS

1. Work by Lee² has been used as the basis for modeling the vertical plane motion of SWATH ships. The general form of his work has been retained in the present modeling; however, the effort reported here has focused on the viscous terms. Alternate semiempirical expressions for body lift terms, cross flow drag coefficients for the body and the fins, and lift curve slope coefficients for the fins have been developed, and improved correlation with experiment is the result.

2. Correlation of added mass and damping coefficients and the exciting force and moment are generally good. Zero speed response correlation is comparable to or better than results based on Hong's³ modifications to Lee's² work. High speed correlation is good and is notably better than previous results shown by Hong.¹⁷ Following sea results no longer display the aberrant behavior which occurred in Lee's² and Hong's¹⁷ SWATH 6A results.

3. The two-dimensional potential flow theory is certainly adequate for the prediction of ship motions of SWATH ships similar to the 6 series.

4. Further experimental work would facilitate refinement of the viscous expressions developed here and would expand the regions of confidence. The following investigations are recommended:

- a. Experimental investigation of C_D for SWATH sections and for circular cylinders at very low K_c would be useful.
- b. Experimental investigation of the effect of fin-fin interference for additional configurations, including ones where the aft fin is larger than the forward fin would be useful.
- c. Experiments of true free-to-surge conditions using radio-controlled models in following waves would aid in the assessment of prediction techniques.
- d. Experimental investigation of C_{55} for existing models, including the 6B, 6C, and 6D, would make it possible to define the body lift component of C_{55} more precisely and to improve the reliability of prediction of responses in following seas at high speeds.

ACKNOWLEDGEMENTS

The authors wish to thank Miss Elizabeth M. Dempsey of DTNSRDC for her informative discussions concerning submarine hydrodynamics and Dr. William R.

McCreight of DTNSRDC for pointing out the existence of the Lloyd data. Ms. Dotti McLean of ORI, Inc. prepared the figures in this report.

REFERENCES

1. Salvesen, N., E.O. Tuck, and O. Faltinsen, "Ship Motions and Sea Loads," Transactions of the Society of Naval Architects and Marine Engineers, Vol. 78 (1970).
2. Lee, C.M., "Theoretical Prediction of Motion of Small-Waterplane-Area, Twin-Hull (SWATH) Ships in Waves," Report DTNSRDC/SPD-76-0046 (Dec 1976).
3. Hong, Y.S., "Improvements in the Prediction of Heave and Pitch Motions for SWATH Ships," Report DTNSRDC/SPD-0928-02 (Apr 1980).
4. Frank, W. and N. Salvesen, "The Frank Close-Fit Ship-Motion Computer Program," DTNSRDC Department of Hydromechanics Research and Development Report 3289 (Jun 1970).
5. Sarpkaya, T., "In-Line and Transverse Forces on Cylinders in Oscillatory Flow at High Reynolds Numbers," Journal of Ship Research, Vol. 21, No. 4 (Dec 1977).
6. Bearman, P.W. and J.M.R. Graham, "Hydrodynamic Forces on Cylindrical Bodies in Oscillatory Flow," Second International Conference on Behavior of Off-Shore Structures, Paper 24 (Aug 1979).
7. Whicker, L.F. and L.F. Fehlner, "Free-Stream Characteristics of a Family of Low-Aspect-Ratio, All-Movable Control Surfaces for Application to Ship Design," David Taylor Model Basin Report 933, Revised Edition (Dec 1958).
8. Lloyd, A.R.J.M., "Roll Stabiliser Fins: Interference at Non-Zero Frequencies," Royal Institute of Naval Architects, Vol. 117 (1975).
9. Cox, G.G. and A.R. Lloyd, "Hydrodynamic Design Basis for Navy Ship Roll Motion Stabilization," Transactions of the Society of Naval Architects and Marine Engineers, Vol. 85 (1977).
10. Dempsey, E.M., "Static Stability Characteristics of a Systematic Series of Stern Control Surfaces on a Body of Revolution," Report DTNSRDC-77-0085 (Aug 1977).
11. Keunig, J.A. Jr., "Forced Oscillation Tests and Motion Measurements with a Small Waterplane Area Twin Hull Ship," Delft University of Technology Report Number 533 (Dec 1981).

12. Lee, C.M. and L.O. Murray, "Experimental Investigation of Hydrodynamic Coefficients of a Small-Waterplane-Area, Twin-Hull Model," Report DTNSRDC/SPD-744-01 (Jan 1977).
13. Fein, J.A. and R. Stahl, "Head and Following Wave Exciting Force Experiments on Two SWATH Configurations," Report DTNSRDC/SPD-0928-01 (Jun 1980).
14. Kallio, J.A., "Seaworthiness Characteristics of a 2900 Ton Small Waterplane Area Twin Hull (SWATH), Report DTNSRDC/SPD-620-03 (Sep 1976).
15. Kallio, J.A., "SWATH 6D Model Experiments in Regular Head and Following Waves With and Without Floodable Struts," Report DTNSRDC/SPD-0914-01 (Feb 1980).
16. Hong, Y.S., "Prediction of Motions of SWATH Ships in Following Seas," Report DTNSRDC/SPD-81-039 (Nov 1981).
17. Hong, Y.S., "Predicted Motions of High-Speed SWATH Ships in Head and Following Seas," Report DTNSRDC/SPD-82-036 (Jul 1982).
18. Newman, J.N. and P. Sclavounos, "The Unified Theory of Ship Motion," Proceedings of the Thirteenth Symposium on Naval Hydrodynamics, Tokyo, Japan (Oct 1980).
19. Lee, C.M., "Approximate Evaluation of Added Mass and Damping Coefficients of Two-Dimensional SWATH Sections," Report DTNSRDC/SPD-78-084 (Oct 1978).
20. Korvin-Kroukovsky, B.V. and W.R. Jacobs, "Pitching and Heaving Motions of a Ship in Regular Waves," Transactions of the Society of Naval Architects and Marine Engineers, Vol. 65 (1957).
21. Newman, J.N., "Marine Hydrodynamics," The MIT Press, Cambridge, Massachusetts (1977), pp. 362-371.
22. "Incompressible Aerodynamics," Edited by B. Thwaites, Oxford University Press (1960), pp. 414-421.
23. Keulegan, G.H. and L.H. Carpenter, "Forces on Cylinders and Plates in an Oscillating Fluid," Journal of Research of the National Bureau of Standards, Vol. 60, No. 5, Research Paper 2857 (May 1958).
24. Lee, C.M. and M. Martin, "Determination of Size of Stabilizing Fins for Small Waterplane Area, Twin-Hull Ships," Report DTNSRDC-4495 (1974).

25. Pitts, W.C., J.N. Nielsen, and G.E. Kaattari, "Lift and Center of Pressure of Wing-Body-Tail Combinations at Subsonic, Transonic, and Supersonic Speeds," NACA Report 1307 (1957).

TABLE 1 - FULL-SCALE PARTICULARS OF SWATH CONFIGURATIONS

Particular	6A ¹	6B ¹	6C ¹	6D ²	SSP ³
Length overall, m	73.15	73.15	73.15	73.15	26.40
Distance between centerlines, m	22.86	22.86	22.86	26.80	12.19
Draft, m	8.13	8.13	8.13	8.13	4.66
Displacement, metric ton	2,946	2,946	2,946	2,946	2,946
Longitudinal CG, aft of nose, m	35.45	35.14	34.72	36.10	13.46
Vertical center of gravity (KG), m	10.36	10.36	10.36	9.00	4.28
Longitudinal metacentric height, m	6.10	11.60	13.70	26.40	5.03

¹As given in Reference 14.

²As given in Reference 15.

³As given in Reference 13.

TABLE 2 - PARTICULARS OF STABILIZING FINS

	Configuration				
	6A ¹	6B ¹	6C ¹	6D ²	SSP ^{3,4}
Forward Fin, Each					
Chord, m	2.59	2.16	2.16	2.59	1.95
Span, m	3.11	2.59	2.59	3.11	1.83
Location, ⁵ m	17.15	17.15	17.15	17.15	2.82
Aft Fin					
Chord, m	4.48	3.73	3.73	4.48	2.38
Span, m	5.36	4.48	4.48	5.36	10.55
Location, ⁵ m	62.24	62.24	62.24	62.24	20.59

¹As given in Reference 14.

²As given in Reference 15.

³As given in Reference 13.

⁴Aft fin spans between the hulls.

⁵Longitudinal distance between lower hull nose and fin quarter chord.

TABLE 3 - NONDIMENSIONALIZATION FACTORS FOR ADDED MASS, DAMPING, WAVE EXCITING FORCE, AND WAVE EXCITING MOMENT

Variable	Nondimensionalization Factor
A_{33}	M
A_{35}, A_{53}	ML
A_{55}	ML^2
B_{33}	$M(g/L)^{1/2}$
B_{35}, B_{53}	$M(gL)^{1/2}$
B_{55}	$ML(gL)^{1/2}$
$F_3^{(e)}$	MgA/L
$F_5^{(e)}$	MgA
ω	$(g/L)^{1/2}$
where	<p>A = Wave amplitude g = Acceleration due to gravity L = Overall ship length M = Mass of Displaced volume</p>

Figure 1 - Comparison between Experiment and Prediction for Added Mass and Damping Coefficients of the SWATH 6A (Bare Hull) for Various Speeds

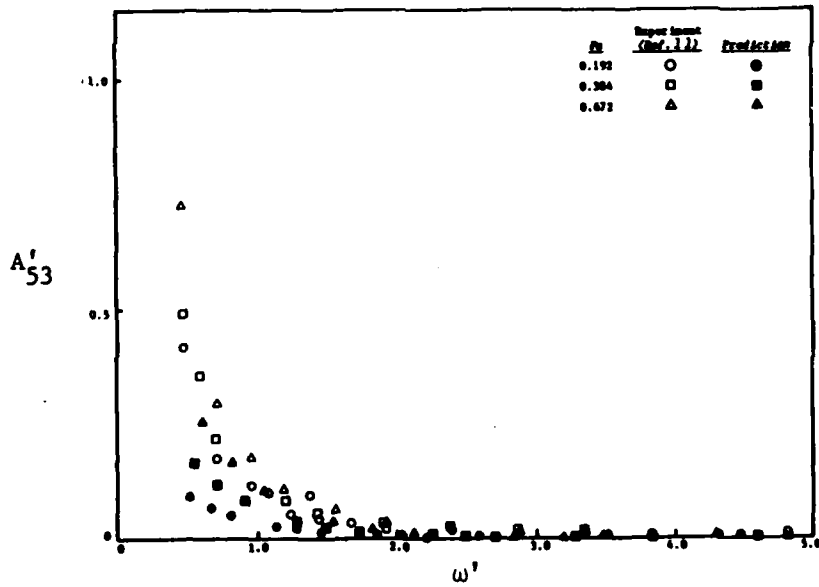
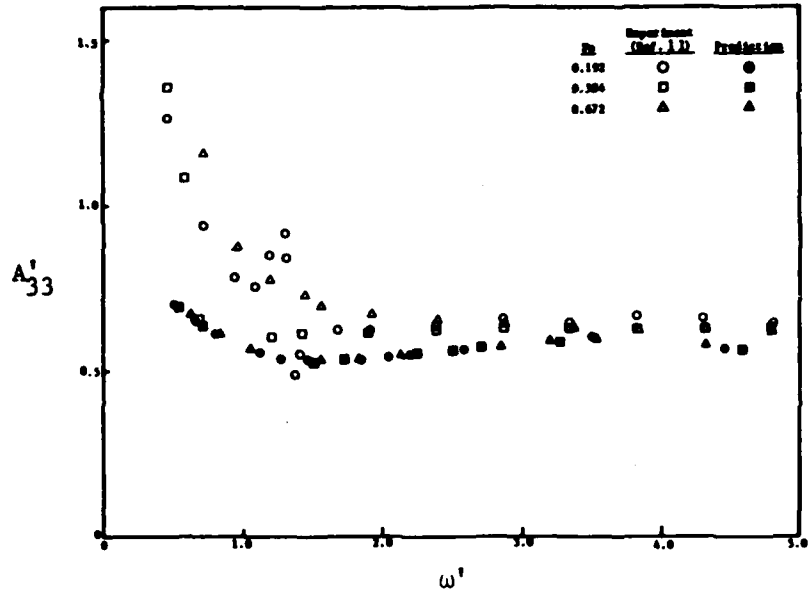


Figure 1a - Added Mass Coefficients A'_{33} and A'_{53}

Figure 1 (Continued)

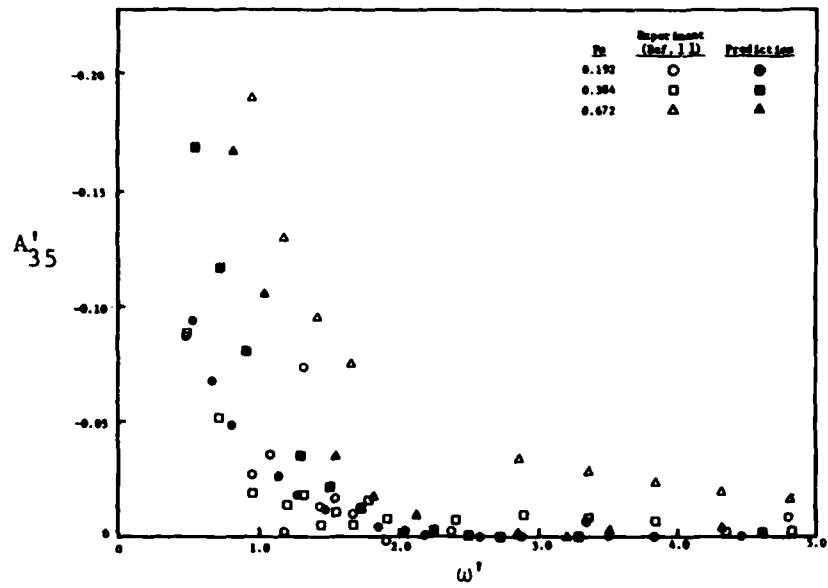
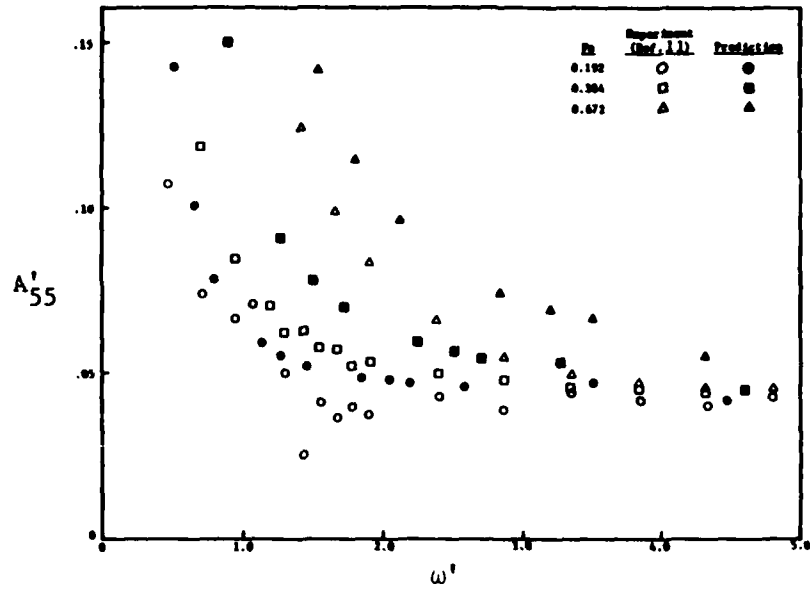


Figure 1b - Added Mass Coefficients A'_{55} and A'_{35}

Figure 1 (Continued)

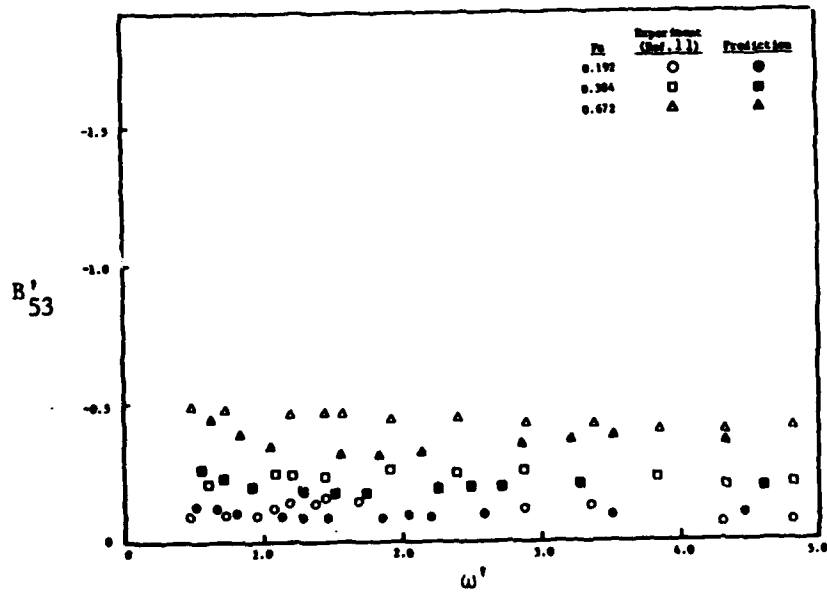
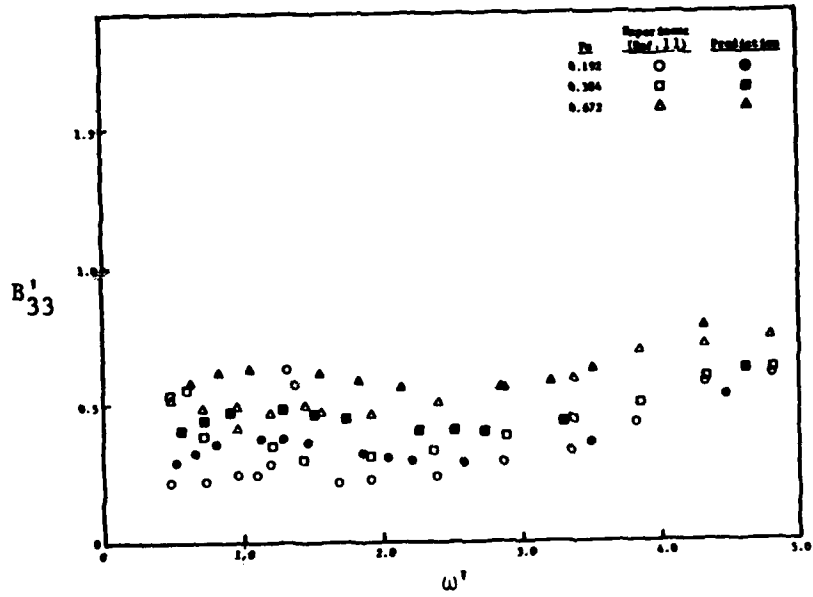


Figure 1c - Damping Coefficients B'_{33} and B'_{53}

Figure 1 (Continued)

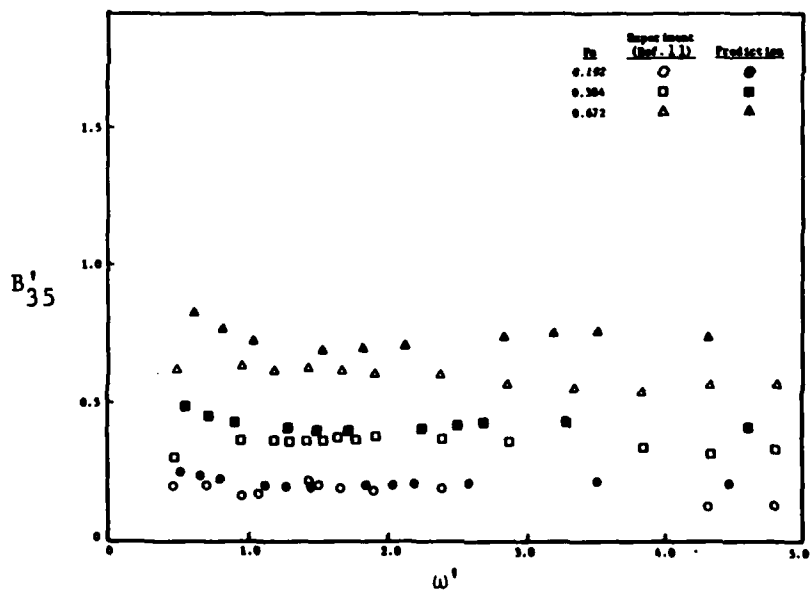
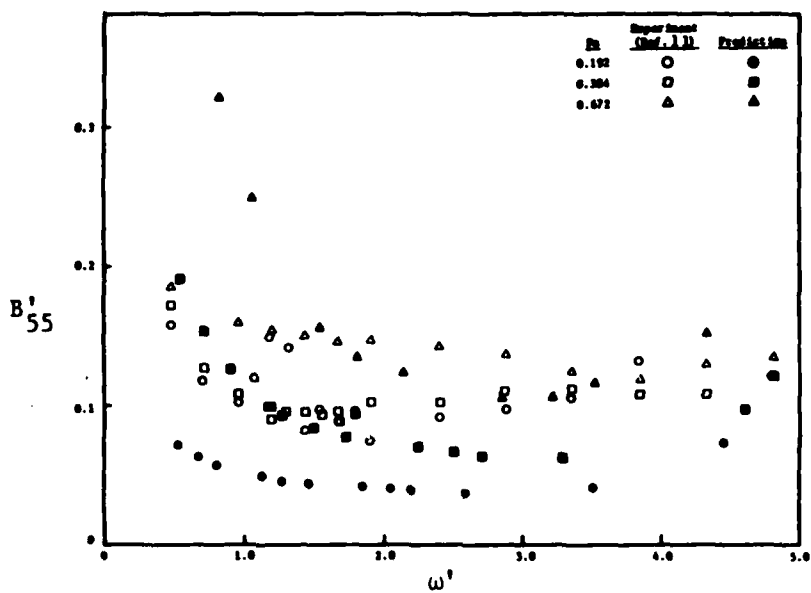


Figure 1d - Damping Coefficients B'_{55} and B'_{35}

Figure 2 - Comparison between Experiment and Prediction of Added Mass and Damping Coefficients for the SWATH 6A

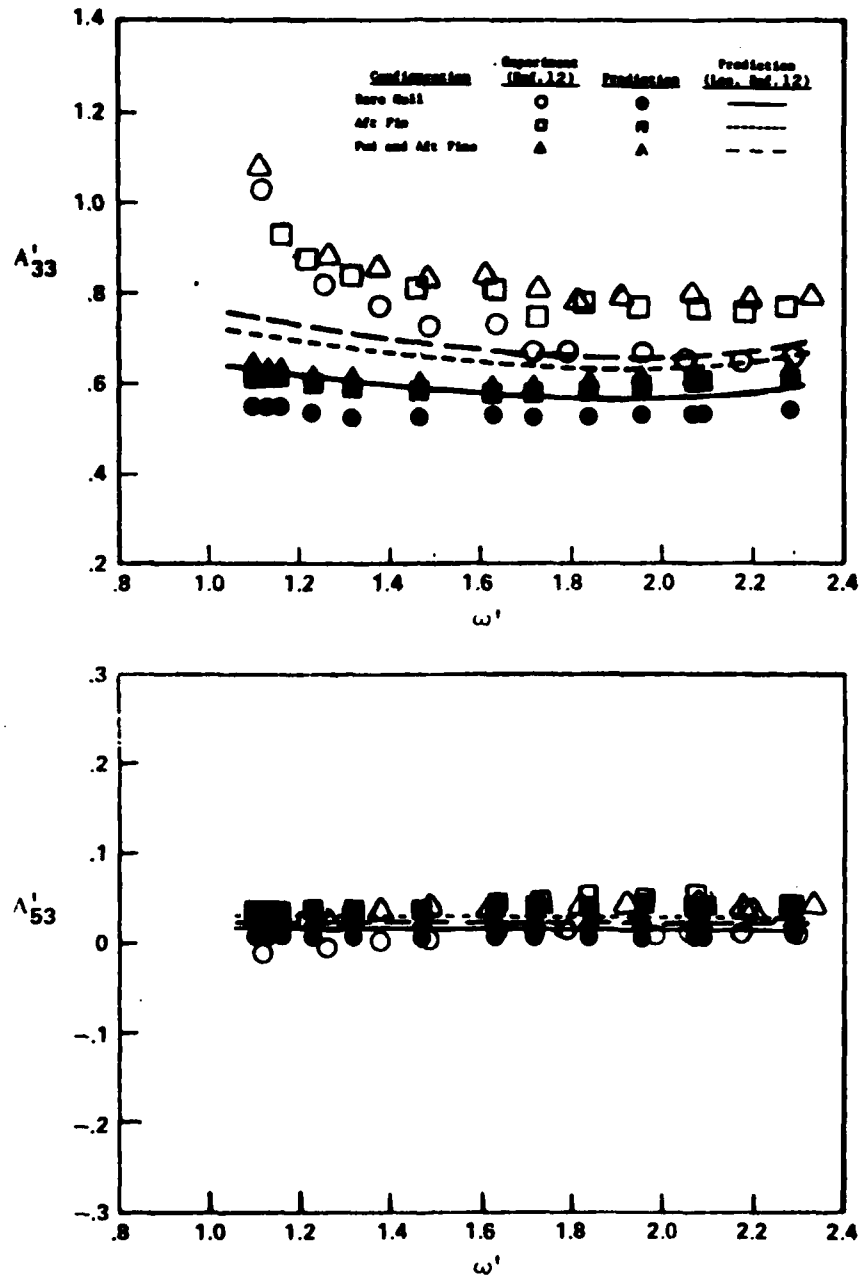


Figure 2a - Added Mass Coefficients A'_{33} and A'_{53} for $F_n = 0.0$

Figure 2 (Continued)

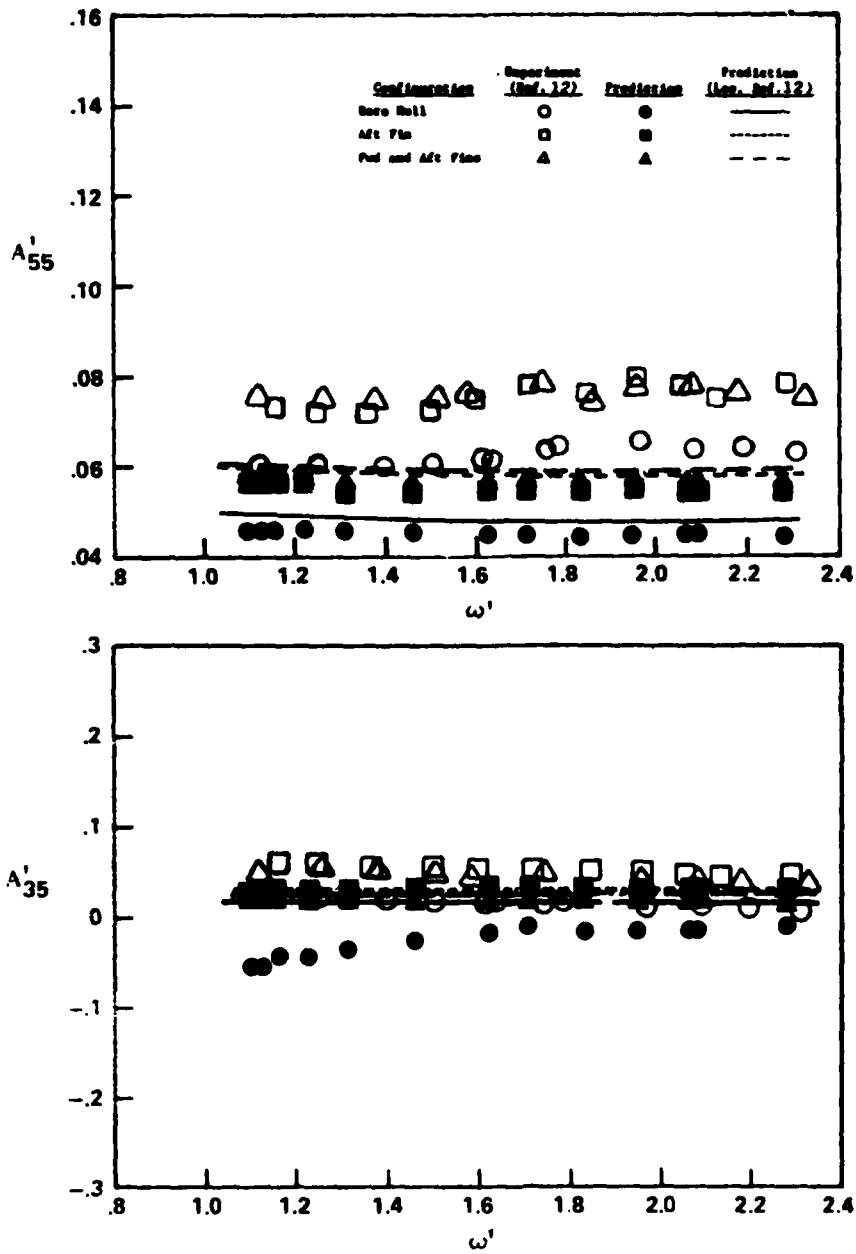


Figure 2b - Added Mass Coefficients A'_{55} and A'_{35} for $F_n = 0.0$

Figure 2 (Continued)

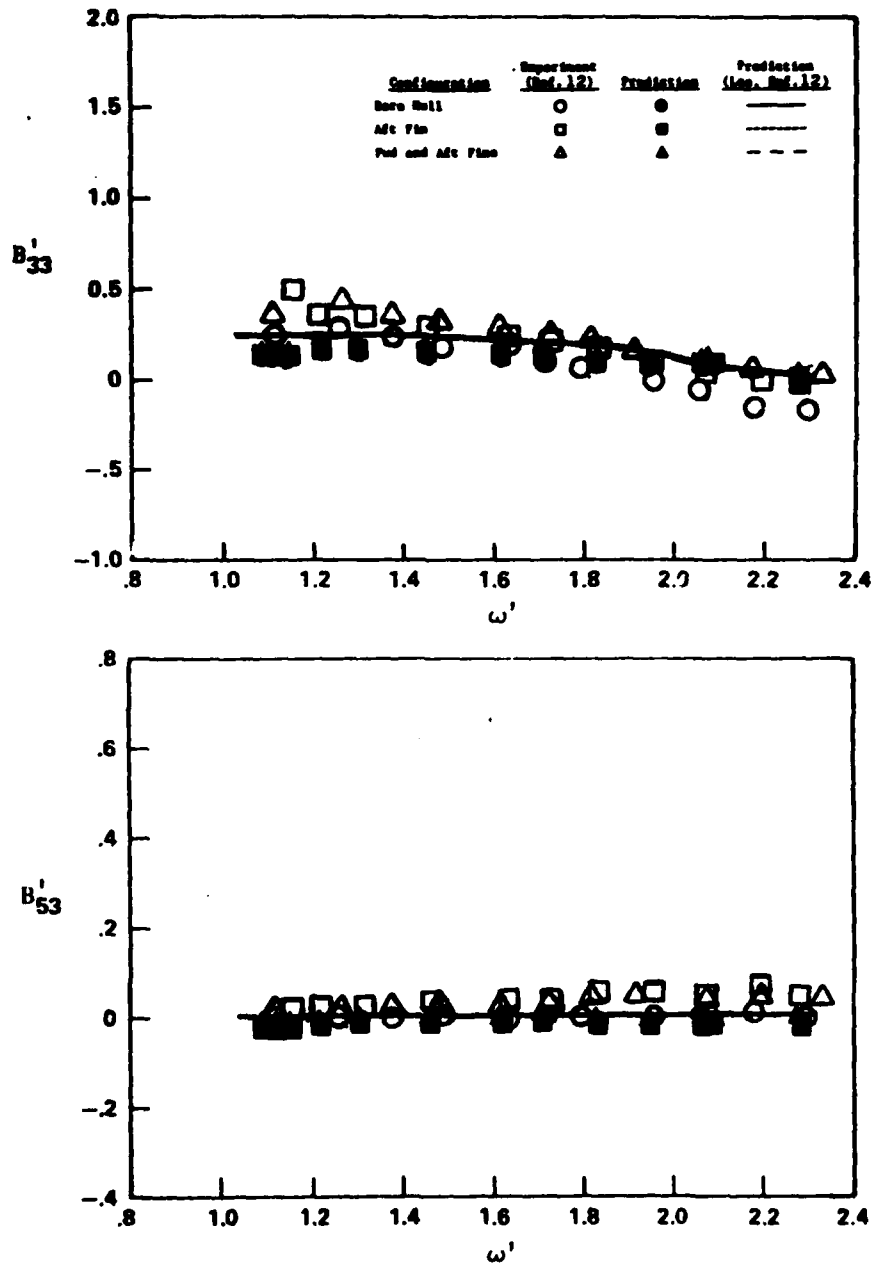


Figure 2c - Damping Coefficients B'_{33} and B'_{53} for $Fn = 0.0$

Figure 2 (Continued)

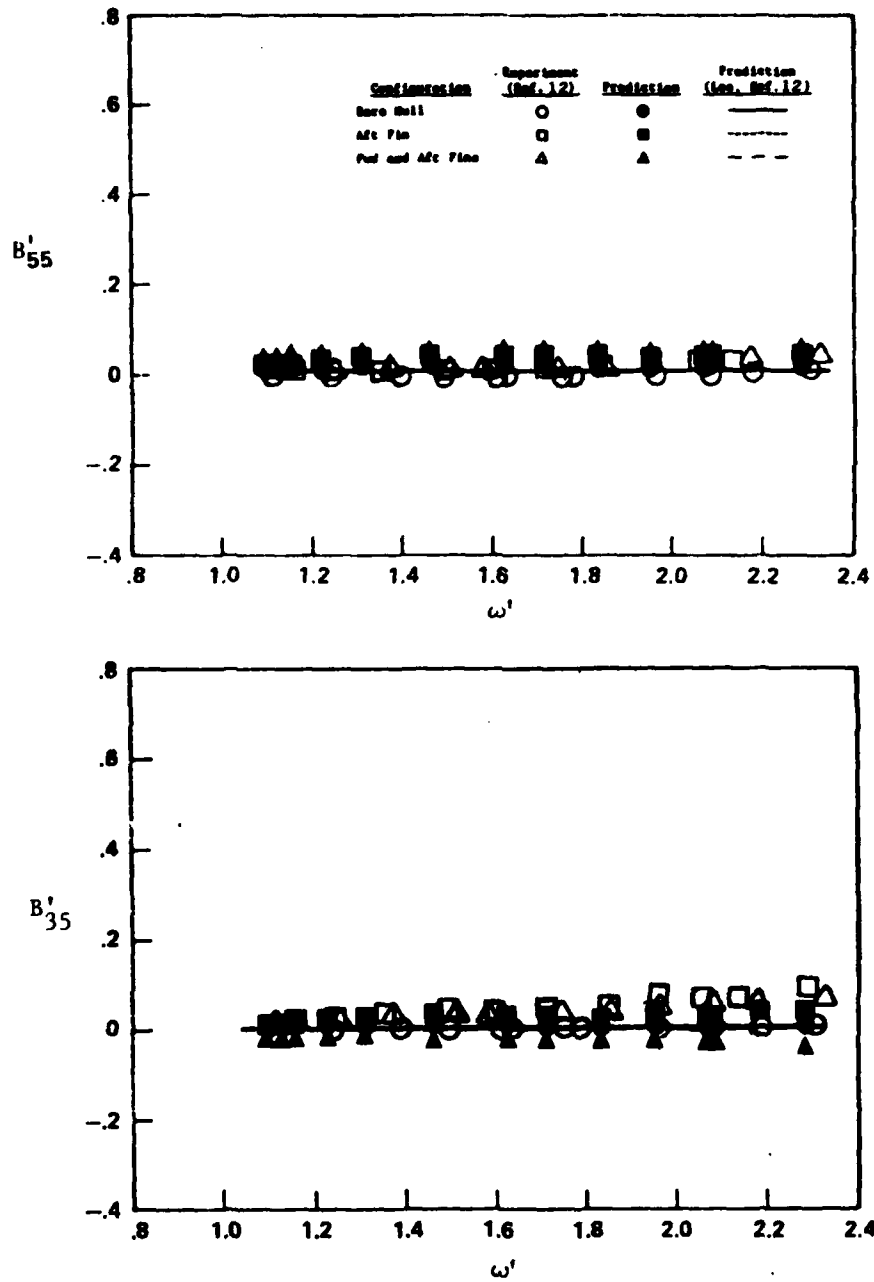


Figure 2d - Damping Coefficients B'_{55} and B'_{35} for $F_n = 0.0$

Figure 2 (Continued)

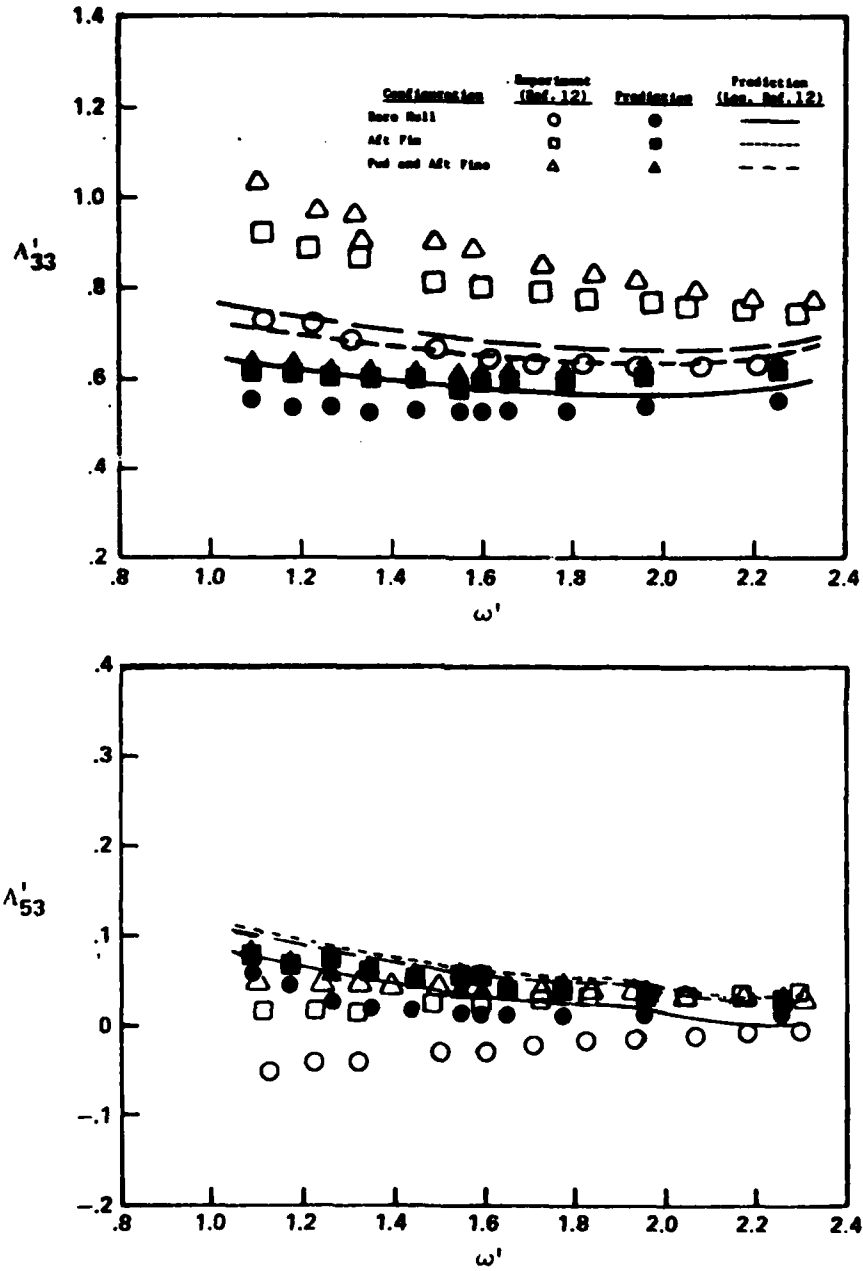


Figure 2e - Added Mass Coefficients A'_{33} and A'_{53} for $F_n = 0.384$

Figure 2 (Continued)

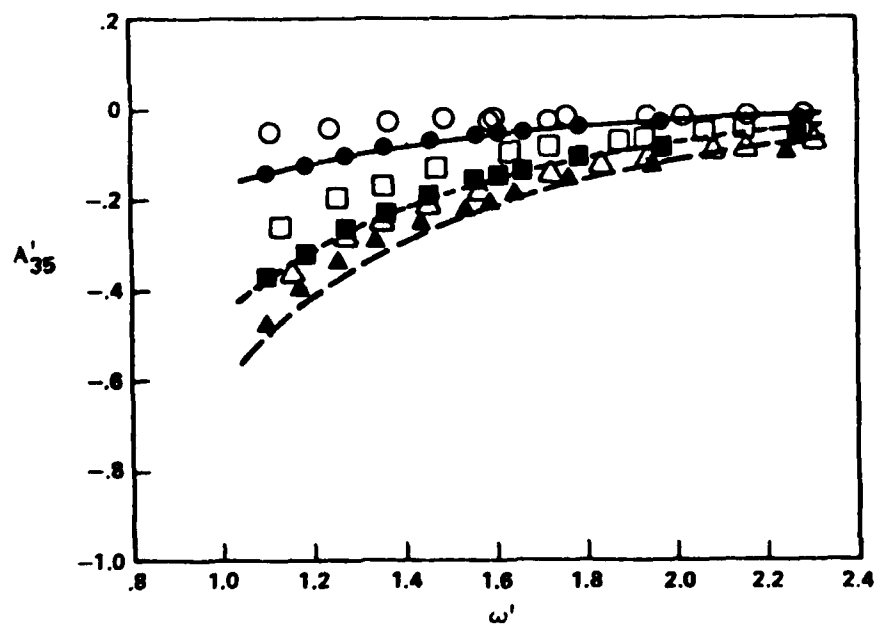
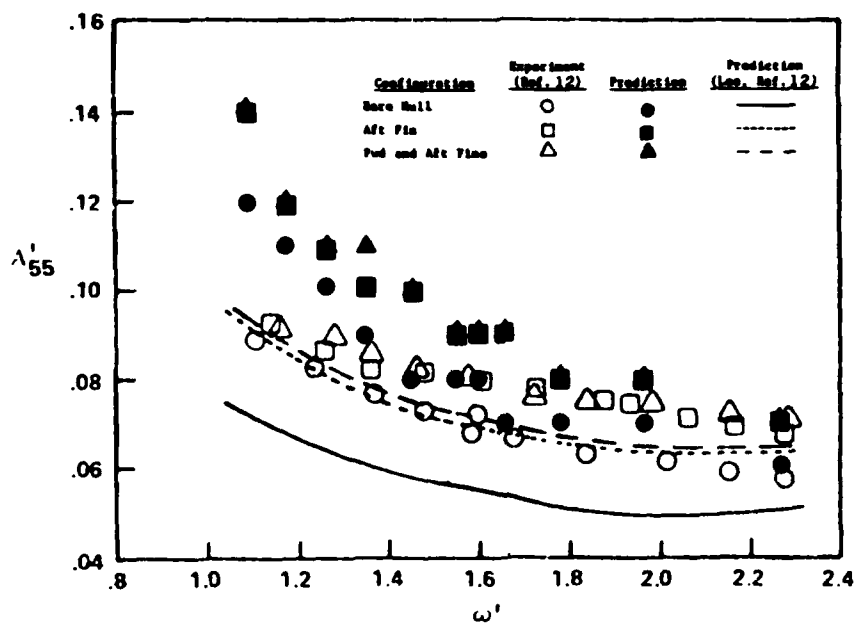


Figure 2f - Added Mass Coefficients A'_{55} and A'_{35} for $F_n = 0.384$

Figure 2 (Continued)

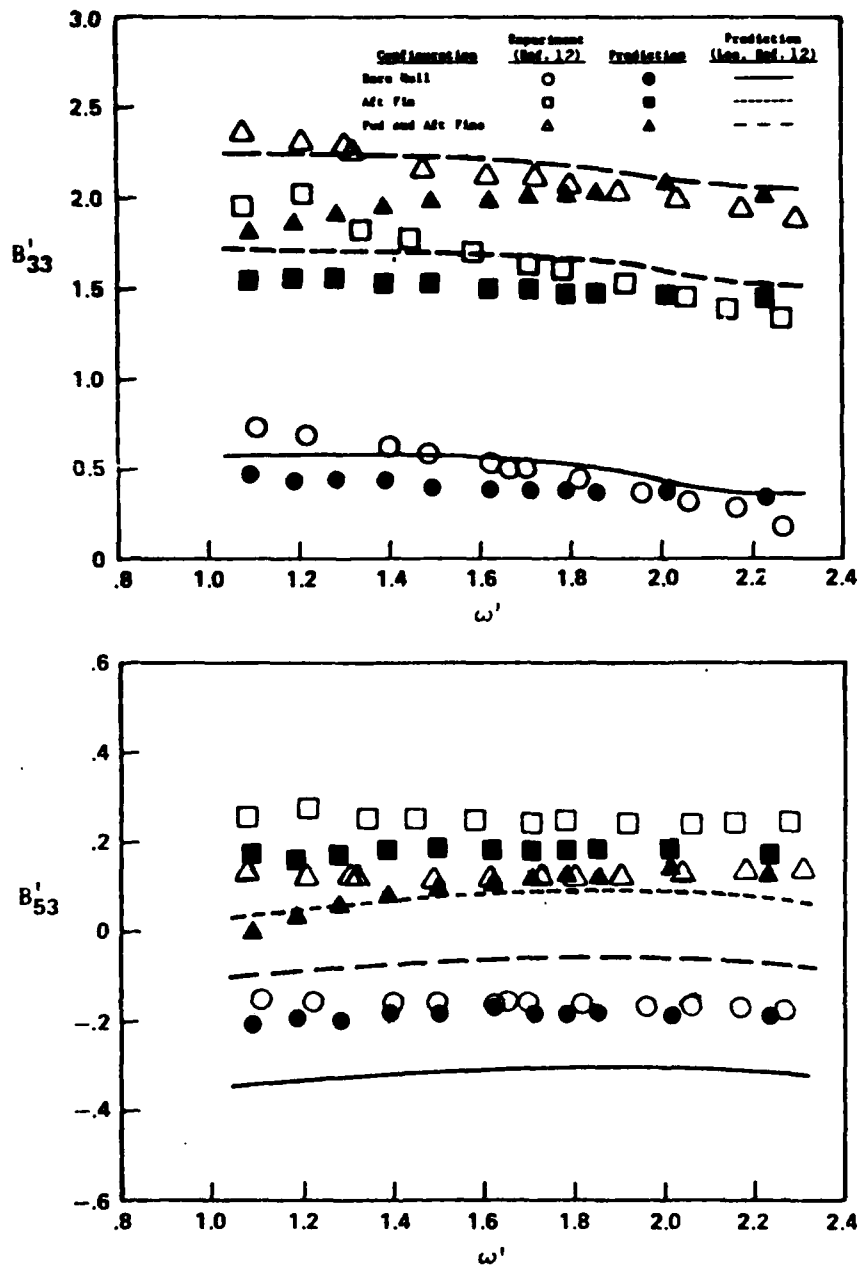


Figure 2g - Damping Coefficients B'_{33} and B'_{53} for $F_n = 0.384$

Figure 2 (Continued)

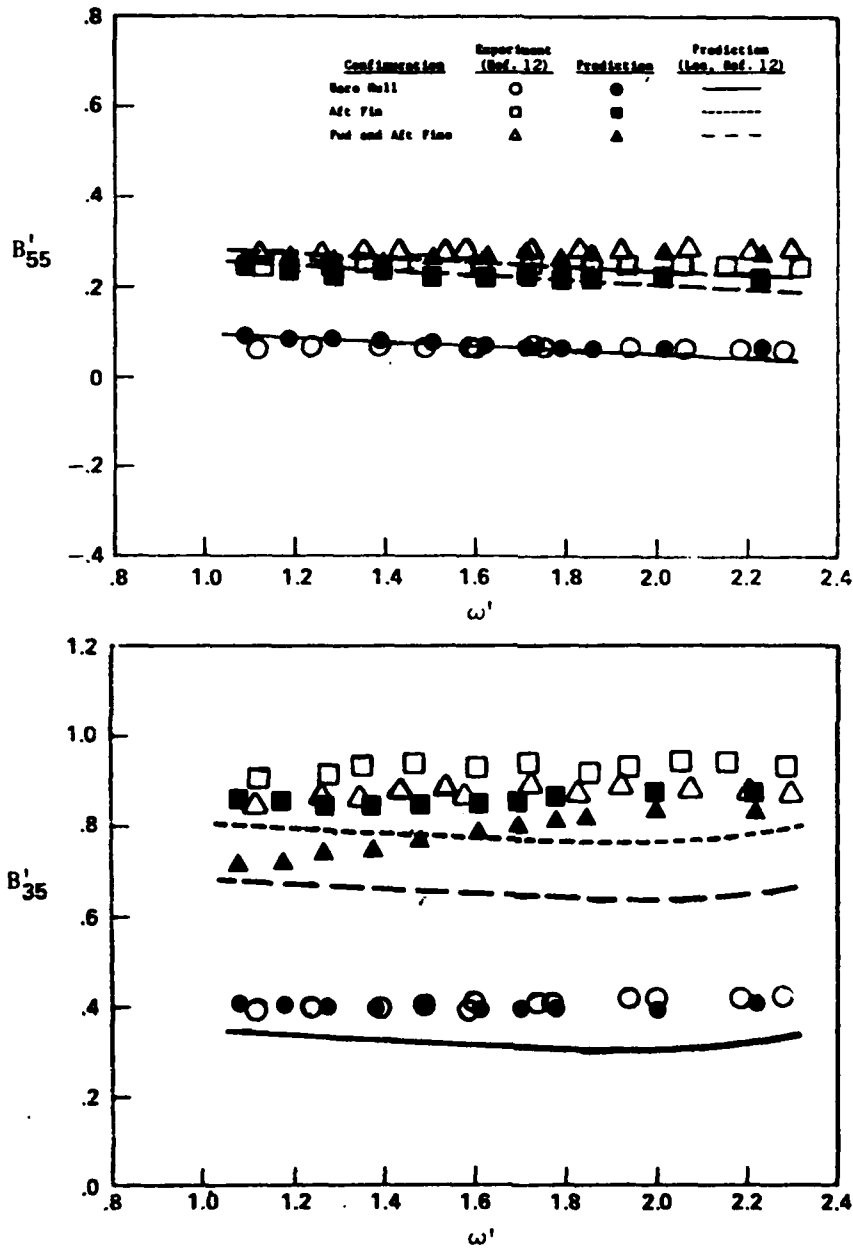


Figure 2h - Damping Coefficients B'_{55} and B'_{35} for $Fn = 0.384$

Figure 2 (Continued)

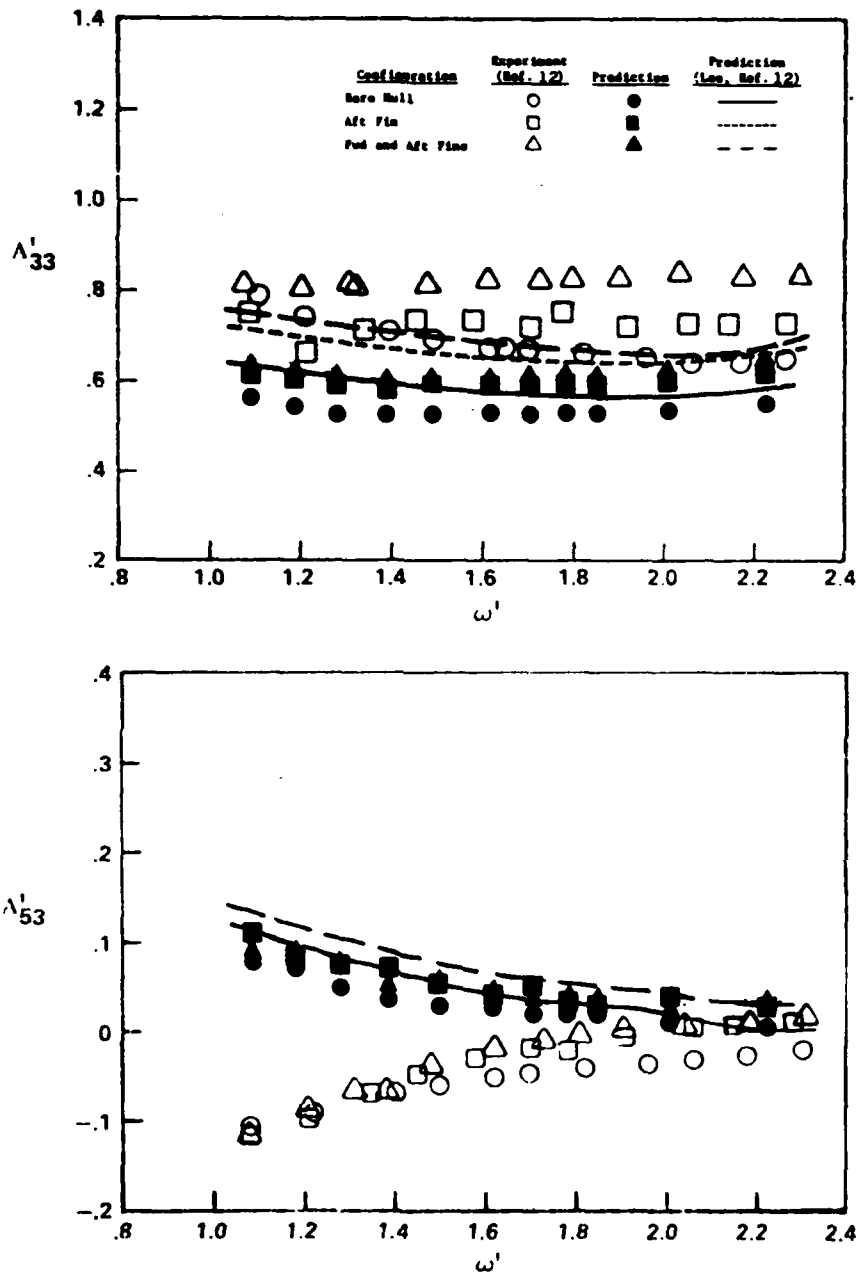


Figure 21 - Added Mass Coefficients A'_{33} and A'_{53} for $Fn = 0.538$

Figure 2 (Continued)

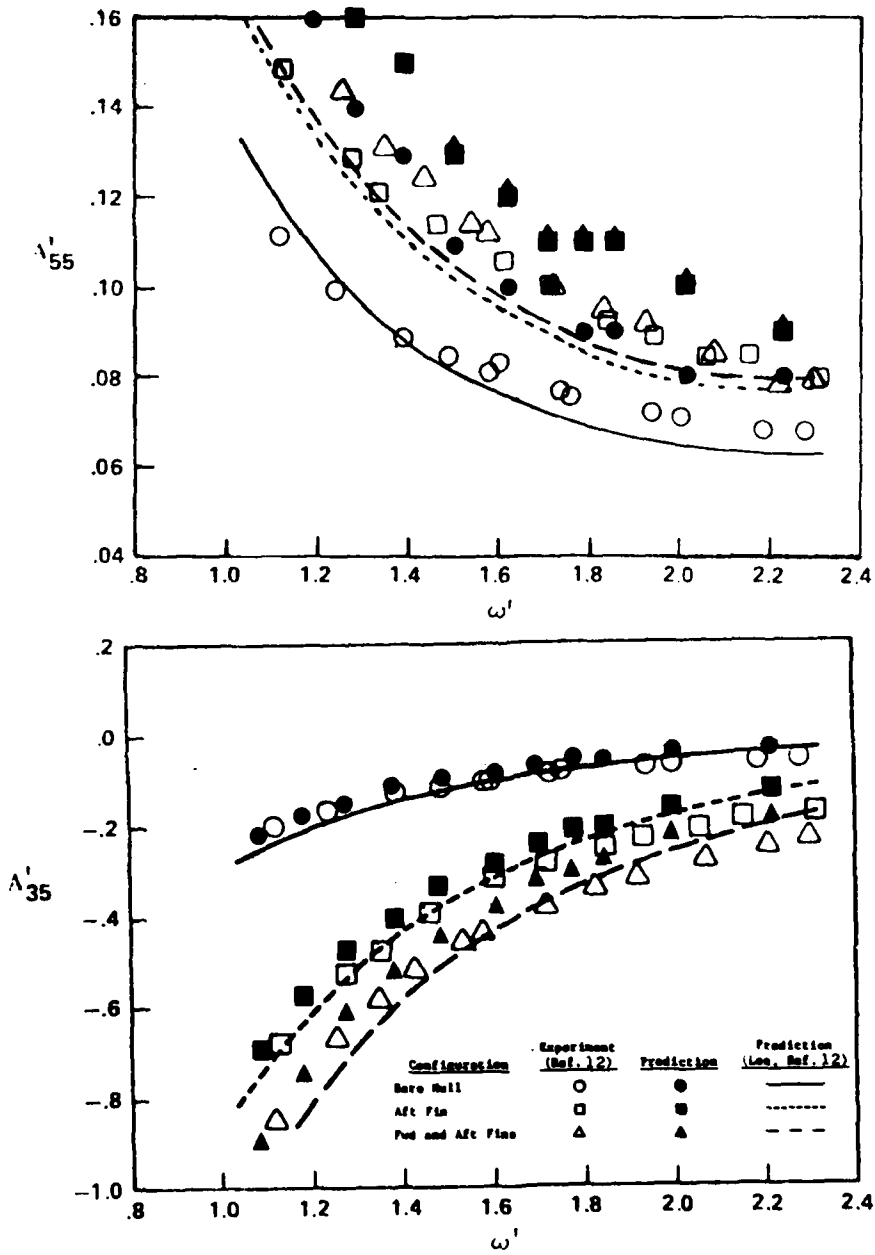


Figure 2j - Added Mass Coefficients A'_{55} and A'_{35} for $Fn = 0.538$

Figure 2 (Continued)

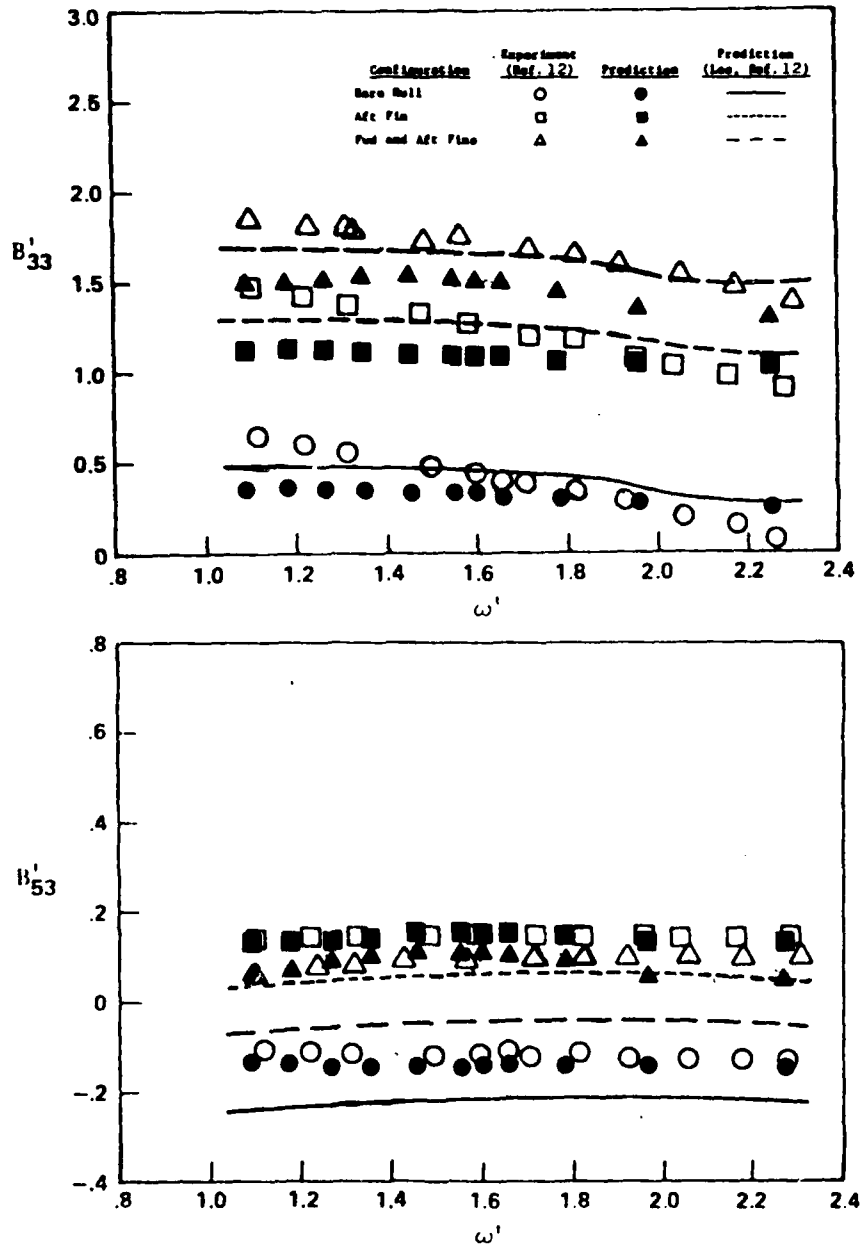


Figure 2k - Damping Coefficients B'_{33} and b'_{53} for $Fn = 0.538$

Figure 2 (Continued)

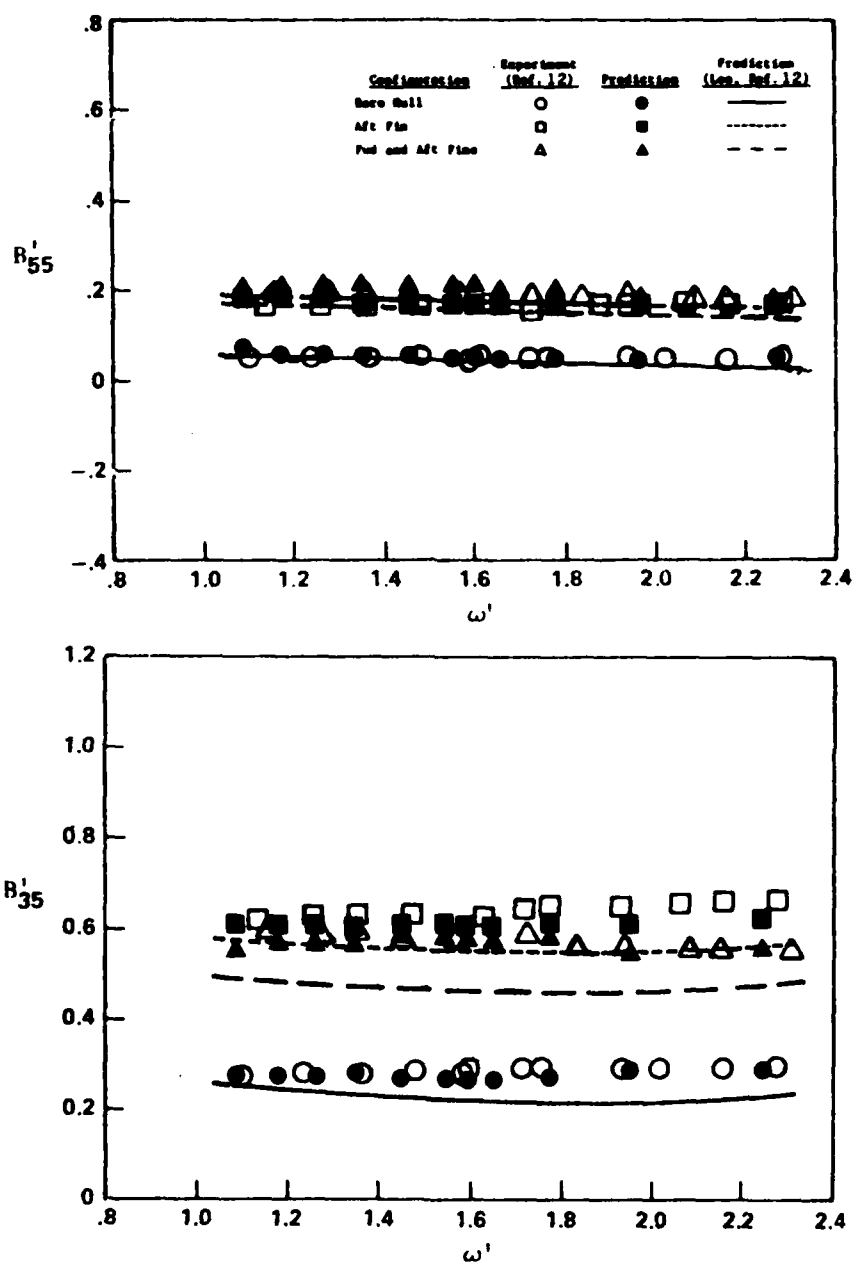


Figure 2d - Damping Coefficients B'_{55} and B'_{35} for $Fn = 0.538$

Figure 3 - Comparison between Experiment and Prediction of Heave
Exciting Force and Pitch Exciting Moment
for the SWATH 6D

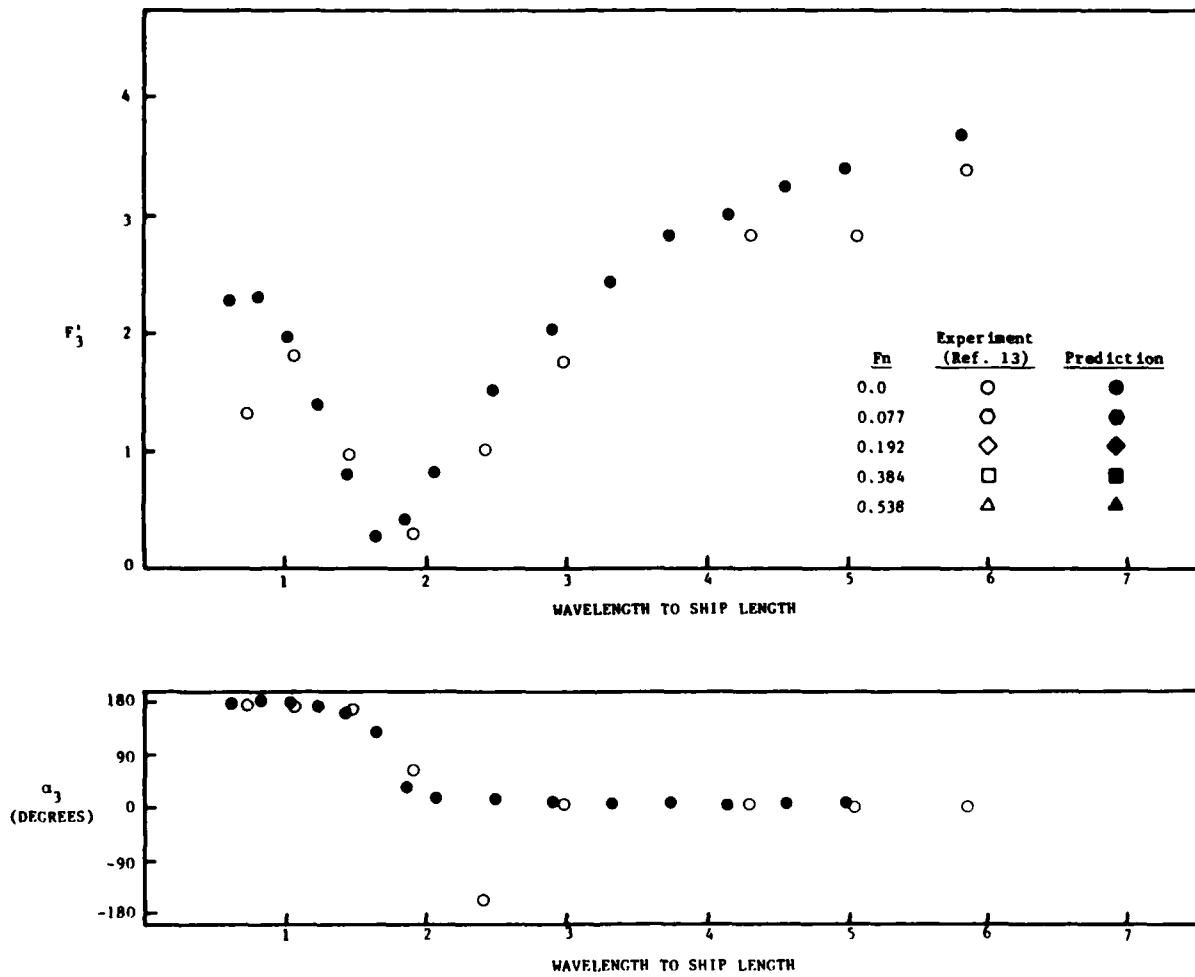


Figure 3a - Heave Force for $F_n = 0.0$ in Head Waves

Figure 3 (Continued)

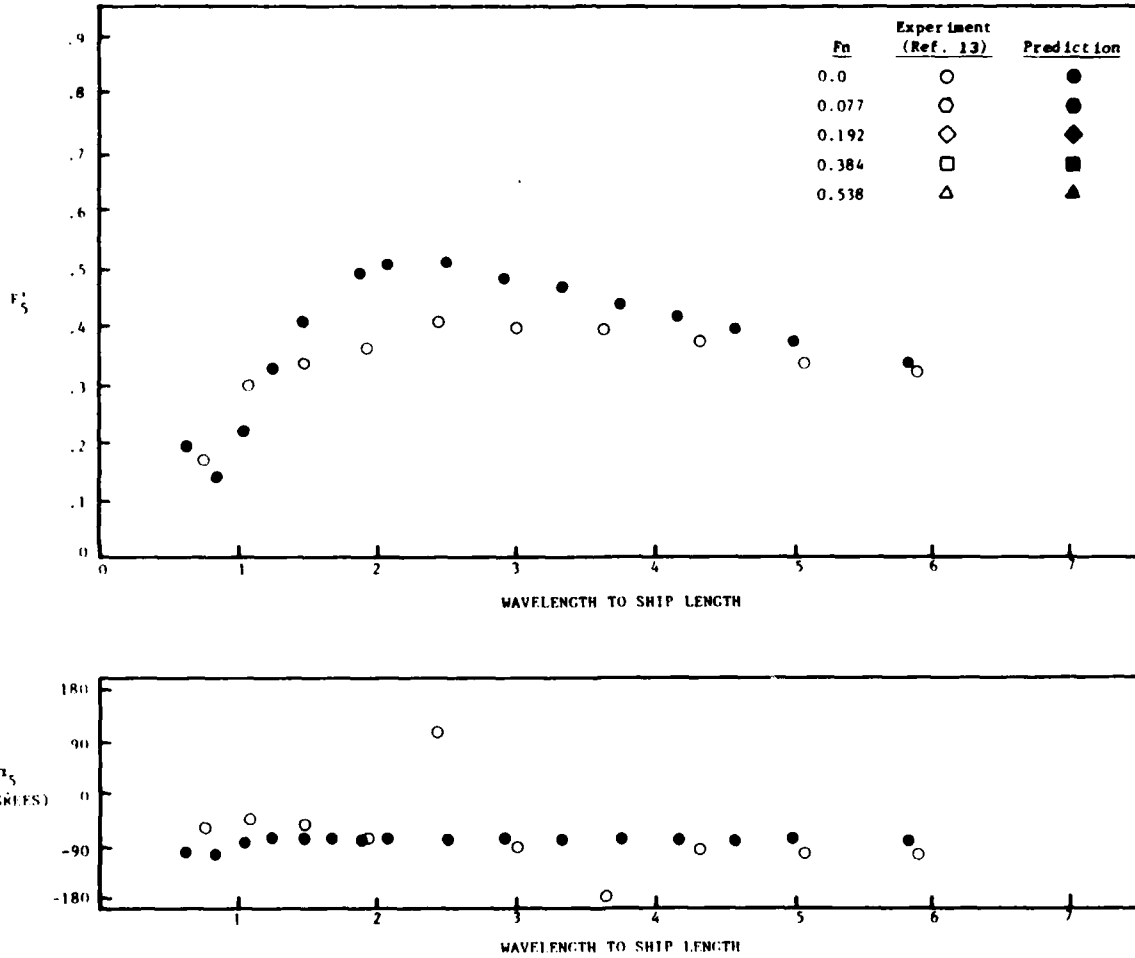


Figure 3b - Pitch Moment for $F_n = 0.0$ in Head Waves

Figure 3 (Continued)

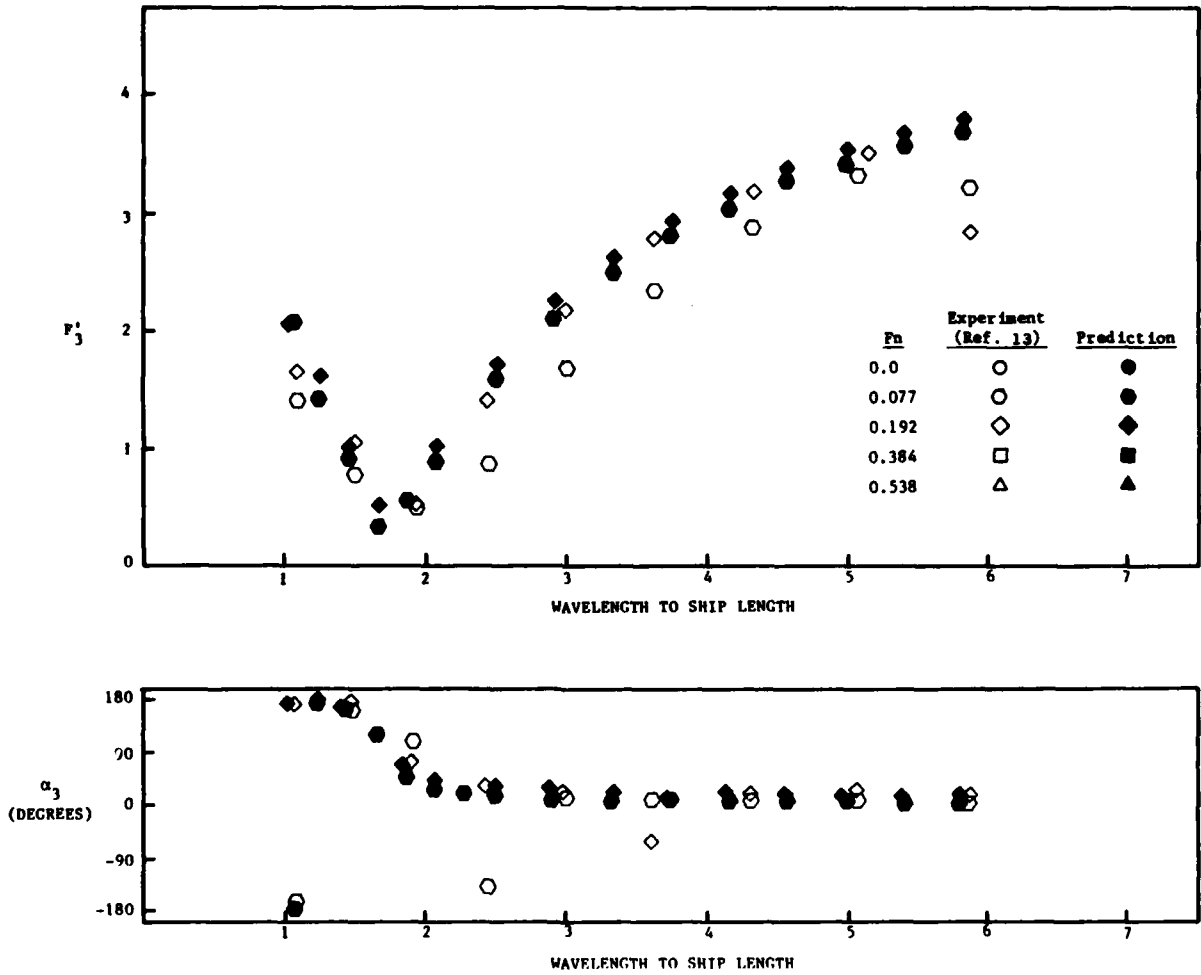


Figure 3c - Heave Force for $F_n = 0.077$ and 0.192 in Head Waves

Figure 3 (Continued)

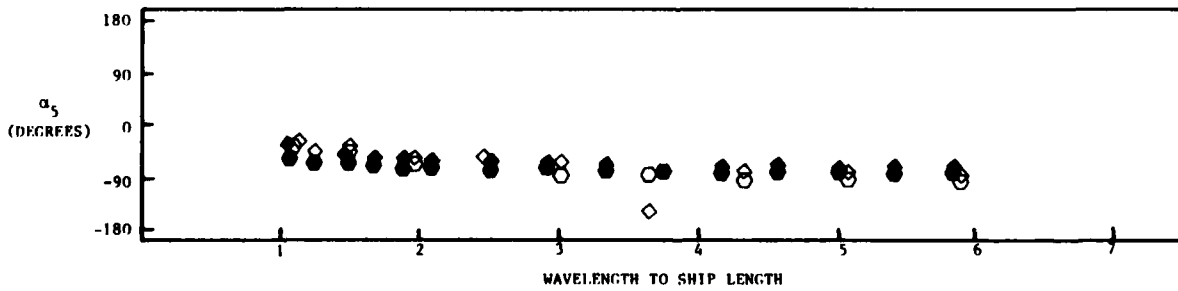
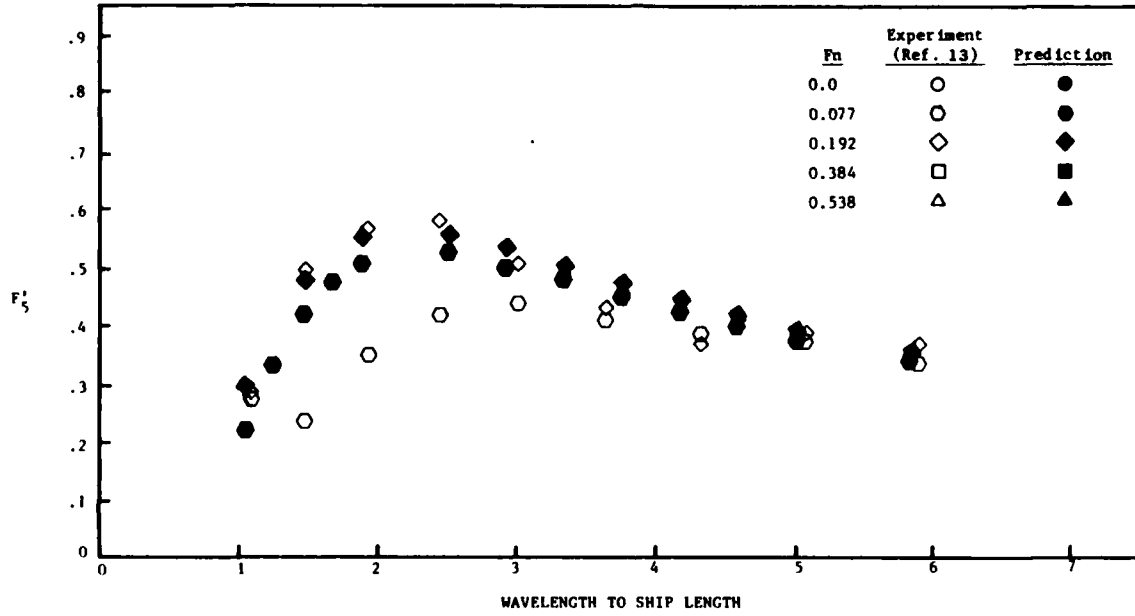


Figure 3d - Pitch Moment at $F_n = 0.077$ and 0.192 in Head Waves

Figure 3 (Continued)

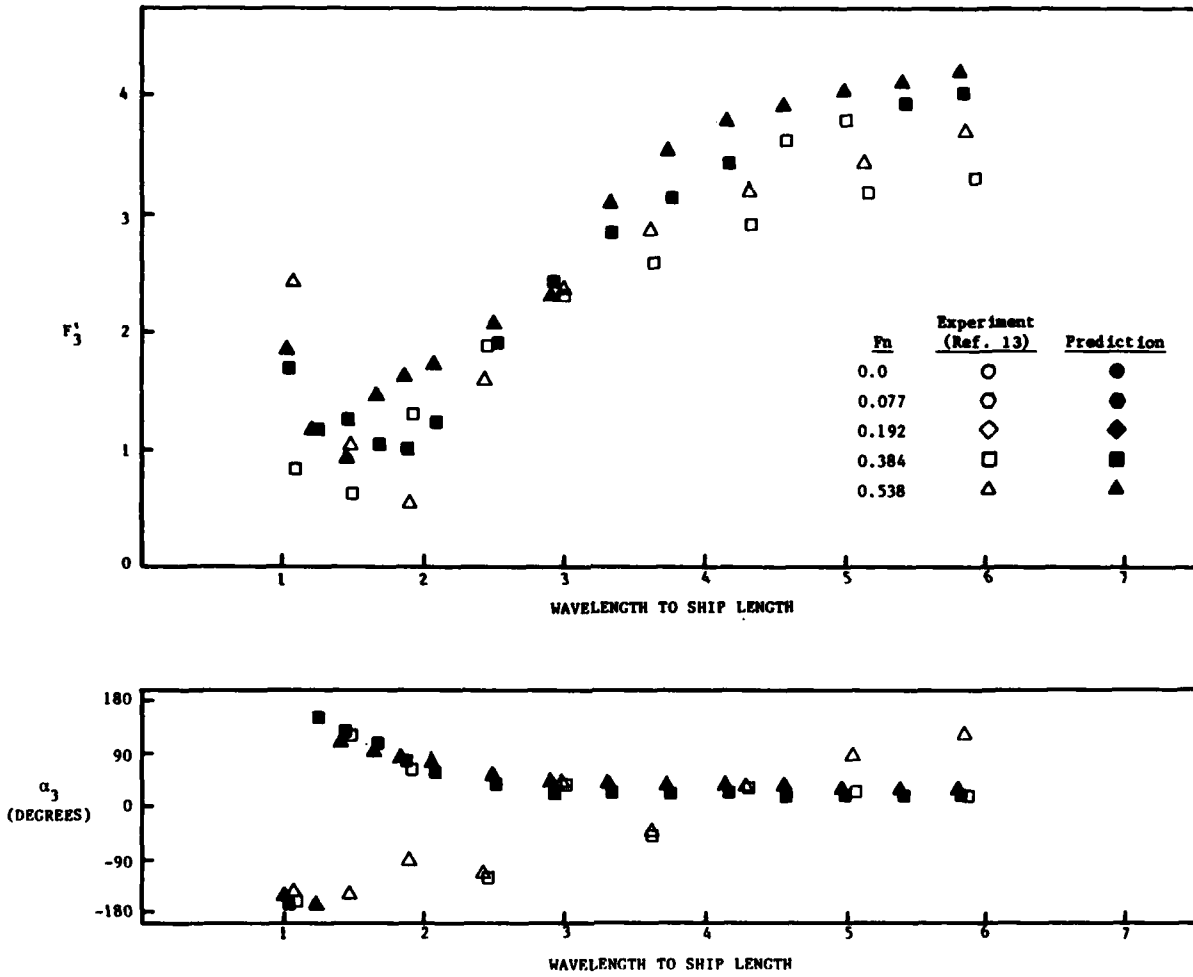


Figure 3e - Heave Force at $F_n = 0.384$ and 0.538 in Head Waves

Figure 3 (Continued)

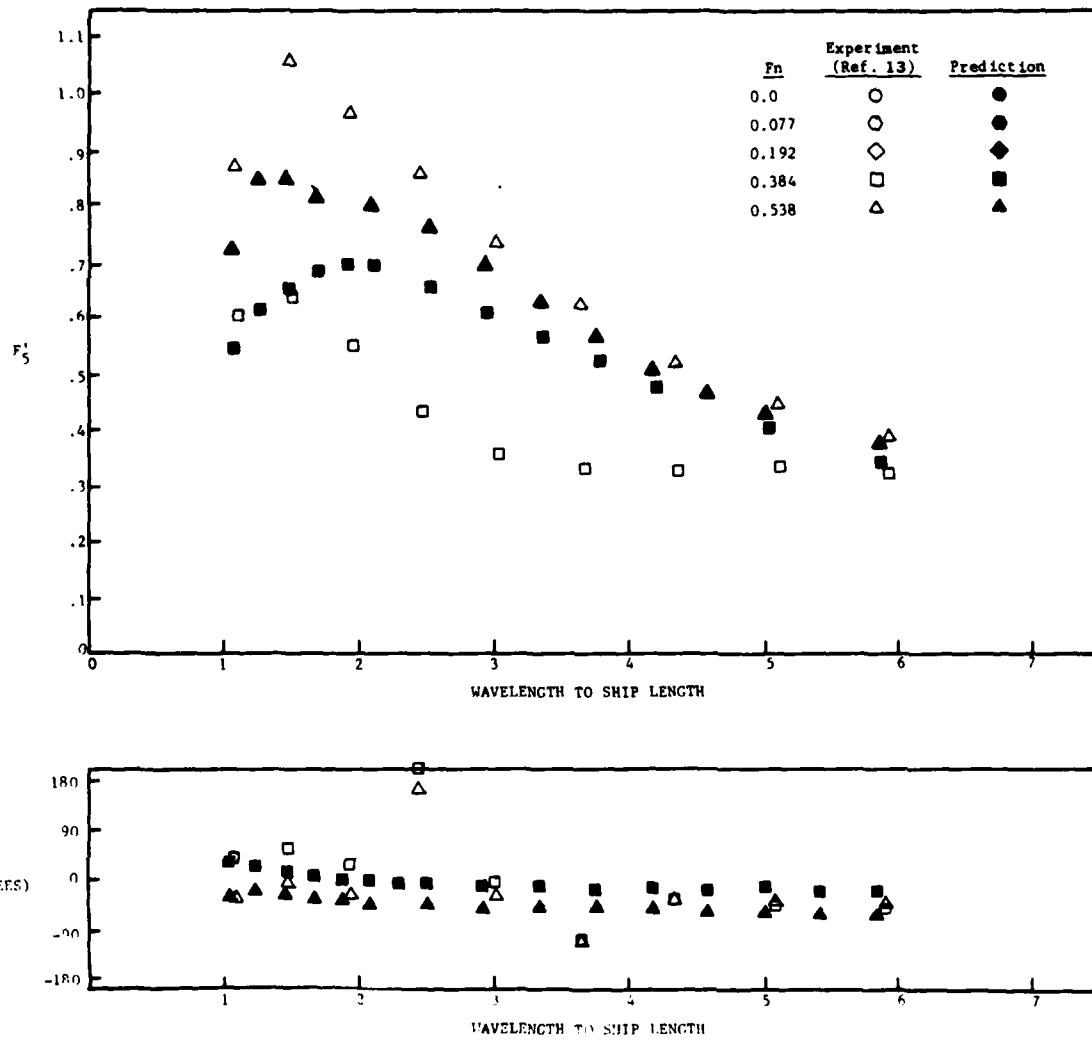


Figure 3f - Pitch Moment at $F_n = 0.384$ and 0.538 in Head Waves

Figure 3 (Continued)

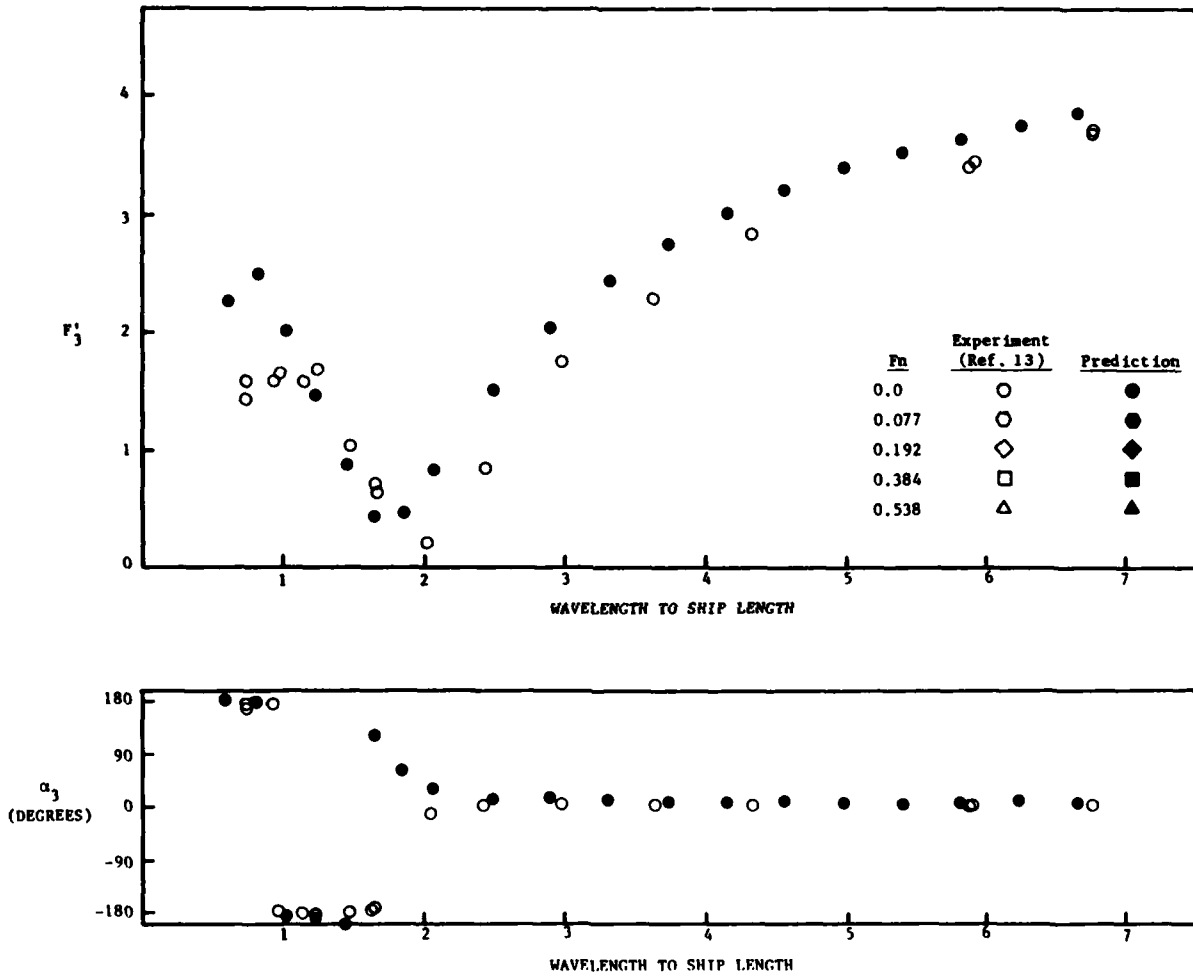


Figure 3g - Heave Force for $F_n = 0.0$ in Following Waves

Figure 3 (Continued)

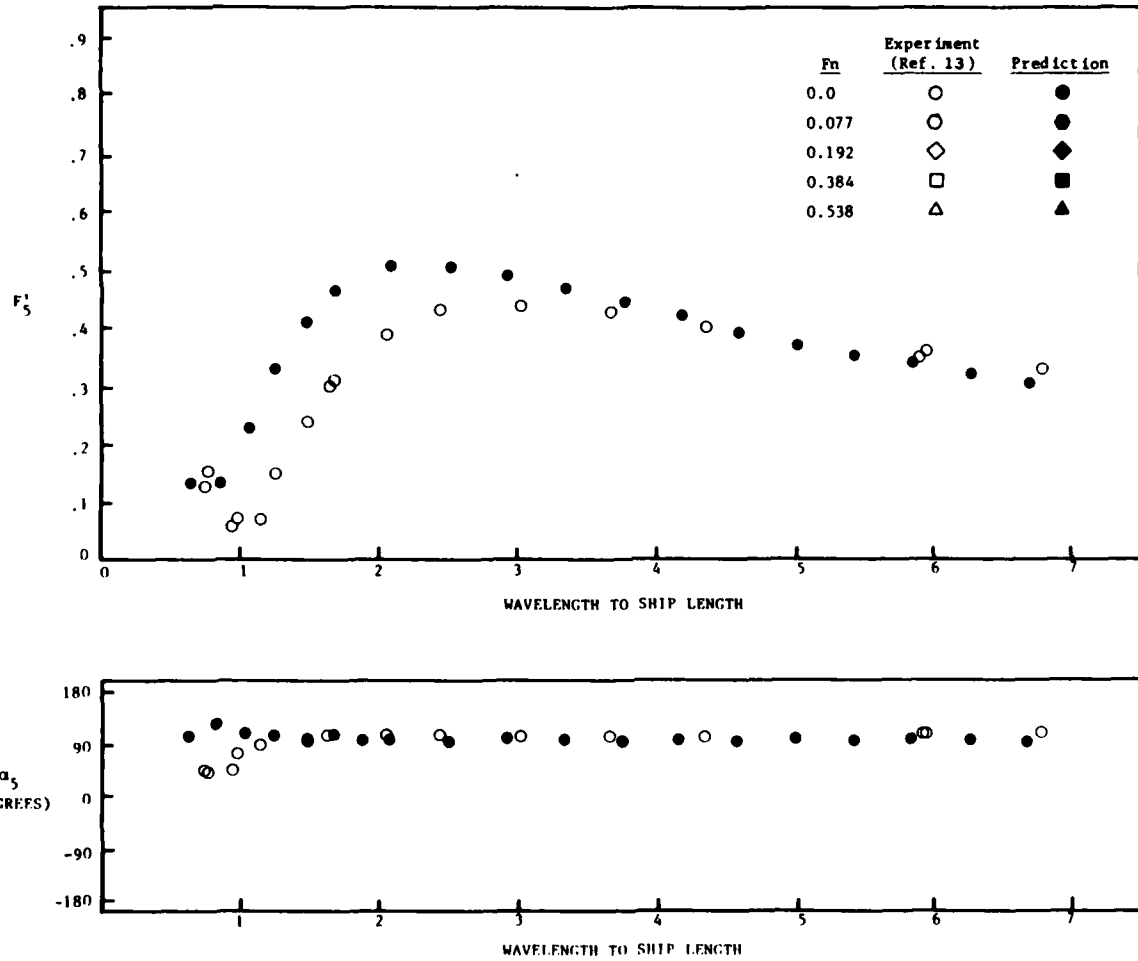


Figure 3h - Pitch Moment for $F_n = 0.0$ in Following Waves

Figure 3 (Continued)

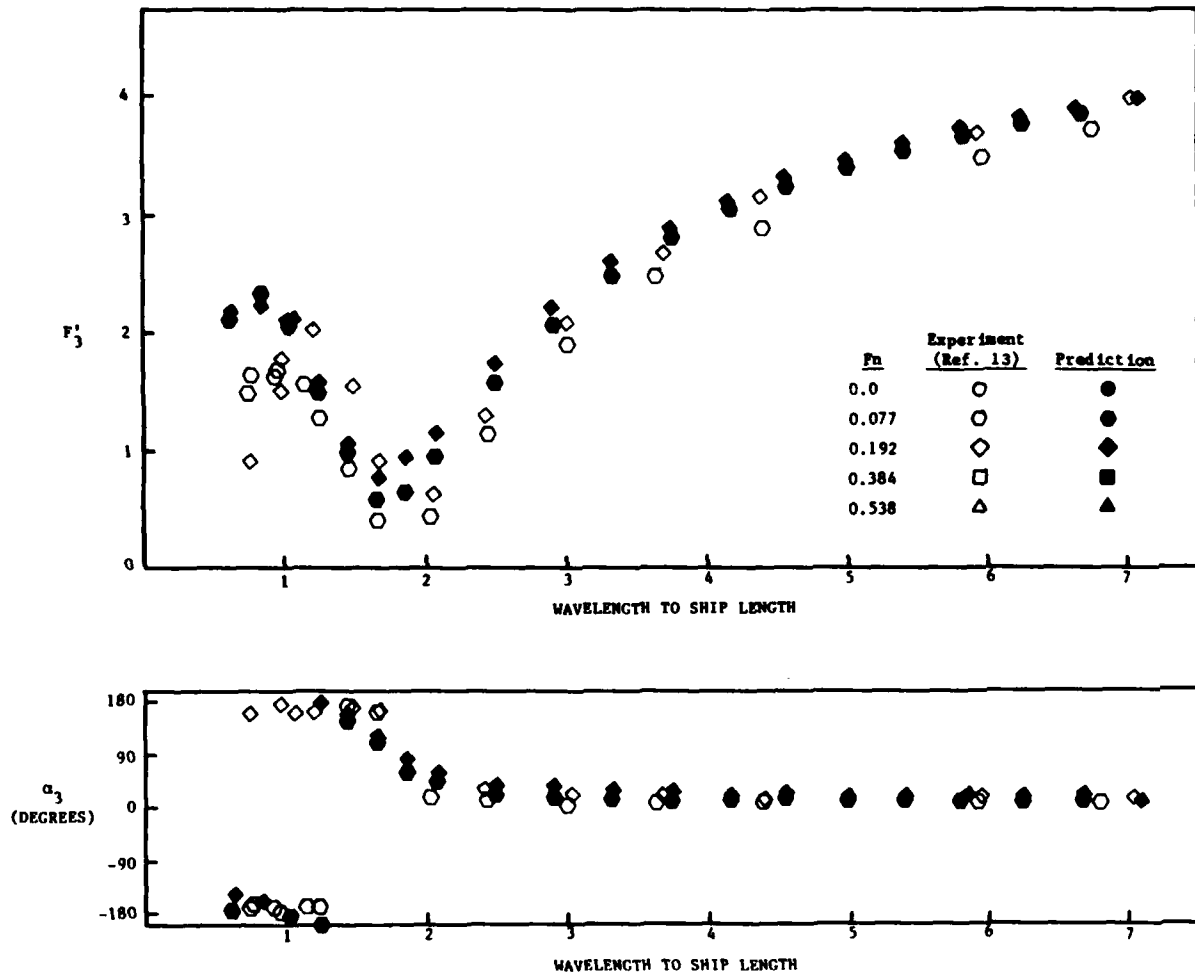


Figure 31 - Heave Force at $F_n = 0.077$ and 0.192 in Following Waves

Figure 3 (Continued)

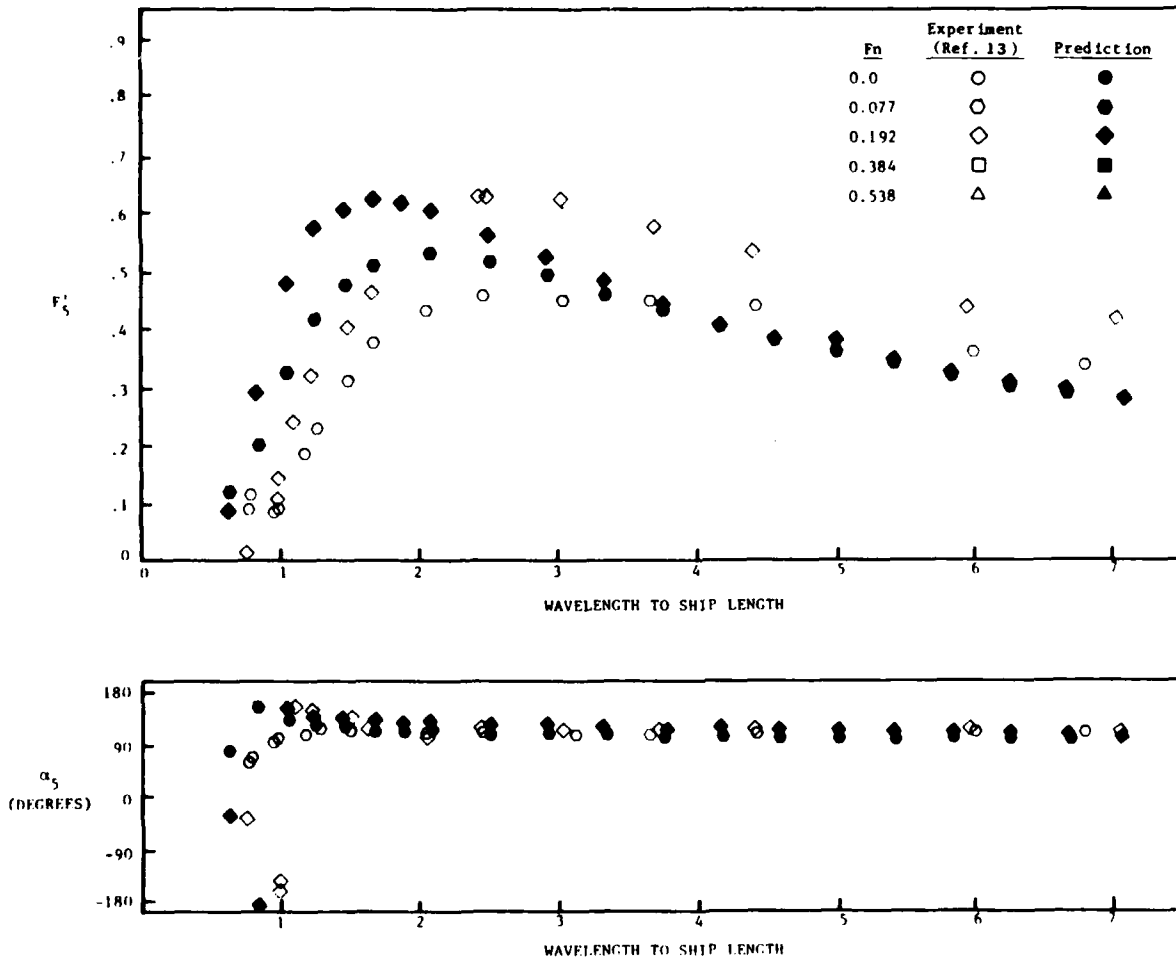


Figure 3j - Pitch Moment at $F_n = 0.077$ and 0.192 in Following Waves

Figure 3 (Continued)

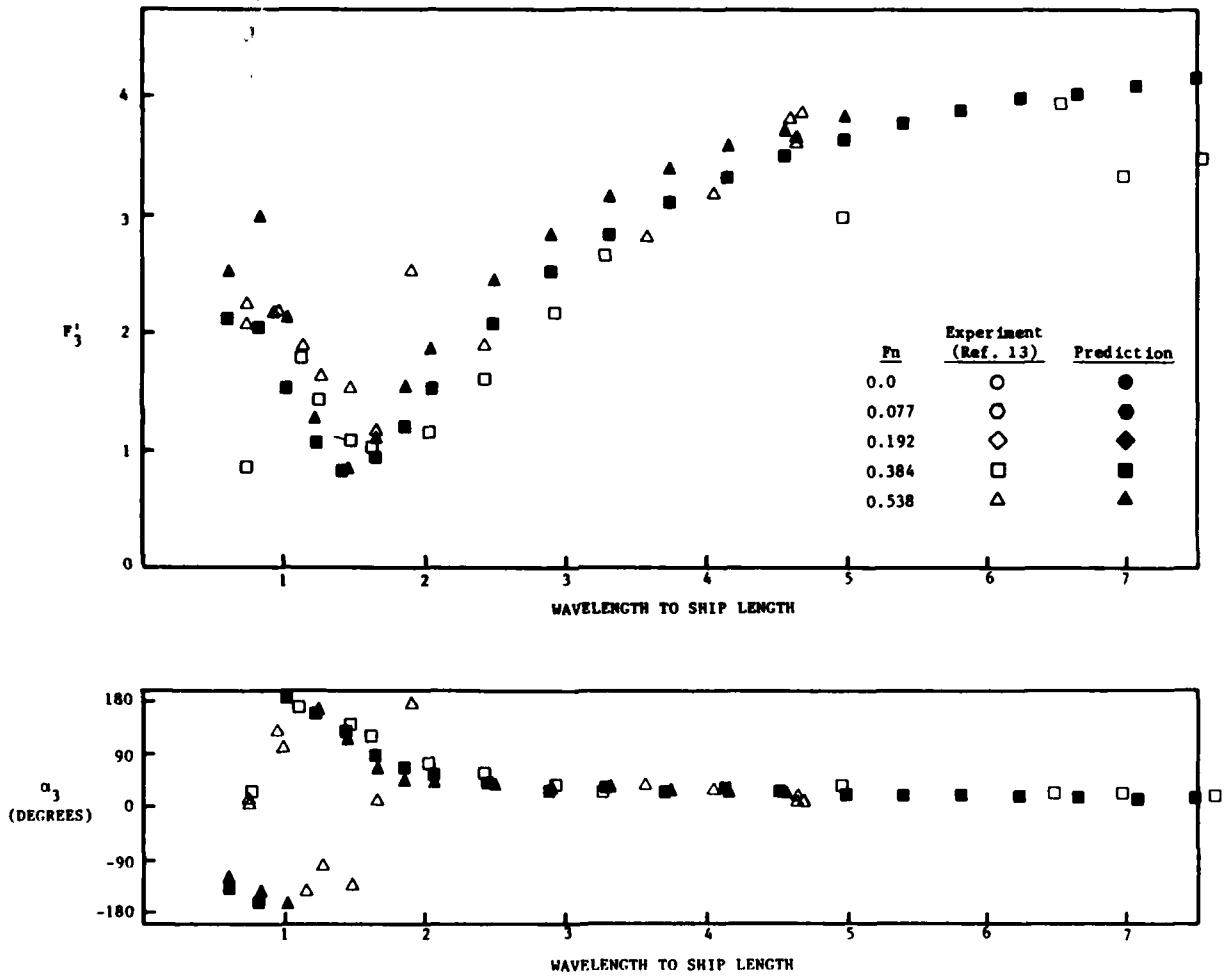


Figure 3k - Heave Force at $F_n = 0.384$ and 0.538 in Following Waves

Figure 3 (Continued)

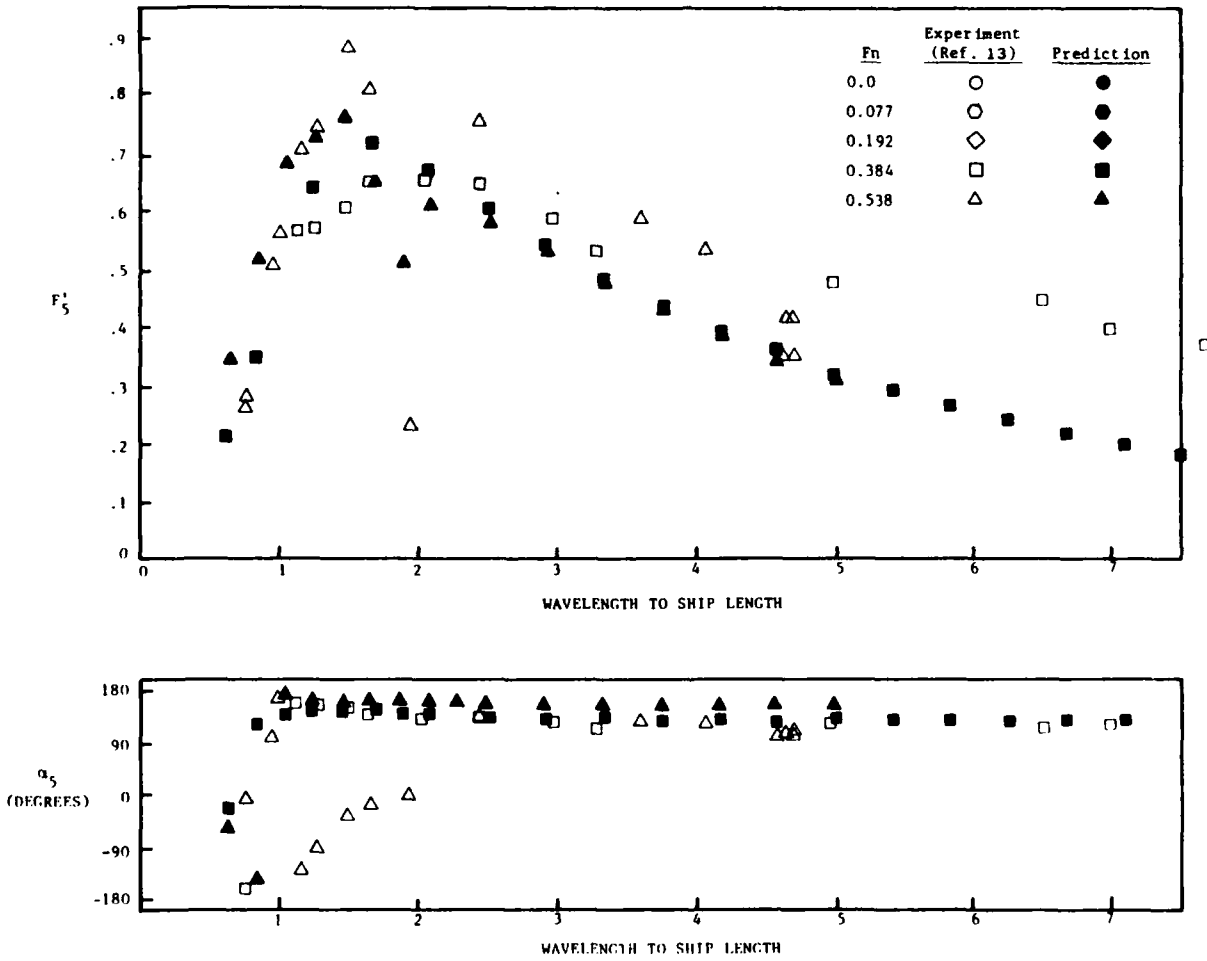


Figure 3l - Pitch Moment at $F_n = 0.384$ and 0.538 in Following Waves

Figure 4 - Comparison between Experiment and Prediction of Heave Exciting Force and Pitch Exciting Moment for the SSP KAIMALINO in Head Waves

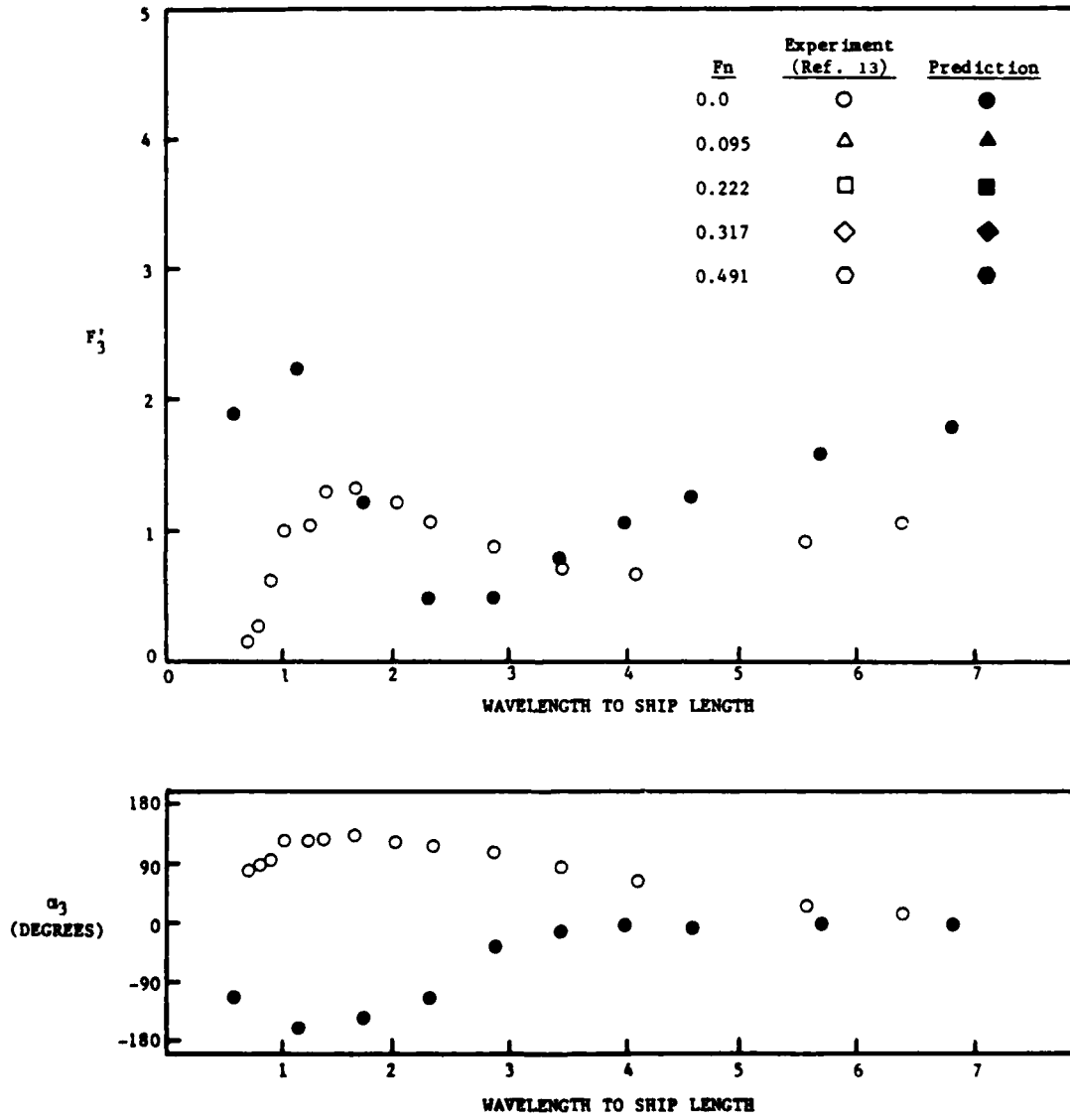


Figure 4a - Heave Force for $F_n = 0.0$

Figure 4 (Continued)

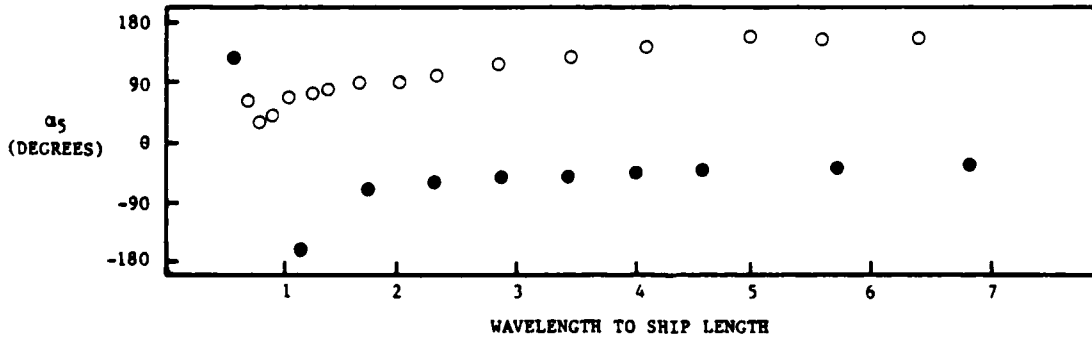
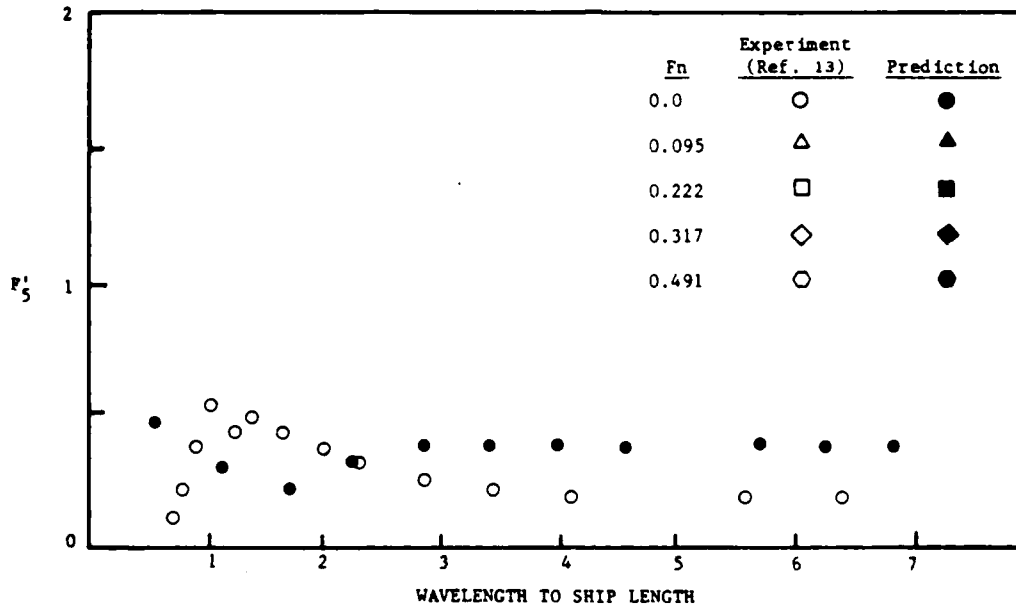


Figure 4b - Pitch Moment for $F_n = 0.0$

Figure 4 (Continued)

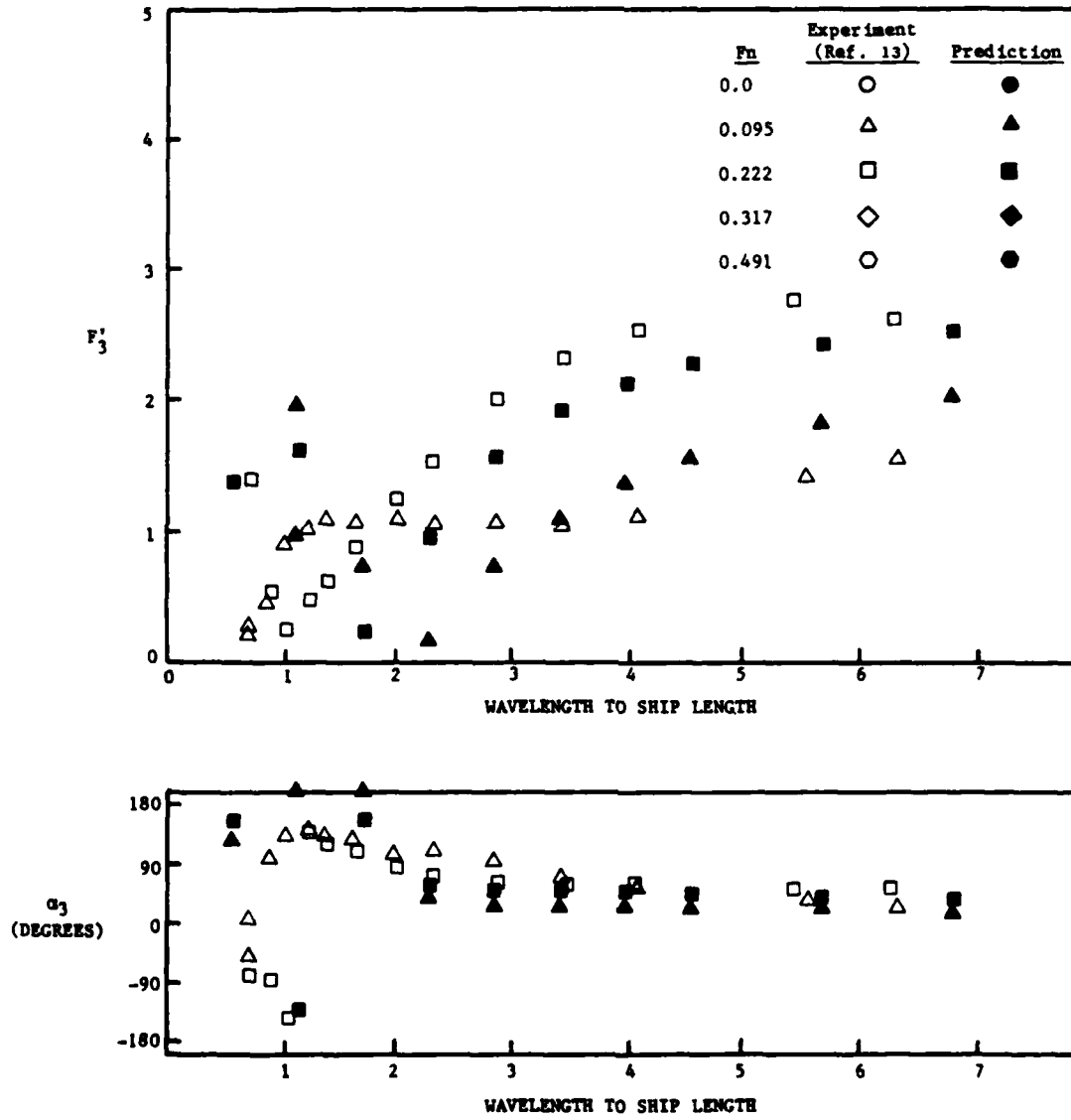


Figure 4c - Heave Force for $F_n = 0.095$ and 0.222

Figure 4 (Continued)

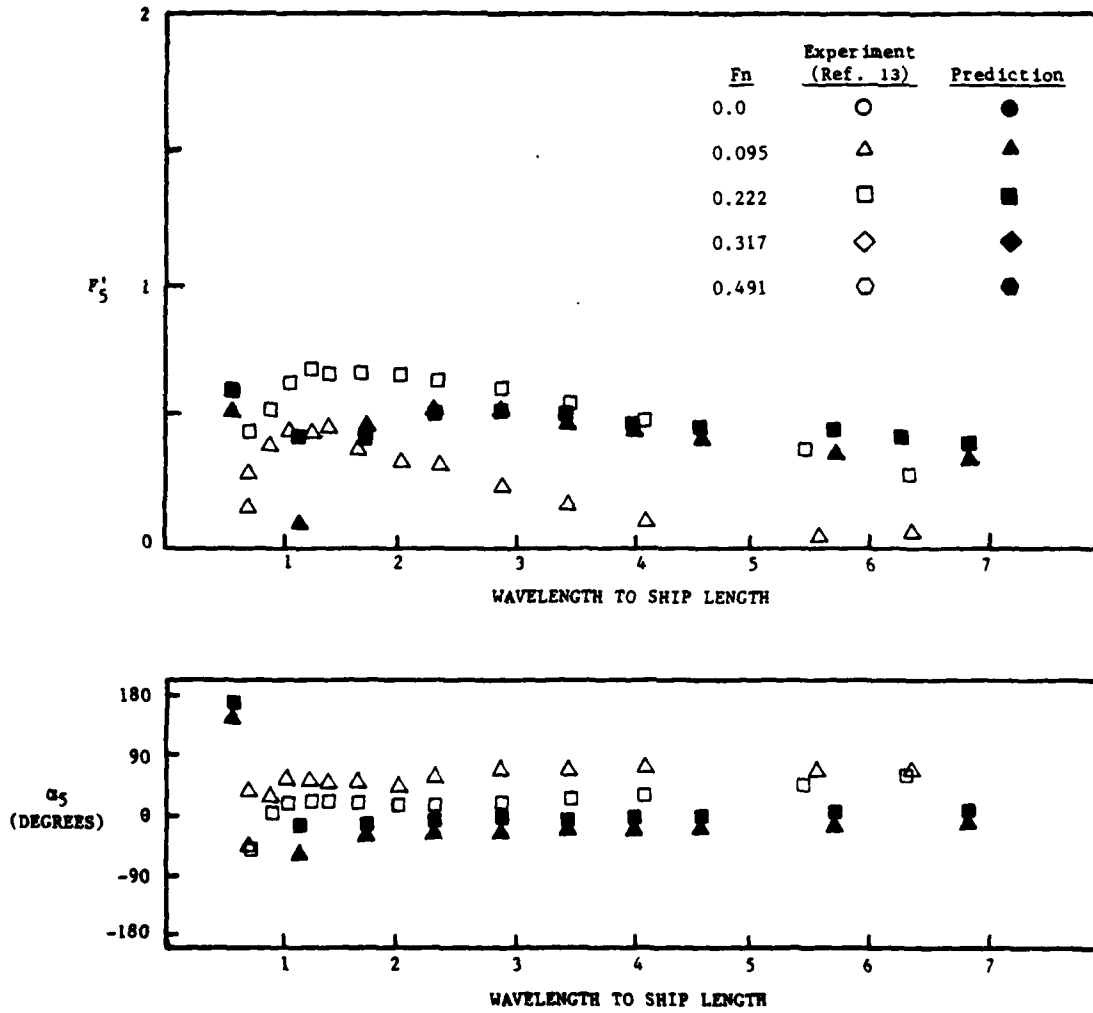


Figure 4d - Pitch Moment for $F_n = 0.095$ and 0.222

Figure 4 (Continued)

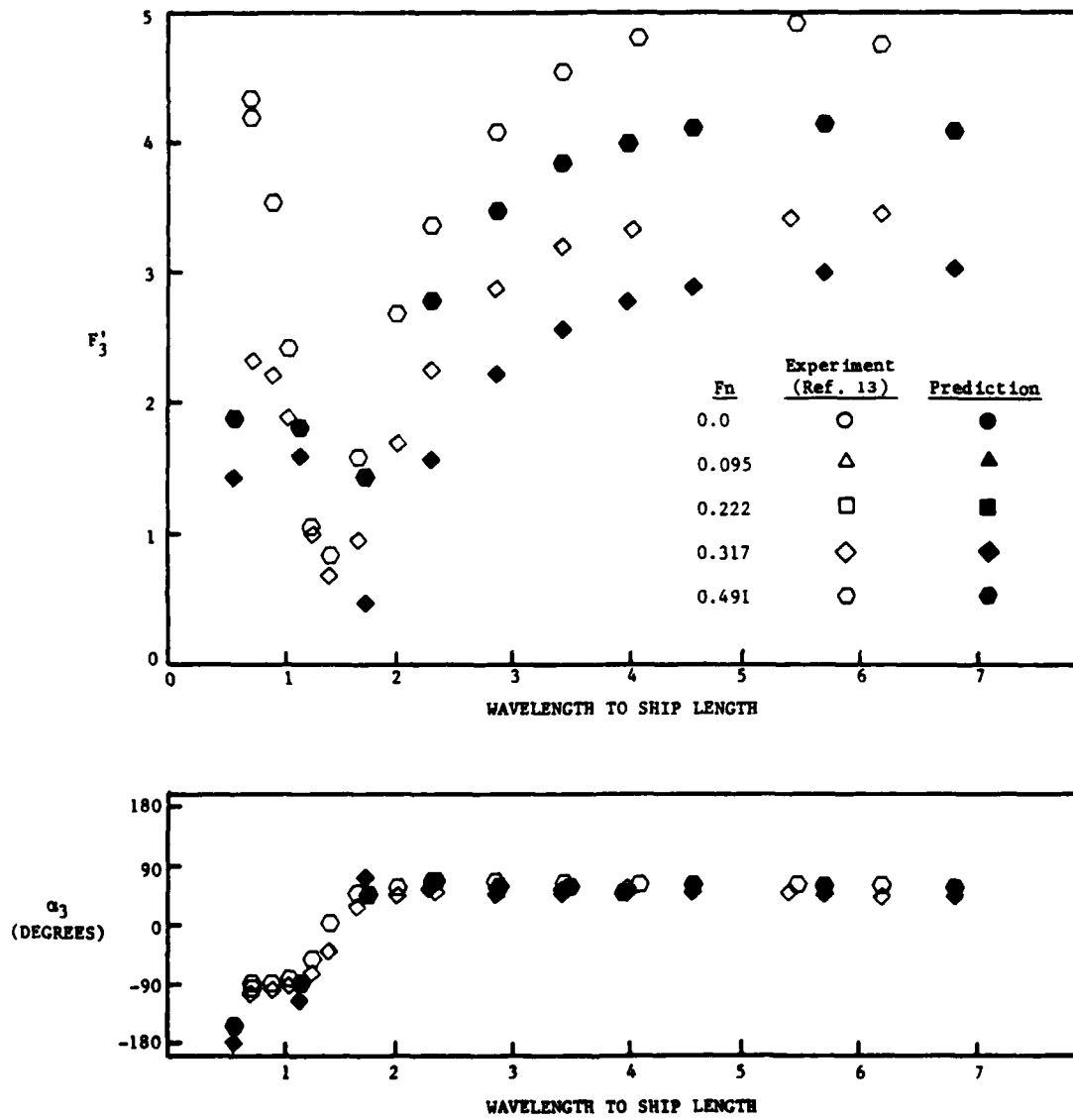


Figure 4e - Heave Force for $F_n = 0.317$ and 0.491

Figure 4 (Continued)

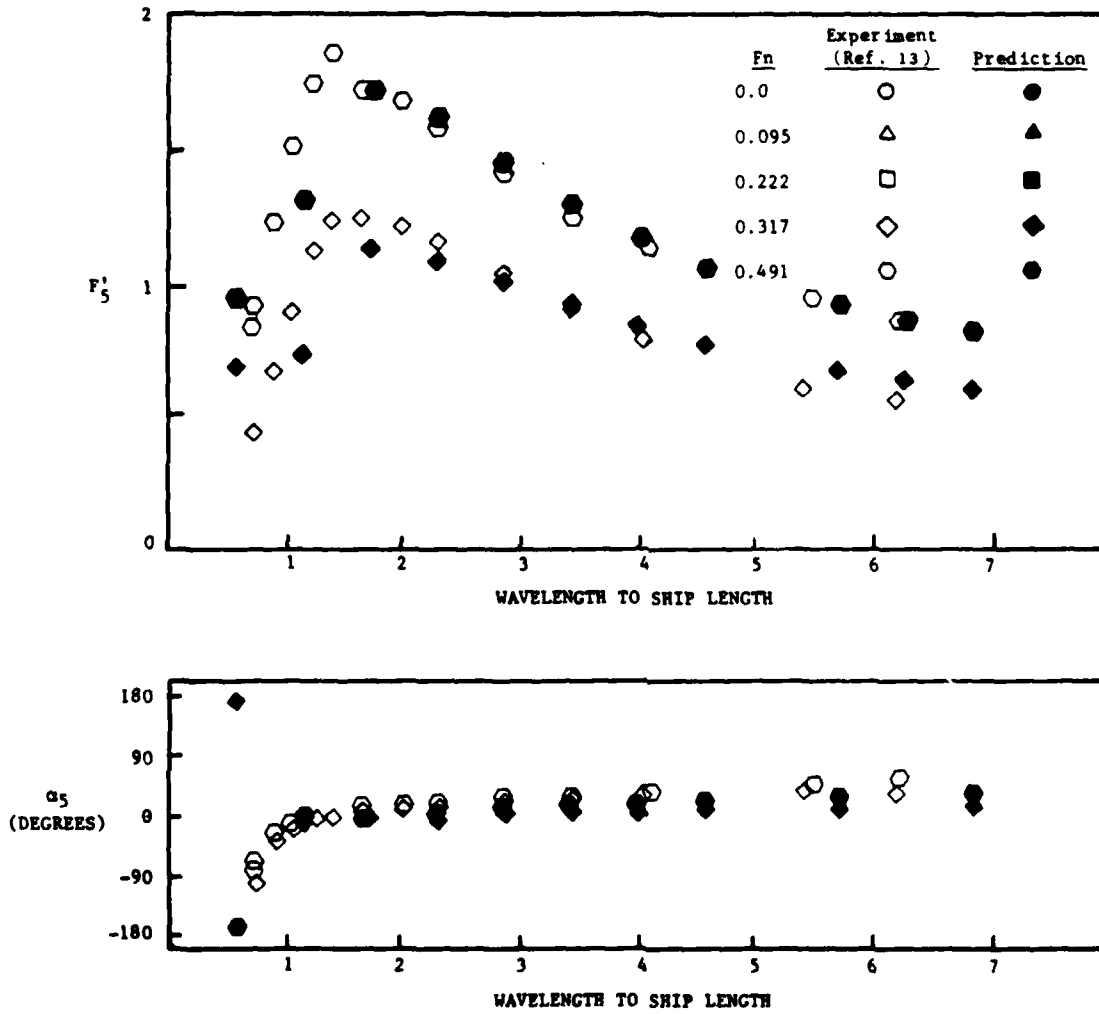


Figure 4f - Pitch Moment for $F_n = 0.317$ and 0.491

Figure 5 - Comparison between Experiment and Prediction of Regular Wave Transfer Functions for the SWATH 6A

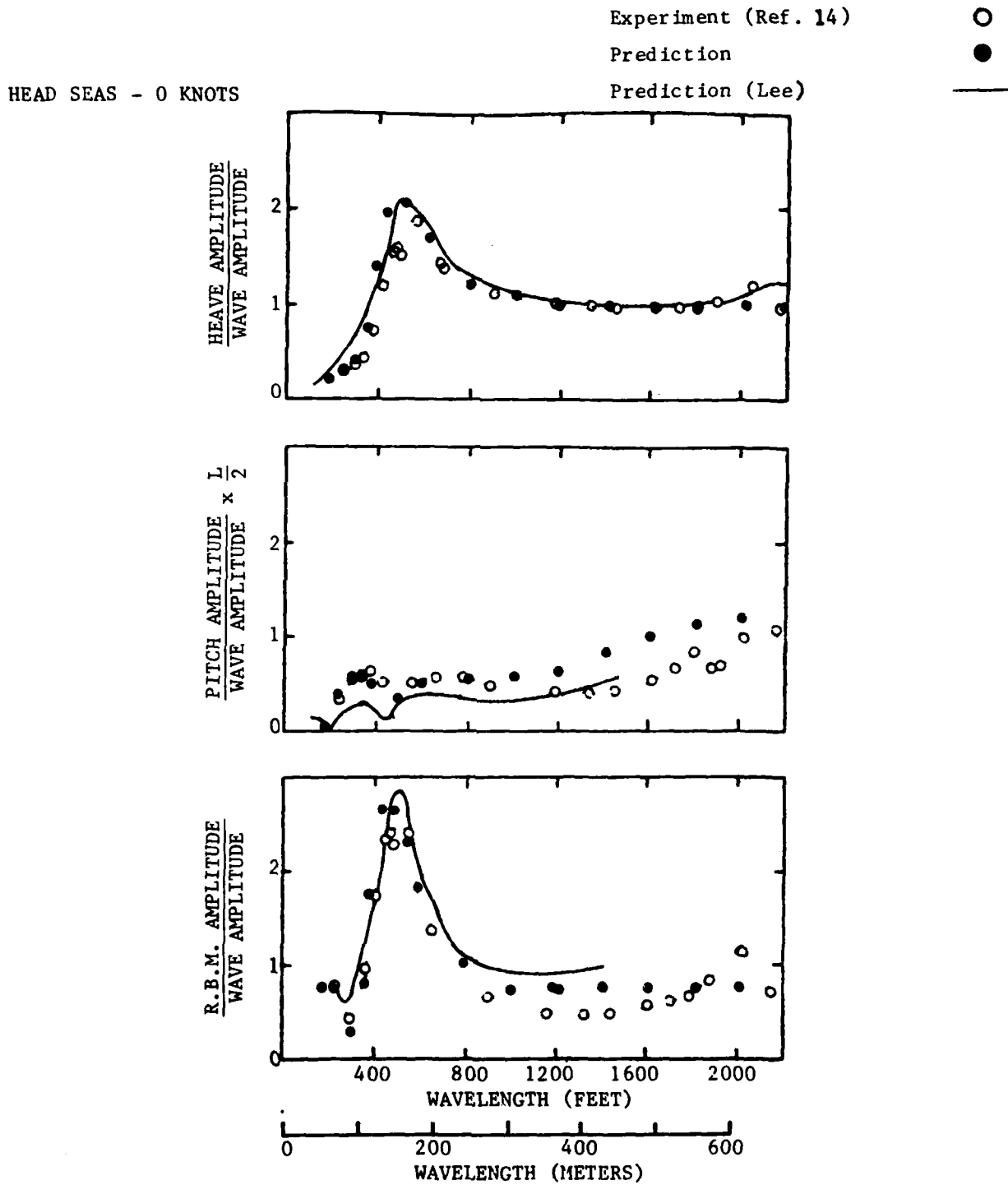


Figure 5a - Responses at 0 Speed in Head Waves

Figure 5 (Continued)

HEAD SEAS - 20 KNOTS

Experiment (Ref. 14)

Prediction

Prediction (Lee)

□

■

—

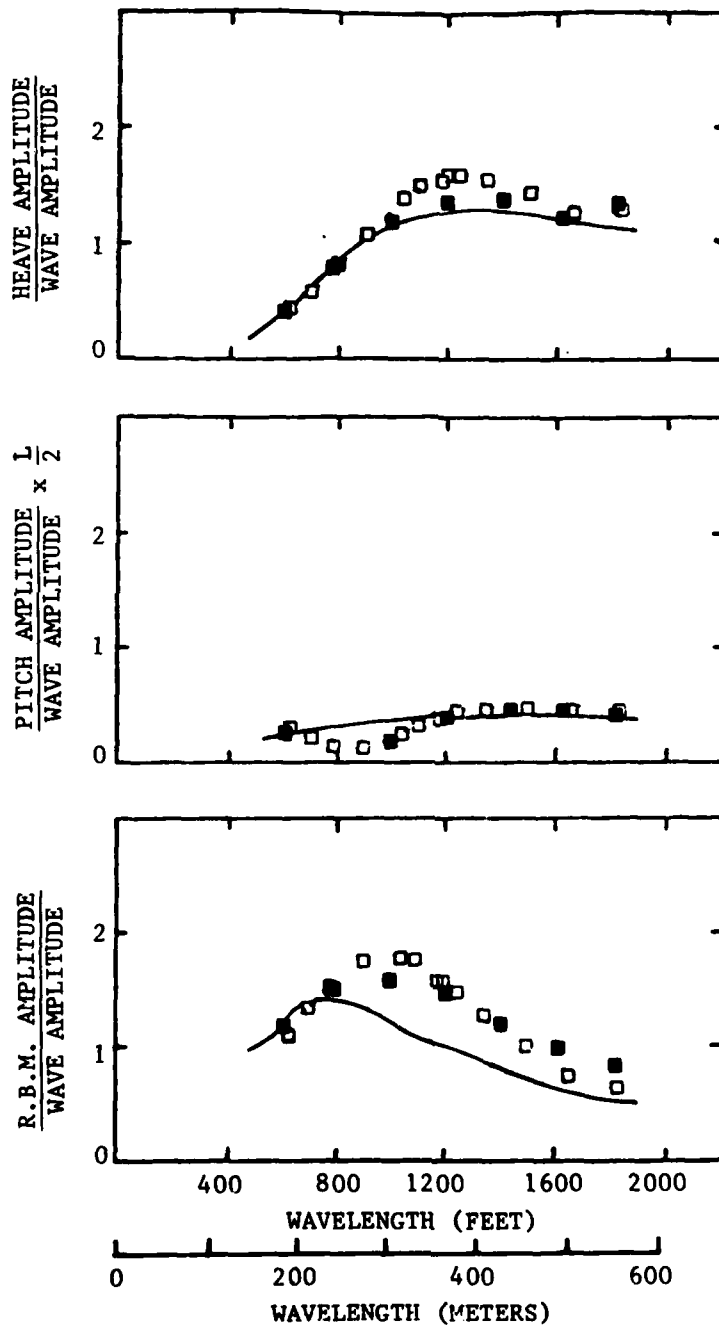


Figure 5b - Responses at 20 Knots in Head Waves

Figure 5 (Continued)

	0 Knots	20 Knots
Experiment (Ref. 14)	○	□
Prediction	●	■
Prediction (Lee)	—	—

BEAM SEAS - 0 KNOTS

BEAM SEAS - 20 KNOTS

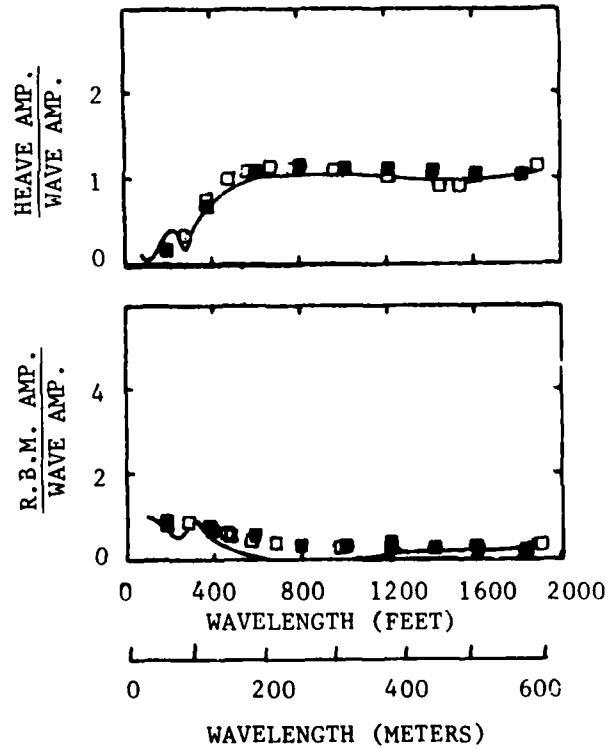
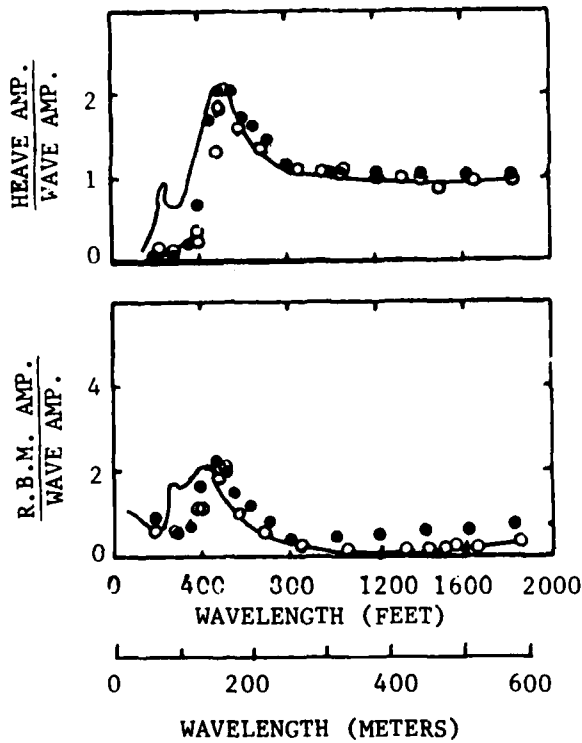


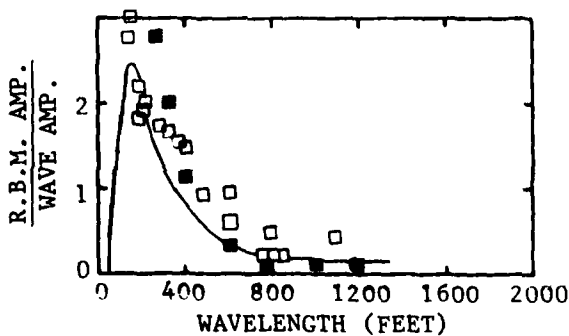
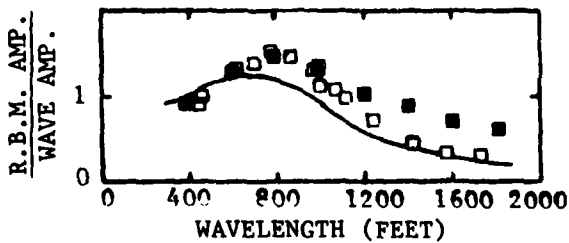
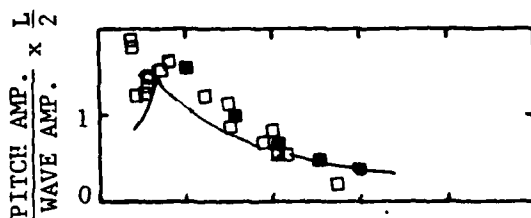
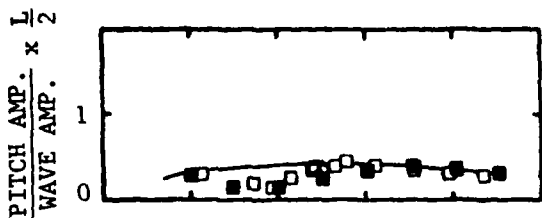
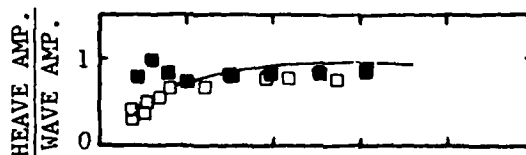
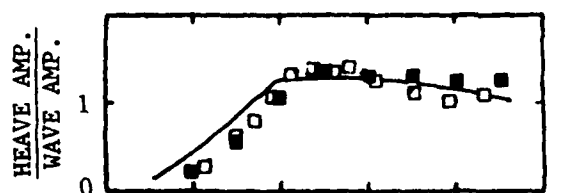
Figure 5c - Responses at 0 and 20 Knots in Beam Waves

Figure 5 (Continued)

Experiment (Ref. 14) □
 Prediction ■
 Prediction (Lee) —

BOW SEAS - 20 KNOTS

QUARTERING SEAS - 20 KNOTS



0 200 400 600
 WAVELENGTH (METERS)

0 200 400 600
 WAVELENGTH (METERS)

Figure 5d - Responses at 20 Knots in Bow and Quartering Waves

Figure 5 (Continued)

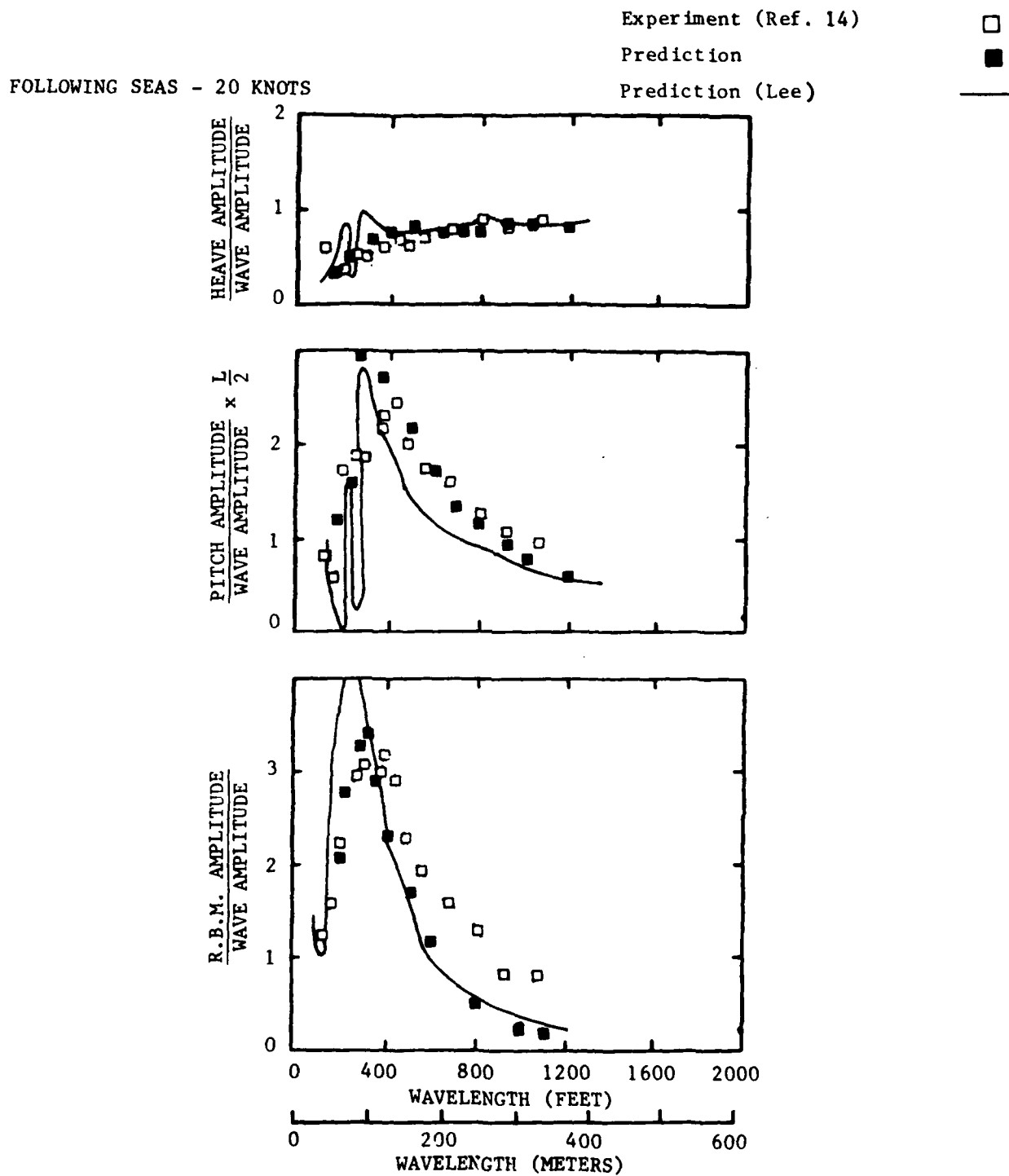


Figure 5e - Responses at 20 Knots in Following Waves

Figure 6 - Comparison between Experiment and Prediction of Regular Wave Transfer Functions for the SWATH 6B

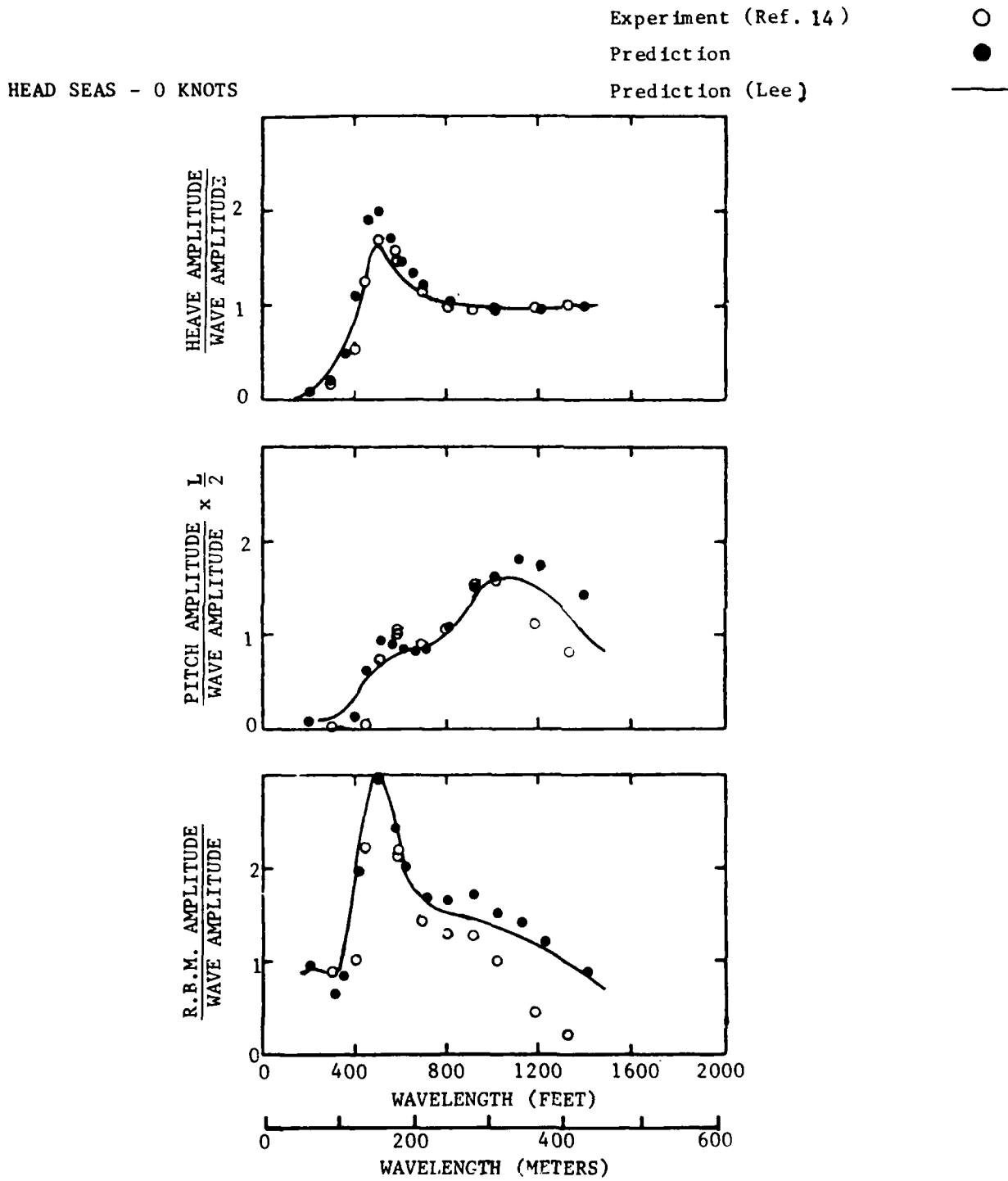


Figure 6a - Responses to Head Waves at 0 Speed

Figure 6 (Continued)

HEAD SEAS - 20 KNOTS

Experiment (Ref. 14)

□

Prediction

■

Prediction (Lee)

—

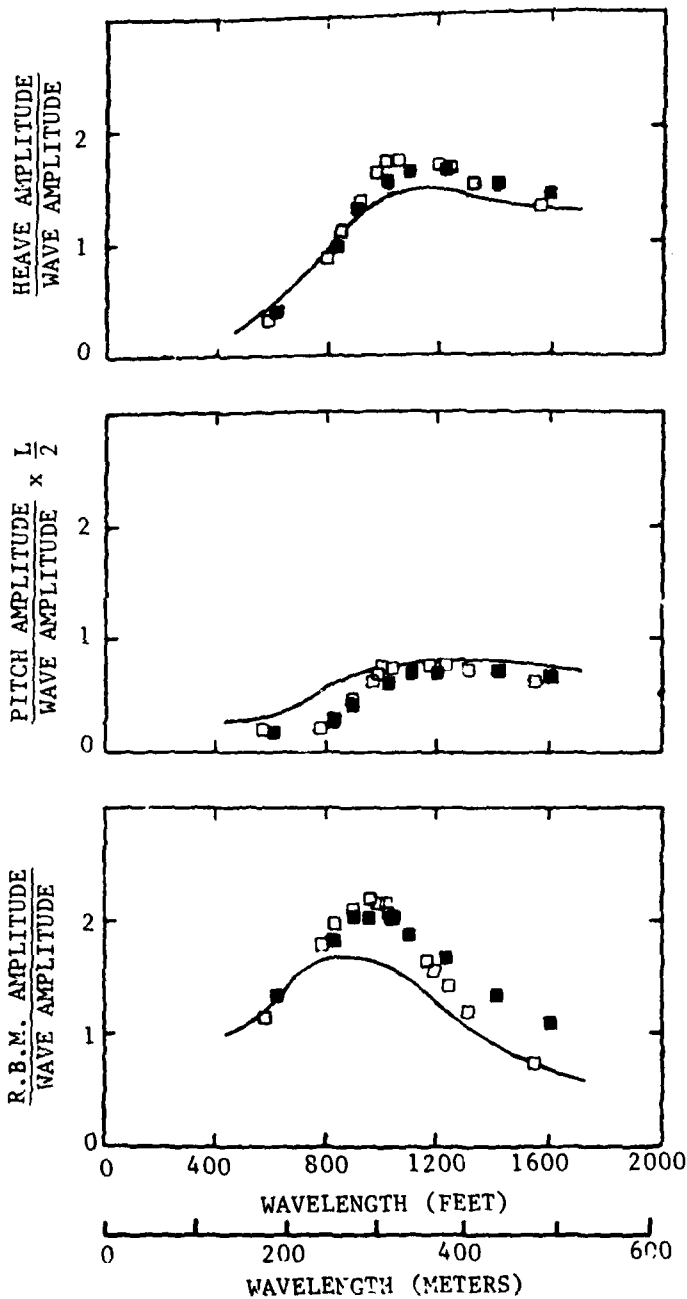


Figure 6b - Responses to Head Waves at 20 Knots

Figure 6 (Continued)

	<u>0 Knots</u>	<u>20 Knots</u>
Experiment (Ref. 14)	○	□
Prediction	●	■
Prediction (Lee)	—	—

BEAM SEAS - 0 KNOTS

BEAM SEAS - 20 KNOTS

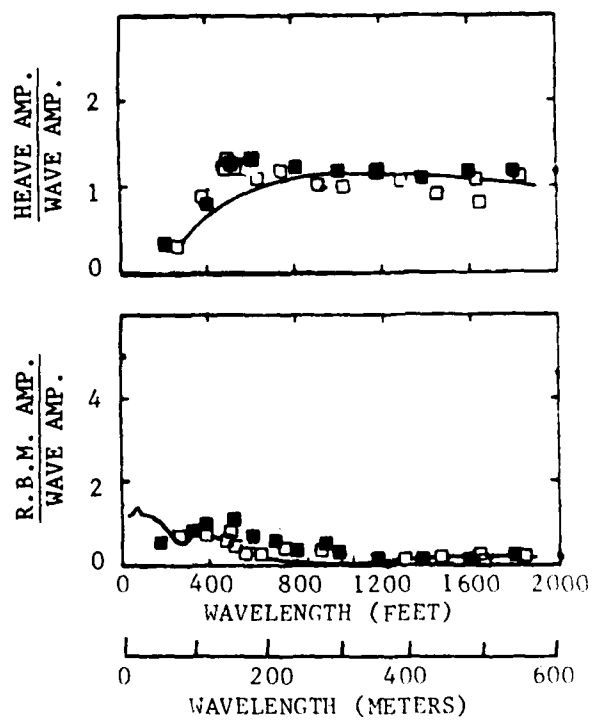
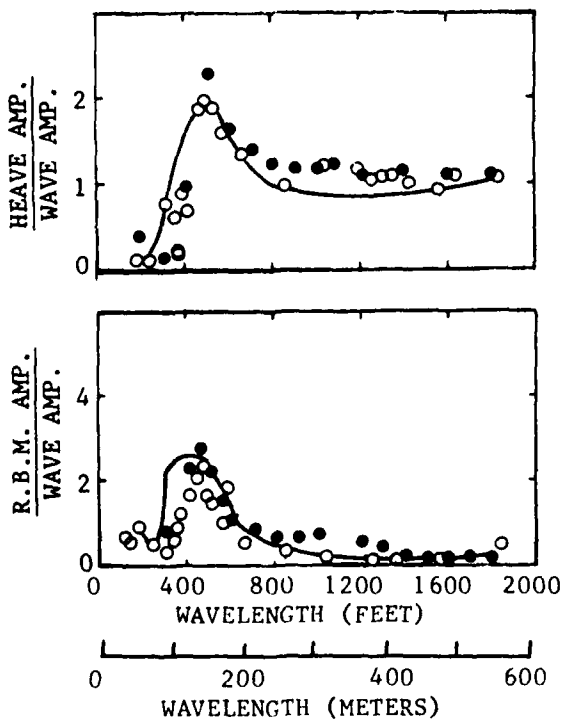


Figure 6c - Responses to Beam Waves at 0 and 20 Knots

Figure 6 (Continued)

Experiment (Ref. 14) □
 Prediction ■
 Prediction (Lee) —

BOW SEAS - 20 KNOTS

QUARTERING SEAS - 20 KNOTS

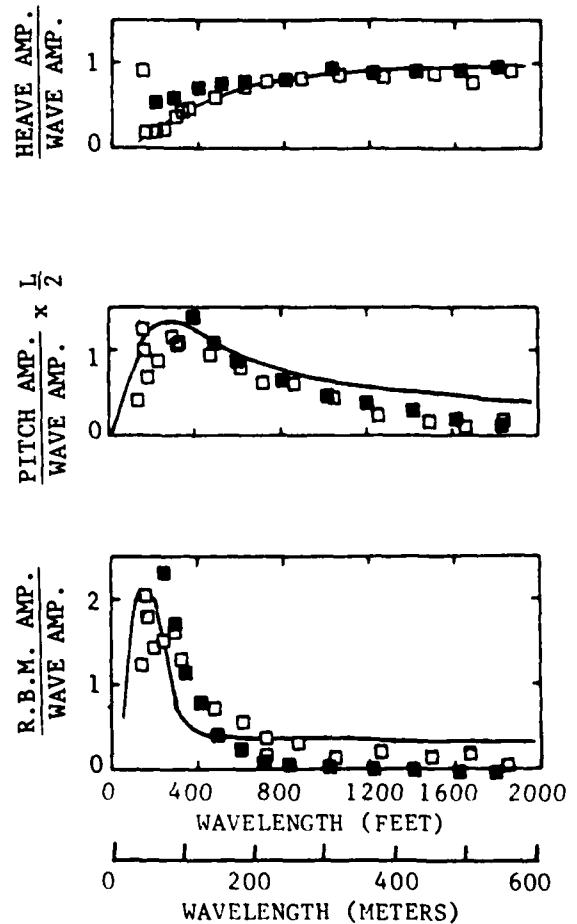
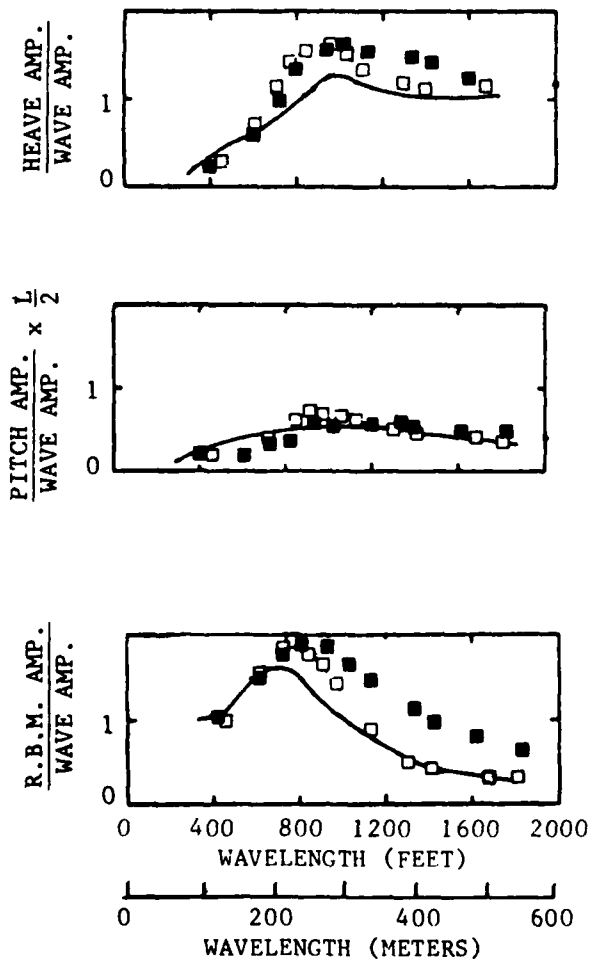


Figure 6d - Responses to Bow and Quartering Waves at 20 Knots

Figure 6 (Continued)

FOLLOWING SEAS - 20 KNOTS

Experiment (Ref. 14)

Prediction

Prediction (Lee)

□

■

—

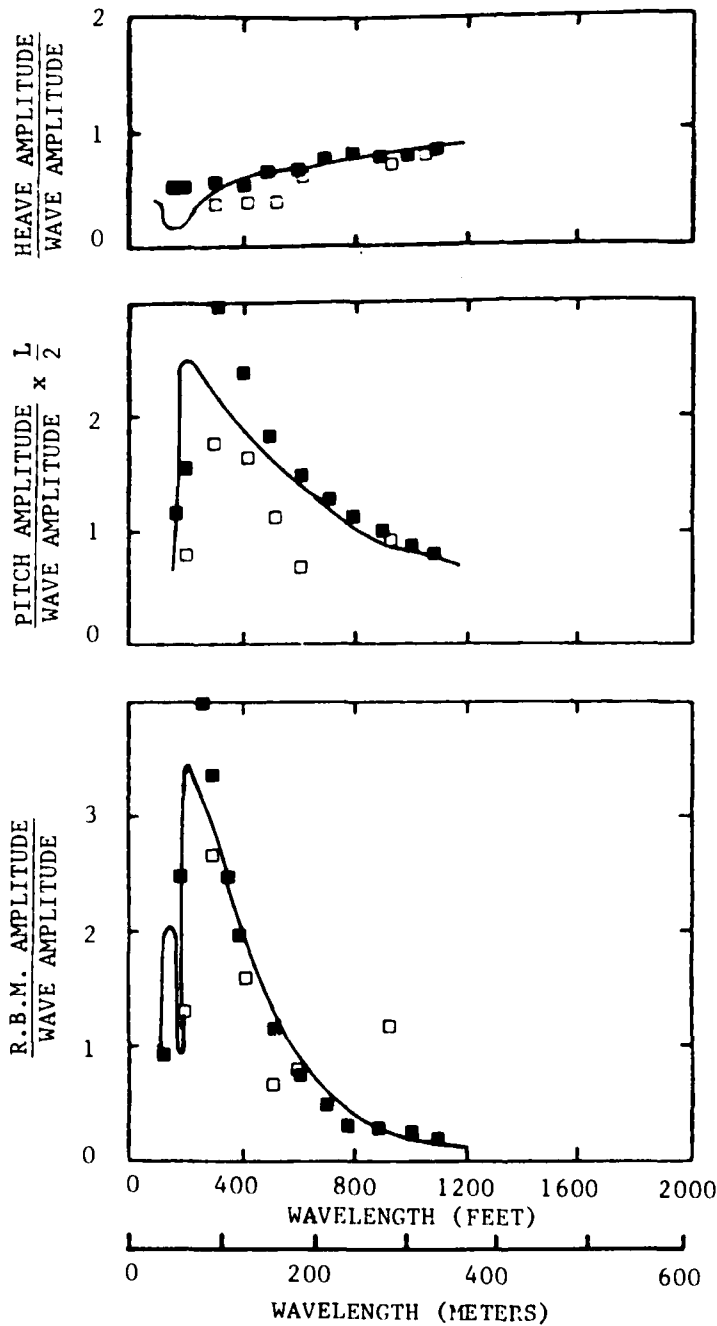


Figure 6e - Responses to Following Waves at 20 Knots

Figure 7 - Comparison between Experiment and Prediction of Regular Wave Transfer Functions for the SWATH 6C

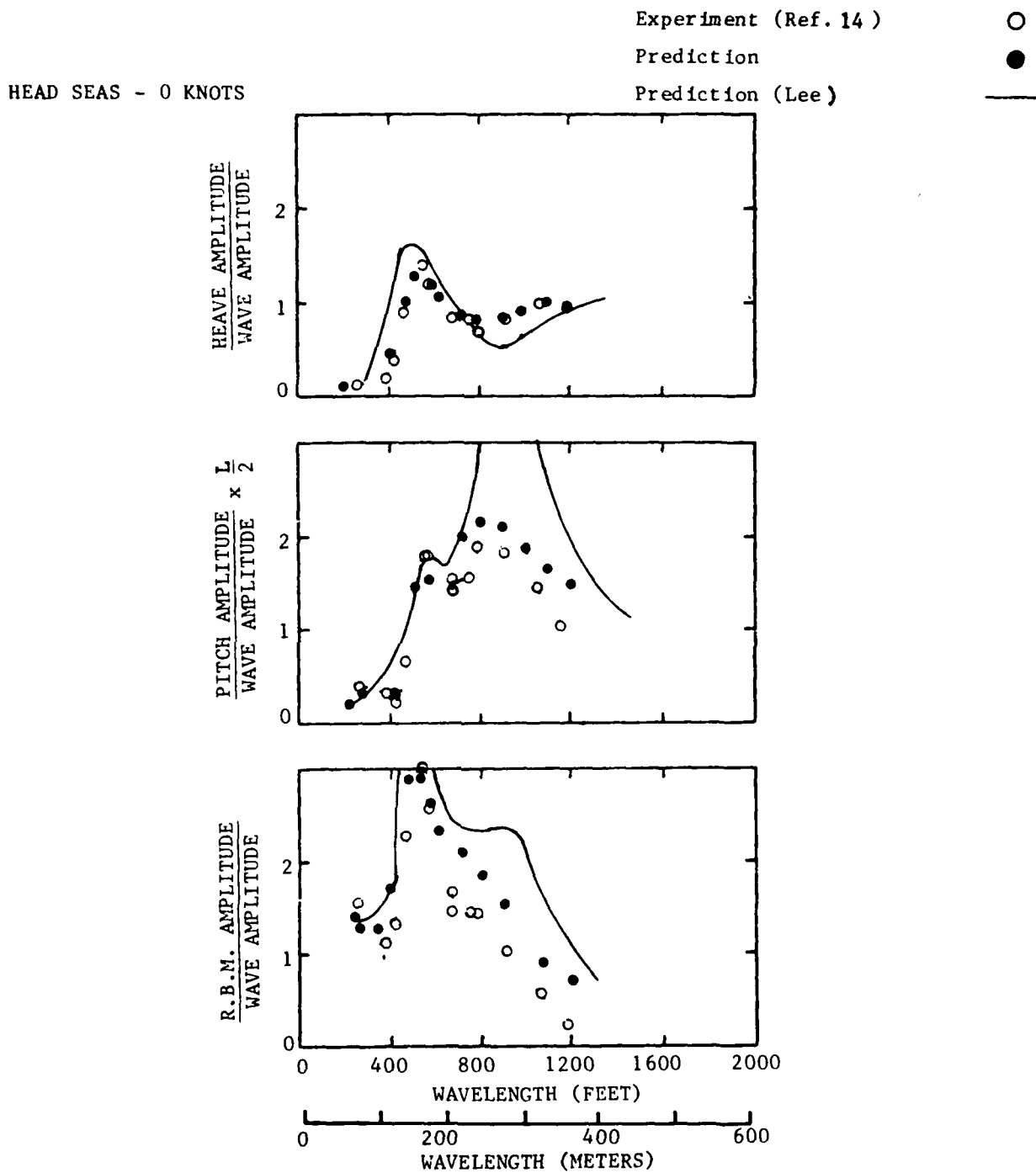


Figure 7a - Responses to Head Waves at 0 Speed

Figure 7 (Continued)

HEAD SEAS - 20 KNOTS

Experiment (Ref. 14)

Prediction

Prediction (Lee)

□

■

—

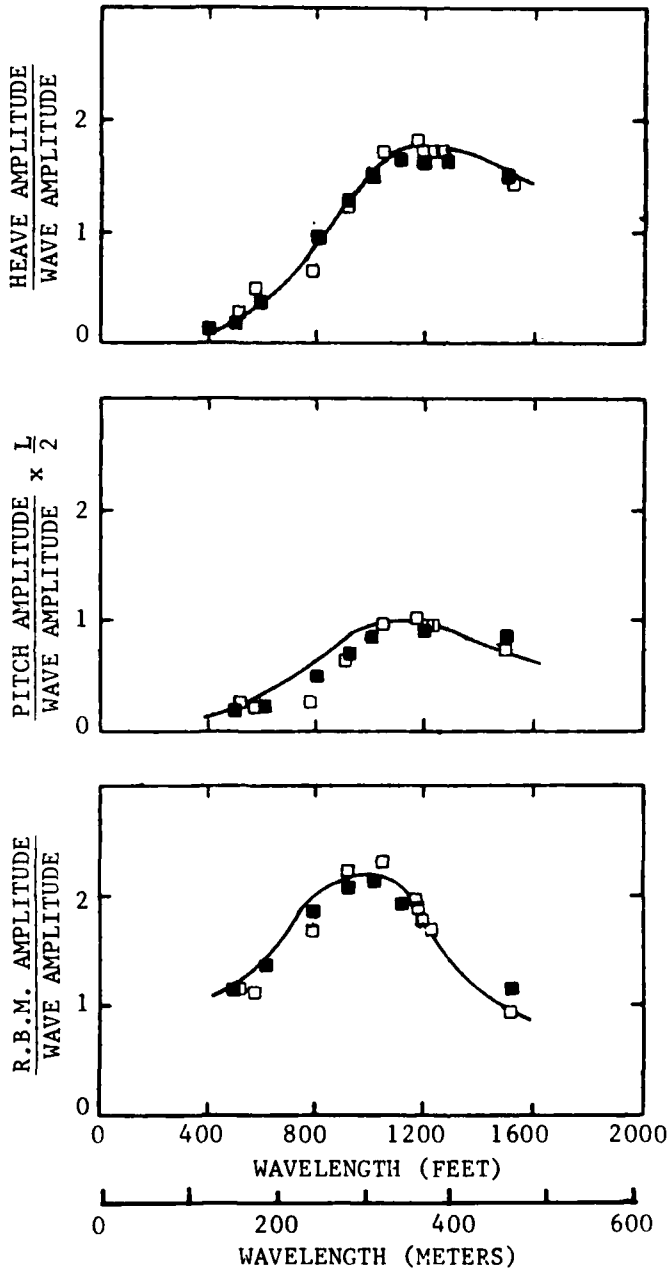


Figure 7b - Responses to Head Waves at 20 Knots

Figure 7 (Continued)

	<u>0 Knots</u>	<u>20 Knots</u>
Experiment (Ref. 14)	○	□
Prediction	●	■
Prediction (Lee)	—	—

BEAM SEAS - 0 KNOTS

BEAM SEAS - 20 KNOTS

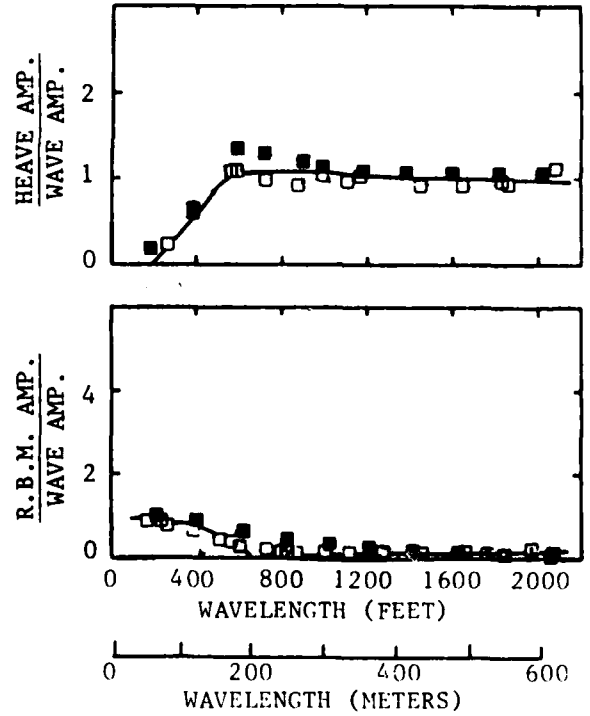
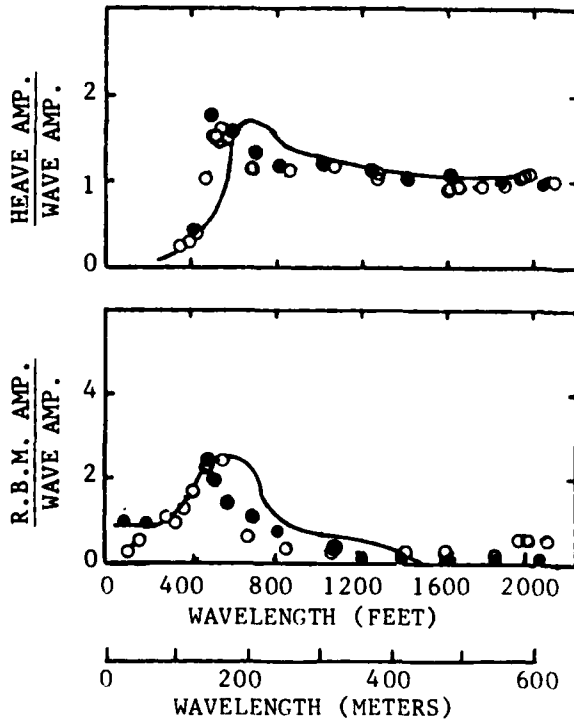


Figure 7c - Responses to Beam Waves at 20 Knots

Figure 7 (Continued)

Experiment (Ref. 14) □
 Prediction ■
 Prediction (Lee) —

BOW SEAS - 20 KNOTS

QUARTERING SEAS - 20 KNOTS

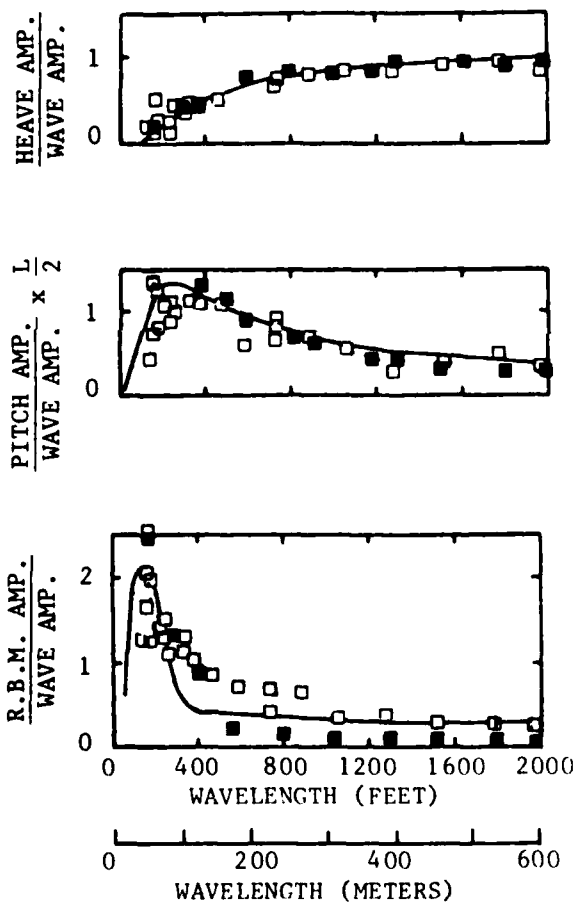
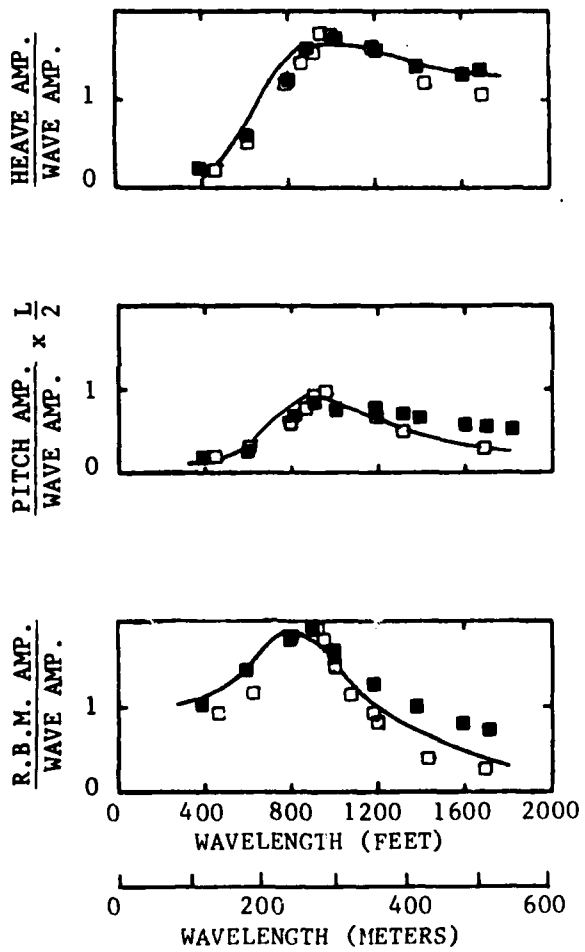


Figure 7d - Responses to Bow and Quartering Waves at 20 Knots

Figure 7 (Continued)

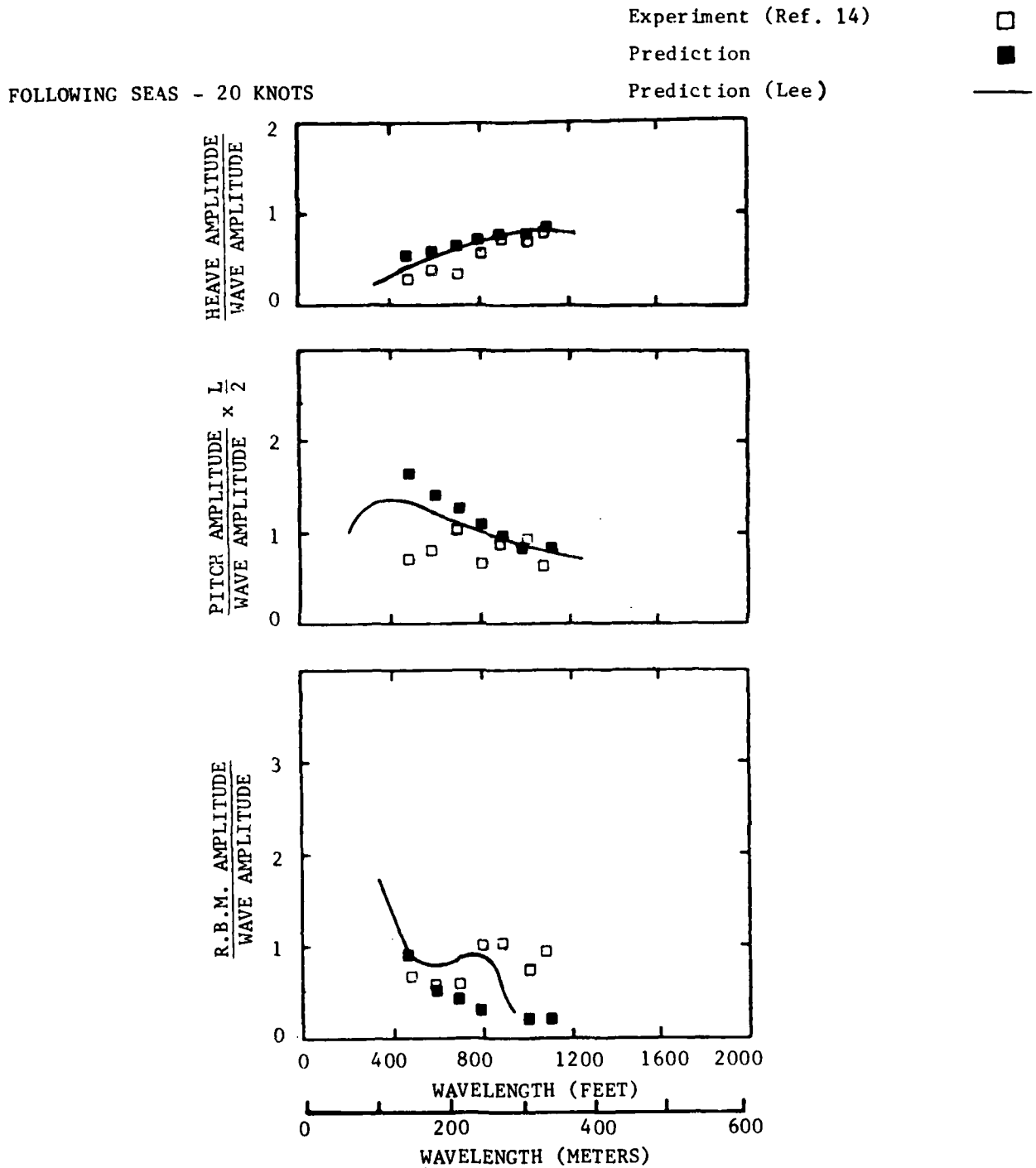


Figure 7e - Responses to Following Waves at 20 Knots

Figure 8 - Comparison between Experiment and Prediction of Regular Wave Transfer Functions for the SWATH 6D

Experiment (Ref. 15) ○

Prediction ●

Prediction (Lee) —

HEAD SEAS - 0 KNOTS

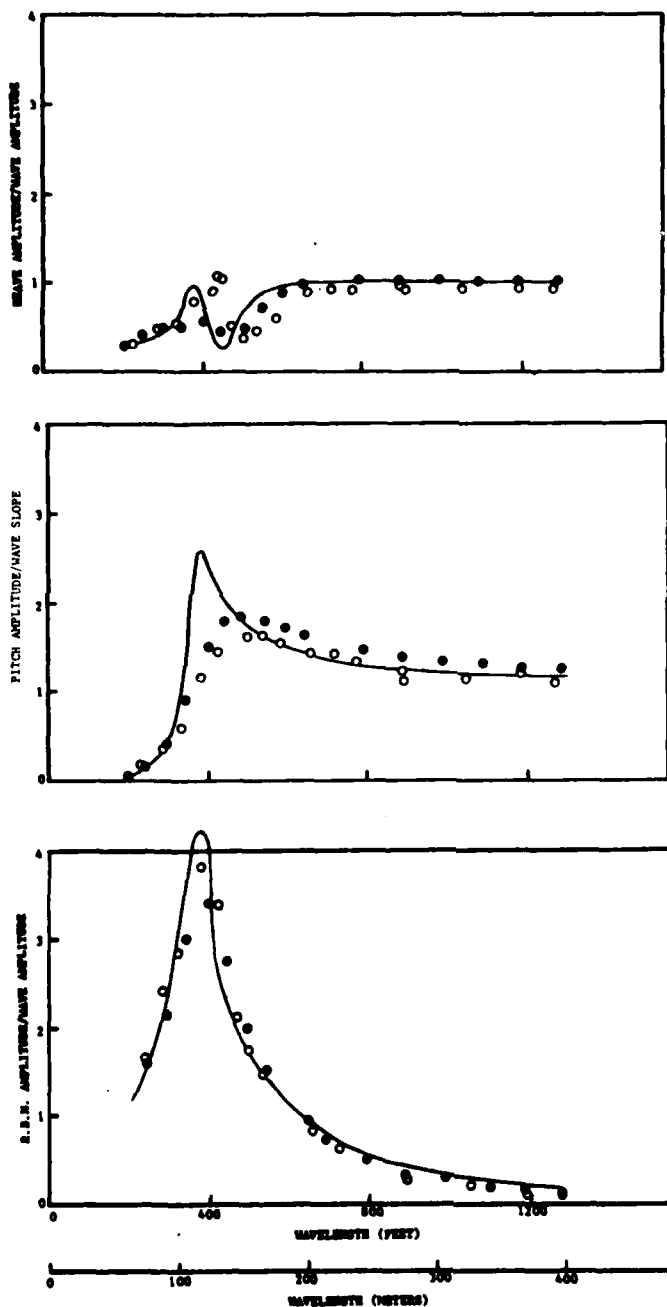


Figure 8a - Responses to Head Waves at 0 Speed

Figure 8 (Continued)

HEAD SEAS - 4 KNOTS

Experiment (Ref. 15) ○

Prediction ●

Prediction (Lee) —

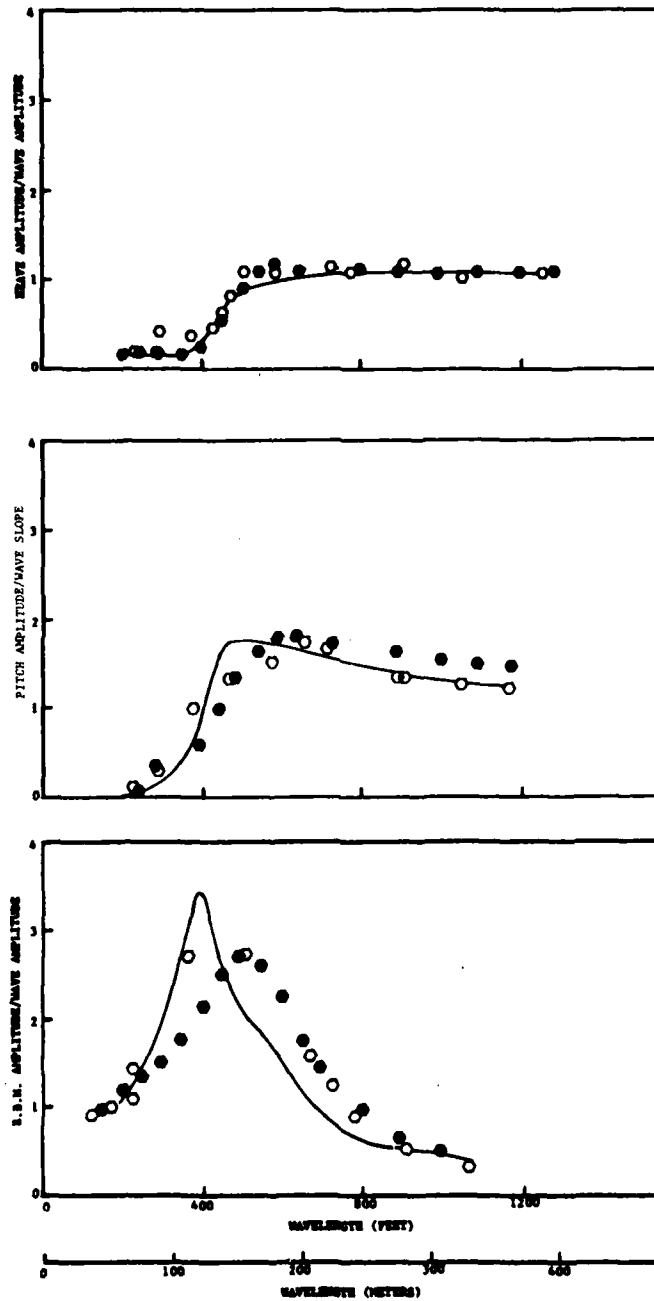


Figure 8b - Responses to Head Waves at 4 Knots

Figure 8 (Continued)

HEAD SEAS - 10 KNOTS

Experiment (Ref. 15) \diamond

Prediction \blacklozenge

Prediction (Lee) —

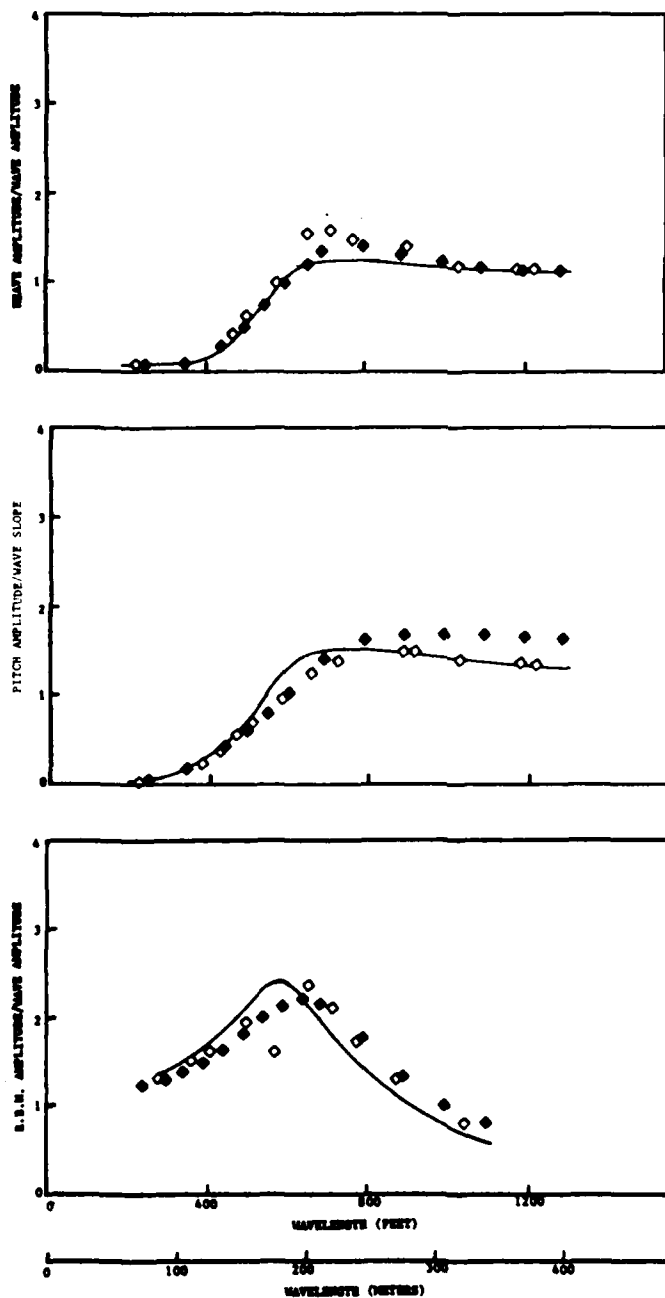


Figure 8c - Responses to Head Waves at 10 Knots

Figure 8 (Continued)

HEAD SEAS - 20 KNOTS

Experiment (Ref. 15)
 Prediction
 Prediction (Lee)

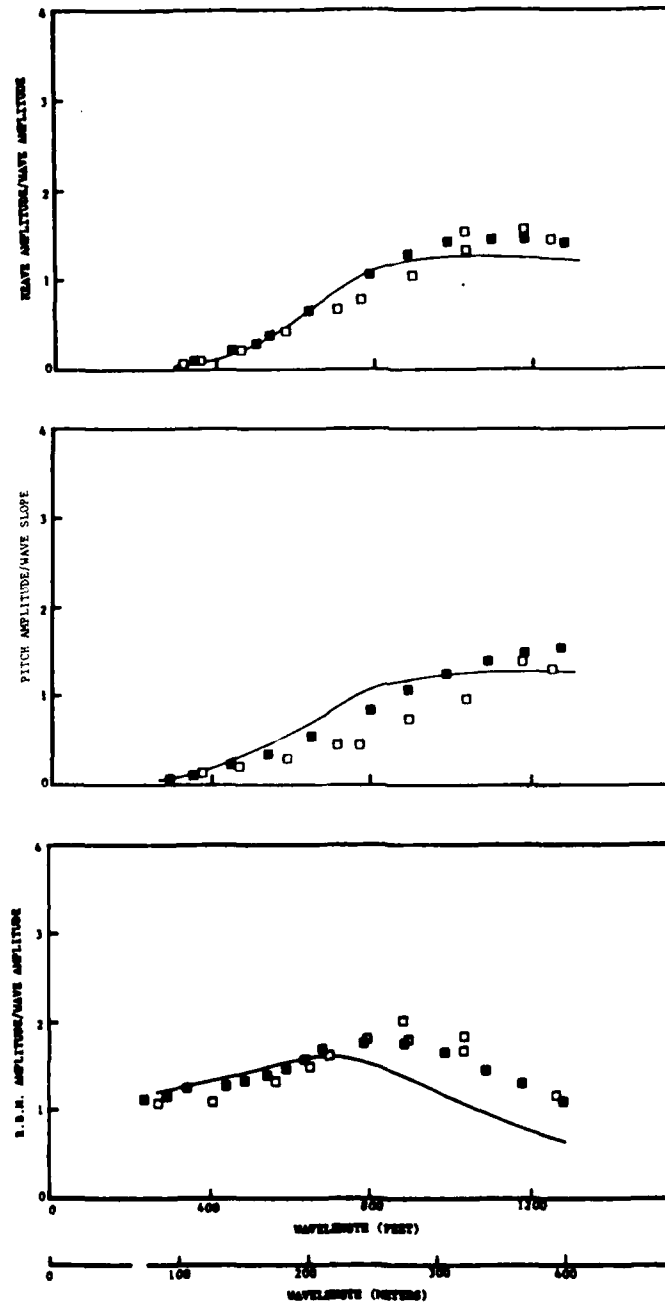


Figure 8d - Responses to Head Waves at 20 Knots

Figure 8 (Continued)

Experiment (Ref. 15) \triangle

Prediction \blacktriangle

Prediction (Lee) —

HEAD SEAS - 28 KNOTS

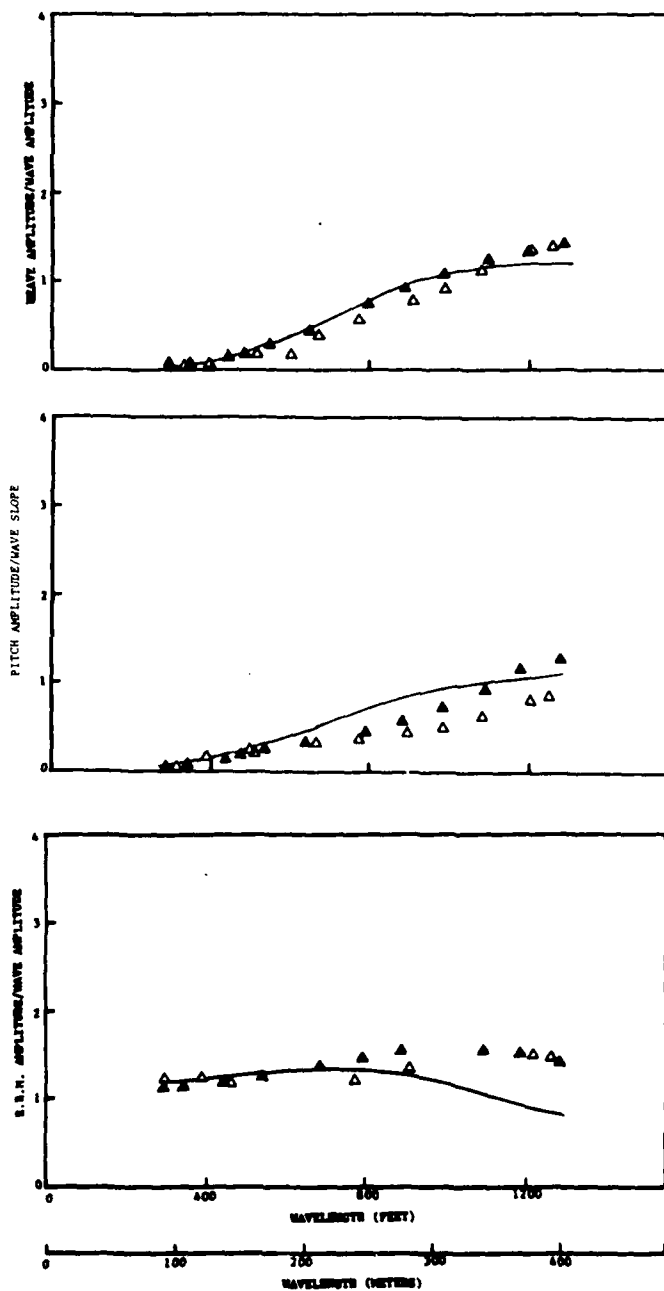


Figure 8e - Responses to Head Waves at 28 Knots

Figure 8 (Continued)

FOLLOWING SEAS - 4 KNOTS

Experiment (Ref. 15)
 Prediction
 Prediction (Lee)

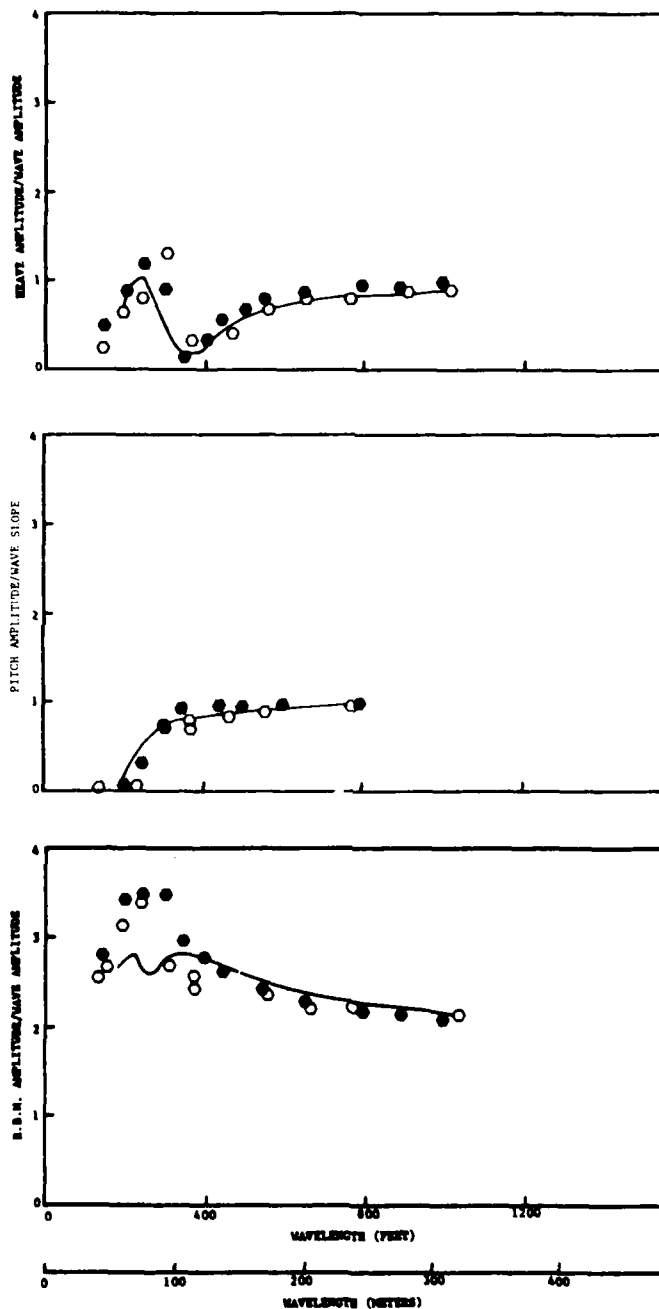


Figure 8f - Responses to Following Waves at 4 Knots

Figure 8 (Continued)

FOLLOWING SEAS - 10 KNOTS

Experiment (Ref. 15) \diamond
 Prediction \blacklozenge
 Prediction (Lee) —

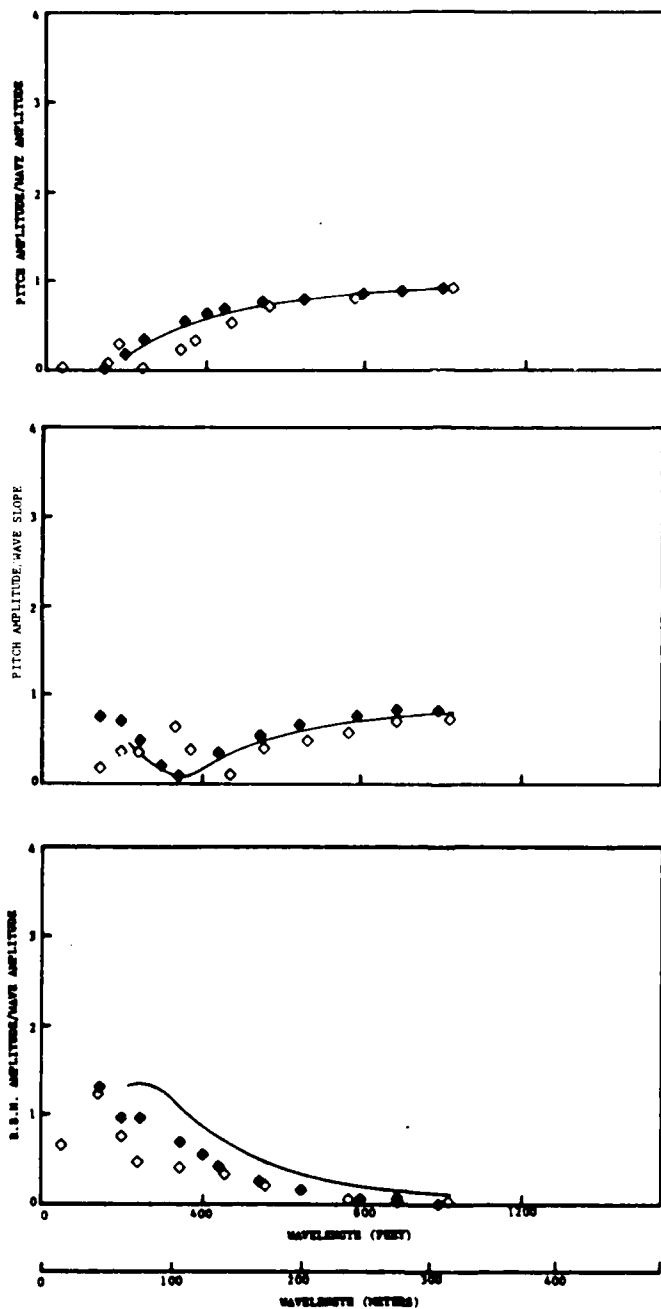


Figure 8g - Responses to Following Waves at 10 Knots

Figure 8 (Continued)

FOLLOWING SEAS - 20 KNOTS

Experiment (Ref. 15) □

Prediction ■

Prediction (Lee) —

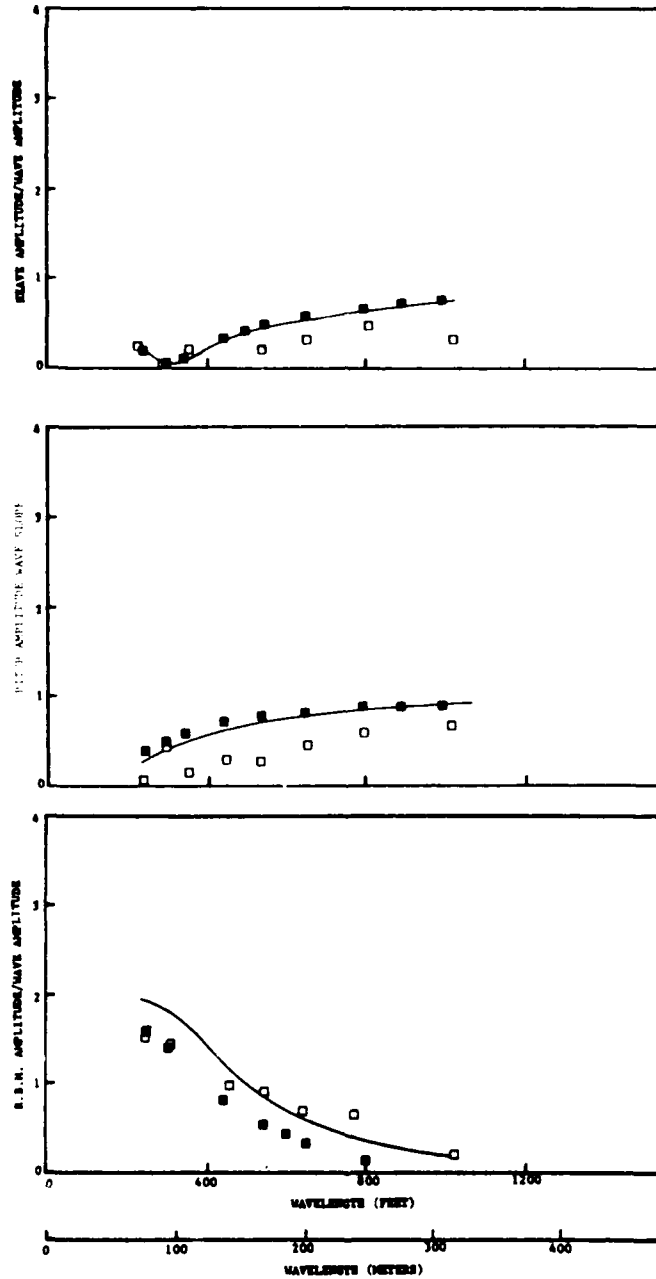


Figure 8h - Responses to Following Waves at 20 Knots

APPENDIX A

FREQUENCY DEPENDENT HYDRODYNAMIC COEFFICIENTS, FORCES AND MOMENTS

$$A_{33} = \int_{\ell} a_{33} dx + \sum_{n=1}^N (m_n + a_{33n})$$

$$A_{35} = - \int_{\ell} x a_{33} dx - \frac{U}{\omega^2} \int_{\ell} b_{33} dx - \sum_{n=1}^N \ell_n (m_n + a_{33n})$$

$$A_{53} = - \int_{\ell} x a_{33} dx + \frac{U}{\omega^2} \int_{\ell} b_{33} dx - \sum_{n=1}^N \ell_n (m_n + a_{33n})$$

$$A_{55} = \int_{\ell} x^2 a_{33} dx + \frac{U^2}{\omega^2} A_{33} + \sum_{n=1}^N \ell_n^2 (m_n + a_{33n})$$

$$B_{33} = \int_{\ell} b_{33} dx + \rho \frac{2}{3\pi} \int_{\ell} C_D \dot{z}_{10}^a dx - \rho U L^2 \left[2.439 ((k_2 - k_1) m')^{4/3} - m' \right]$$

$$+ \frac{\rho}{2} \sum_{n=1}^N A_n \left[\frac{4}{3\pi} C_{Dn} (\dot{z}_{so} + \dot{z}_{po}) + U C_{L\alpha_n} \right]$$

$$B_{35} = - \int_{\ell} x b_{33} dx + U A_{33} - \rho \frac{2}{3\pi} \int_{\ell} C_D \dot{z}_{10}^a x dx + 0.207 \rho U L^3 (k_2 - k_1) m'$$

$$- \frac{\rho}{2} \sum_{n=1}^N \ell_n A_n \left[\frac{4}{3\pi} C_{Dn} (\dot{z}_{so} + \dot{z}_{po}) + U C_{L\alpha_n} \right]$$

$$B_{53} = -\int_{\ell} x b_{33} dx - U A_{33} - \rho \frac{2}{3\pi} \int_{\ell} C_D \dot{z}_{10} x a dx + 0.207 \rho U L^3 (k_2 - k_1) m'$$

$$- \frac{\rho}{2} \sum_{n=1}^N \ell_n A_n \left[\frac{4}{3\pi} C_{D_n} (\dot{z}_{so} + \dot{z}_{po}) + U C_{L\alpha_n} \right]$$

$$B_{55} = \int_{\ell} x^2 b_{33} dx + \frac{U^2}{\omega^2} \int_{\ell} b_{33} dx + \rho \frac{2}{3\pi} \int_{\ell} C_D \dot{z}_{10} x^2 a dx$$

$$- \rho U L^4 \frac{[0.207 (k_2 - k_1) m']^2}{2.439 [(k_2 - k_1) m']^{4/3} - m'}$$

$$+ \frac{\rho}{2} \sum_{n=1}^N \ell_n^2 A_n \left[\frac{4}{3\pi} C_{D_n} (\dot{z}_{so} + \dot{z}_{po}) + U C_{L\alpha_n} \right]$$

$$C_{33} = \rho g A_w$$

$$C_{35} = -\rho g \int_{\ell} x B dx - \rho U^2 L^2 \left[2.439 ((k_2 - k_1) m')^{4/3} - m' \right] + \frac{\rho}{2} U^2 \sum_{i=1}^N A_n C_{L\alpha_n}$$

$$C_{53} = -\rho g \int_{\ell} x B dx$$

$$C_{55} = \rho g \int_{\ell} x^2 B dx - Mg \overline{BG} - \rho U^2 L^3 0.278 (k_2 - k_1) m' - \frac{\rho}{2} U^2 \sum_{n=1}^N \ell_n A_n C_{L\alpha_n}$$

$$F_1^{(e)} = 2\rho g A \int_{\ell} e^{ikx \cos\beta} \left(\frac{\pi}{4} e^{-kd_1} \left(a \frac{db}{dx} + b \frac{da}{dx} \right) + e^{-kt_s} t_s \frac{dB}{dx} \right) dx$$

$$F_3^{(e)} = A \int_{\ell} \left[\rho g e^{ikx \cos\beta} (B - kS) - \omega \omega_o e^{+ikx \cos\beta - kd_s} \left(a_{33} + \frac{1}{\omega} b_{33} \right) \right] dx$$

$$- i\rho \frac{2}{3\pi} \omega_o A \int_{\ell} a_{C_D} e^{k(-d_1 + ix \cos\beta)} (|\dot{z}_{1s}| e^{ikS_D \sin\beta}$$

$$+ |\dot{z}_{1p}| e^{-ikS_D \sin\beta}) dx - \frac{i\rho}{2} \omega_o A a_o U \int_{\ell} a_{S_D} e^{k(-d_1 + ix \cos\beta)} \cos(kS_D \sin\beta) dx$$

$$- i\rho \frac{2}{3\pi} \omega_o A \sum_{n=1}^N A_n C_{D_n} e^{k(-d_{1n} + i\ell_n \cos\beta)} (|\dot{z}_{so}| e^{ikS_D \sin\beta}$$

$$+ |\dot{z}_{po}| e^{-ikS_D \sin\beta}) - \frac{i\rho}{2} \omega_o A U \sum_{n=1}^N A_n C_{L\alpha_n} e^{k(-d_{1n} + i\ell_n \cos\beta)} \cos(kS_{D_n} \sin\beta)$$

$$F_5^{(e)} = -\rho Ag \int_{\ell} x e^{ikx \cos\beta} (B - kS) dx + \omega \omega_o A \int_{\ell} \left(x - \frac{U}{i\omega} \right) e^{ikx \cos\beta - kd_s} \left(a_{33} + \frac{1}{\omega} b_{33} \right) dx$$

$$+ i\rho \frac{2}{3\pi} \omega_o A \int_{\ell} x a C_D e^{k(-d_1 + ix \cos\beta)} (|\dot{z}_{1s}| e^{ikS_D \sin\beta} + |\dot{z}_{1p}| e^{-ikS_D \sin\beta}) dx$$

$$+ i\rho \frac{2}{3\pi} \omega_o A \sum_{n=1}^N \ell_n A_n C_{Dn} e^{k(-d_{1n} + i\ell_n \cos\beta)} (|\dot{z}_{so}| e^{ikS_{Dn} \sin\beta}$$

$$+ |\dot{z}_{po}| e^{-ikS_{Dn} \sin\beta}) + i \frac{\rho}{2} \omega_o A a_o U \int_{\ell} x a e^{k(-d_1 + ix \cos\beta)} \cos(kS_D \sin\beta) dx$$

$$+ i \frac{\rho}{2} \omega_o A U \sum_{n=1}^N \ell_n A_n C_{Ln} e^{k(-d_{1n} + i\ell_n \cos\beta)} \cos(kS_{Dn} \sin\beta) + d_{eF_1}^{(e)}$$

where integrations are along ship length with the origin at the LCG. Contributions from both hulls are included in the integrations.

$$AR = \frac{a + 2s}{c}$$

A_n = Projected area of n^{th} stabilizing fin

A_w = Waterplane area

$$a_o = \frac{-L^2 (2.439((k_2 - k_1)m')^{4/3} - m')}{\int_{\ell} a dx}$$

a_{33} = Heave added mass coefficient of two-dimensional section

$$a_{33n} = \text{Added mass of stabilizing fin} \approx \rho \frac{\pi}{4} s c^2$$

b_{33} = Heave damping coefficient of two-dimensional section

$$C_D = \left(1.0 - \frac{B}{a} \frac{b}{a}\right) C_{D_{SARPKAYA}} \quad (\text{see Figure 9 for } C_{D_{SARPKAYA}})$$

$$C_{D_n} = C_D \text{ for } n^{\text{th}} \text{ stabilizing fin modeled by flat plate with } d = 2s$$

(see Figure 10)

$$C_{L\alpha_n} = \frac{1.8 \pi AR}{1.8 + (AR^2 + 4.0)^{1/2}} C_{Lz_n} \quad (\text{with } C_{L\alpha_n} \text{ for aft fins is corrected according to data in Table 4})$$

$$C_{Lz_n} = \begin{cases} 1.0 - \frac{0.2556}{(a+2s)/a} \left[\left(\frac{a+2s}{a} \right)^2 - 0.1612 \right]^{1/2} \\ - 0.6366 \sin^{-1} \frac{0.4015}{(a+2s)/a} & \text{if for aft fin } \frac{a_{\max}}{a} \geq 2 \\ 1.0 & \text{otherwise} \end{cases}$$

$$d_e = - \left(1 - \frac{Bt_s}{S + Bt_s} \right) d_1$$

$$k_1 = \frac{\alpha_o}{2 - \alpha_o}$$

$$k_2 = \frac{\beta_o}{2 - \beta_o}$$

M = Mass of displaced volume of SWATH ship

$$m' = \frac{M}{\rho L^3}$$

m_n = Mass of stabilizing fin $\approx \rho \frac{\pi}{4}$ (sct)

N = Total number of fins

$$S = \frac{\pi}{4} ab$$

S_{D_n} = Transverse distance between fin's centroid and the ship's centerline

t_s = Draft of strut

$$\dot{z}_{10} = |\dot{z}_{1s}| + |\dot{z}_{1p}|$$

$$\dot{z}_{so} = \dot{\xi}_3 - l_n \dot{\xi}_5 - \dot{\zeta}_v(l_n, -S_{D_n}, -d_{1n})$$

$$\dot{z}_{po} = \dot{\xi}_3 - l_n \dot{\xi}_5 - \dot{\zeta}_v(l_n, S_{D_n}, -d_{1n})$$

$$\dot{z}_{1s} = \dot{\xi}_3 - x \dot{\xi}_5 - \dot{\zeta}_v(x, -S_D(x), -d_1(x))$$

$$\dot{z}_{1p} = \dot{\xi}_3 - x \dot{\xi}_5 - \dot{\zeta}_v(x, S_D(x), -d_1(x))$$

$$\alpha_o = 2 \frac{(1 - \epsilon^2)}{\epsilon^3} \left(\frac{1}{2} \ln \frac{(1 + \epsilon)}{(1 - \epsilon)} - \epsilon \right)$$

$$\beta_o = \frac{1}{\epsilon^2} - \frac{1 - \epsilon^2}{2\epsilon^3} \ln \frac{(1 + \epsilon)}{(1 - \epsilon)}$$

$$\epsilon = \left(1 - \left(\frac{a_{\max}}{L} \right)^2 \right)^{1/2}$$

$$\dot{\zeta}_v(x, y, z) = i\omega_o A e^{kz + ikx \cos\beta - iky \sin\beta}$$

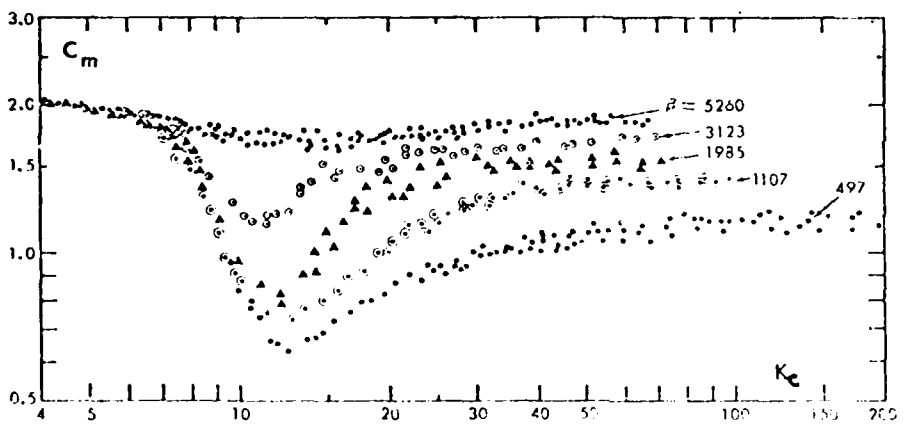
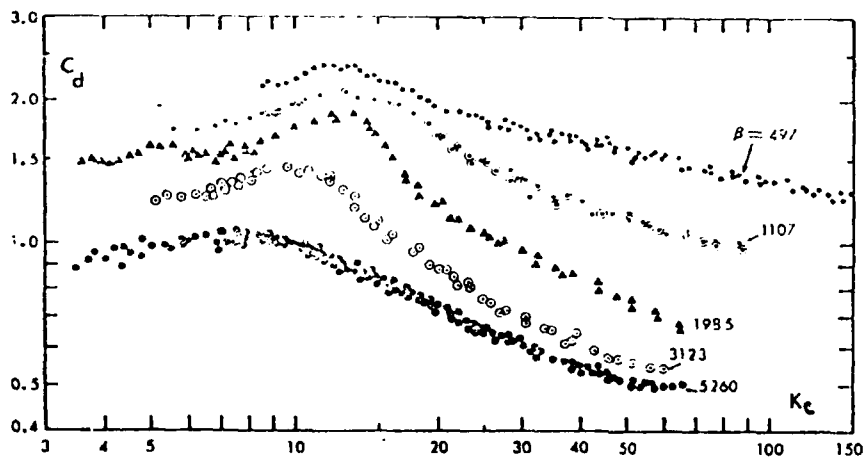


Figure 9 - Drag and Inertia Coefficients versus Keulegan-Carpenter Number for Constant Values of the Frequency Parameter (From Reference 5)

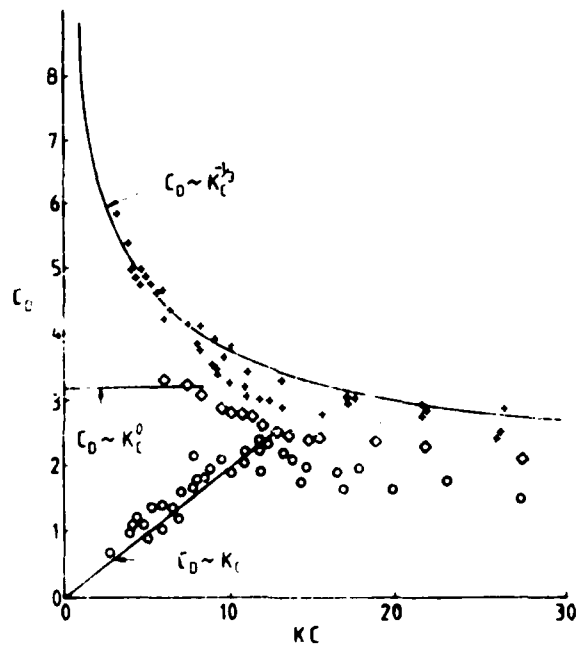


Figure 10 - The Drag Coefficient of Flat Plate (+),
 Diamond (◇) and Circular (○) Cylinders
 at Low KC (From Reference 6)

TABLE 4 - RATIO OF LIFT ON AFT FIN TO LIFT ON FORWARD FIN FOR
 VARIOUS FIN SEPARATIONS AND OSCILLATION FREQUENCY
 TO SPEED RATIOS (FROM REFERENCES 8 AND 9)

$\frac{x}{s} \backslash \frac{\omega s}{U}$	0.00	0.04	0.08	0.12	0.16	0.20
10	0.412	0.544	0.643	0.824	1.076	1.221
15	0.462	0.638	0.846	1.046	1.180	1.109
20	0.529	0.732	1.000	1.151	1.110	0.971
25	0.614	0.816	1.099	1.132	1.011	0.897
20	0.706	0.853	1.118	1.006	0.912	0.853

where x = distance between leading edges of fins
 s = span
 U = forward speed
 ω = oscillation frequency

APPENDIX B
POTENTIAL FLOW COMPONENTS

In Reference 2, Lee discusses the potential flow added mass and damping coefficients for oscillating twin cylinders. The source distribution method is applied. This technique requires a substantial amount of computer time and consequently limits the number of configurations which can be evaluated. John Dalzell* initiated an effort to approximate the potential flow added mass and damping coefficients. The goal of his work was to develop expressions which would approximate the potential flow coefficients resulting from the Frank Close Fit Technique⁴ which is utilized in References 1 and 2. Lee¹⁹ also developed expressions for heave added mass and damping and extended the approximate approach to the transverse plane. Dalzell* then modified his work further and extended it to include the transverse plane and elliptical as well as circular lower hull sections. Dalzell's expressions for approximating the heave added mass and damping coefficients for two-dimensional sections have been used in results in this report. His work correlates well with results from the Frank Close Fit for a variety of strut-lower hull configurations. Consequently, the expressions developed in this report for the viscous components can be expected to result in similar values when used in conjunction with potential flow results obtained using Frank Close Fit Technique or the Dalzell Approximation Technique. One consequence of using the Dalzell Approximation Technique is that the distribution of the potential on the two-dimensional section is unavailable, necessitating approximations in the exciting forces and moment.

The potential flow exciting force and moment include the incident wave potential and a diffraction potential. Salvesen, Tuck and Faltinsen¹ show that the exciting force and moment $F_3^{(e)}$ and $F_5^{(e)}$ are

$$F_3^{(e)} = \rho A \int (f_3(x) + h_3(x)) dx$$

$$F_5^{(e)} = \rho A \int \left[x(f_3(x) + h_3(x)) + \frac{U}{i\omega} h_3(x) \right] dx$$

* As described by Dalzell in Stevens Institute of Technology reports with limited distribution.

where the sectional incident wave contribution, which is often referred to as the Froude-Krylov force, is defined by

$$f_3(x) = g e^{ikx \cos\beta} \int_{C_x} n_3 e^{-iky \sin\beta} e^{kz} dl$$

and the sectional diffraction contribution is defined by

$$h_3(x) = -\omega_0 e^{ikx \cos\beta} \int_{C_x} (in_3 + n_2 \sin\beta) e^{-iky \sin\beta} e^{kz} \psi_3 dl$$

where ρ is the mass density of water, A is the wave amplitude, ω_0 is the wave frequency, ω is the wave encounter frequency, k is the wave number, β is the heading of the ship relative to the incident wave, U is the forward speed of the ship, n_2 and n_3 are unit normals, ψ_3 is the velocity potential, and dl is an element of an arc along the cross-section C_x . (End-effect terms have been excluded here since they are unnecessary for SWATH configurations.)

Korvin-Kroukovsky²⁰ made the assumption that an average depth can be utilized so that the term e^{kz} can be moved outside the integral. Salvesen, Tuck and Faltinsen investigated this approach. The complex potential can be expanded in a Taylor series. If $\exp(-iky \sin\beta)$ is expanded through order k and symmetry about the $y=0$ axis is assumed then

$$\begin{aligned} f_3(x) &= g e^{ikx \cos\beta} e^{-kd_3} \int_{C_x} n_3 dl \\ &= g e^{ikx \cos\beta} e^{-kd_3} B \end{aligned}$$

where B is the local waterline beam and d_3 is an appropriate average depth.

Similarly, $h_3(x)$ becomes

$$h_3(x) \approx -\frac{1}{\rho} \omega \omega_0 e^{ikx \cos\beta} e^{-kd_s} (a_{33}(\omega) + \frac{i}{\omega} b_{33}(\omega)) \quad (B.1)$$

where d_s is an average depth and a_{33} and b_{33} are the sectional added mass and damping coefficients.

Newman²¹ follows a different approach. In his evaluation of the Froude-Krylov force, Newman expands the exponential under the integrand giving

$$\begin{aligned}
 f_3(x) &= g e^{ikx \cos \beta} \int_{C_x} n_3 (1 - iky \sin \beta + kz) dl \\
 &= g e^{ikx \cos \beta} [B(x) - kS(x)] \quad (B.2)
 \end{aligned}$$

$S(x)$ is the local sectional area. For SWATH sections with wall-sided struts, the argument can be made that since n_3 is zero along the strut, the closed curve can be approximated by the ellipse. This approximation which provides good correlation with Frank Close Fit results has been utilized here. It leads to $S(x)$ including only the area of the ellipse for SWATH sections. This form of $f_3(x)$ has an advantage over the previous form since expansion of the exponential eliminates the need for an equivalent depth.

Application of Equations (B.1) and (B.2) for $h_3(x)$ and $f_3(x)$ makes it possible to evaluate the exciting heave force and pitch moment if the sectional added mass and damping are known and an appropriate average depth is used. Solution for d_s using numerical results from the Frank Close Fit Technique and from Equation (B.2) for SWATH sections indicates that d_s can be approximated by

$$d_s(x) = \left(1 + \frac{Bt_s}{\frac{\pi}{4} ab + Bt_s} \right) d_1$$

where B is the beam, t_s is the draft of the strut, and d_1 is the distance between the mean waterline and the center of the ellipse.

When the potentials on the surface of the body are unknown, approximations to the surge exciting force and the center of surge force are necessary. The surge exciting force, $F_1^{(e)}$, is given by

$$F_1^{(e)} = \rho g A \int_{\ell} e^{ikx \cos \beta - iky \sin \beta} \int_{C(x)} e^{-kz} n_1 dx$$

and can be approximated by

$$F_1^{(e)} = 2\rho g A \int_{\ell} e^{ikx \cos\beta} \left(\frac{\pi}{4} e^{-kd_1} \left(a \frac{db}{dx} + b \frac{da}{dx} \right) + e^{-kt_s} \frac{dB}{dx} \right) dx$$

Evaluation of the expressions in Reference 3 for various SWATH sections using the Frank Close Fit Technique led to an approximation for d_e , the center of surge force

$$d_e = - \left(1 - \frac{Bt_s}{\frac{\pi ab}{4} + Bt_s} \right) d_1$$

That is, the exciting moment due to surge can be expressed by $d_e F_1^{(e)}$.

AD-A130 516

VERTICAL PLANE MOTIONS OF SWATH (SMALL WATERPLANE AREA
TWIN HULL) SHIPS I. (U) DAVID W TAYLOR NAVAL SHIP
RESEARCH AND DEVELOPMENT CENTER BET..

3/2

UNCLASSIFIED

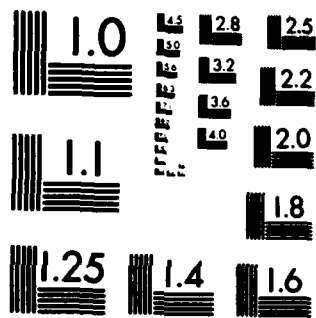
K K MCCREIGHT ET AL. JUN 83

F/G 20/4

NL



			END
			DATE
			FILMED
			8 83
			DTIC



MICROCOPY RESOLUTION TEST CHART
NATIONAL BUREAU OF STANDARDS-1963-A

APPENDIX C
VISCOUS COMPONENTS

Lee² utilized an equation described in Reference 22 to model the viscous damping of SWATH ships. The vertical force F_v on a slender moderately inclined body is expressed as

$$F_v = \frac{1}{2} \rho U^2 A_p \sin\alpha |\sin\alpha| (a_o |\cot\alpha| + C_D)$$

where ρ is the density of water, U is the ship speed, A_p is the projected area of the body, α is the trim angle, a_o is the viscous lift coefficient and C_D is the cross flow drag coefficient. For air ships with circular cross sections, experimental work indicates that a_o is about 0.07 and C_D is between 0.4 and 0.7.²² (Lee² suggests using 0.07 and 0.5, respectively.)

Substituting $w/U = \sin\alpha$ and assuming small α this becomes

$$F_v = \frac{1}{2} \rho A_p (a_o U^2 \alpha + C_D w|w|) \quad (C.1)$$

Following Lee, w is the relative fluid velocity and can be defined as

$$w = \dot{\xi}_3 - x\dot{\xi}_5 + y\dot{\xi}_4 - \dot{\zeta}_v(x, \pm S_D(x), -d_1(x), t)$$

where $d_1(x)$ is the depth of submergence of the maximum breadth of a section. The relative velocity of the fluid induced by the incoming wave, $\dot{\zeta}_v$, is given by

$$\dot{\zeta}_v(x, y, z, t) = -i\omega_o A e^{kz + ikx \cos\beta - iky \sin\beta} e^{-i\omega t}$$

The angle of incidence of flow is given by

$$\alpha = \xi_5 + (\dot{\xi}_3 - x\dot{\xi}_5 + y\dot{\xi}_4 - \dot{\zeta}_v(x, \pm S_D(x), d_1(x))) / U$$

The equation for the vertical force F and the pitch moment M are assumed to be

$$F = \int_L F_v(x) dx$$

$$M = - \int x F_v(x) dx$$

where $F_v(x)$ is given by Equation (C.1).

When the necessary algebra and integrations along the body have been performed, and the equilinearization approximation has been applied the viscous contributions become²:

$$B_{33}^* = \rho \frac{2}{3\pi} C_D \int \dot{z}_{10} a(x) dx + \frac{\rho}{2} a_0 U \int a(x) dx \quad (C.2)$$

$$B_{35}^* = B_{53}^* = -\rho \frac{2}{3\pi} C_D \int x \dot{z}_{10} a(x) dx - \frac{\rho}{2} a_0 U \int xa(x) dx \quad (C.3)$$

$$B_{55}^* = \rho \frac{2}{3\pi} C_D \int x^2 \dot{z}_{10} a(x) dx + \frac{\rho}{2} a_0 U \int x^2 a(x) dx \quad (C.4)$$

$$C_{35}^* = \frac{\rho}{2} a_0 U^2 \int a(x) dx \quad (C.5)$$

$$C_{55}^* = - \frac{\rho}{2} a_0 U^2 \int xa(x) dx \quad (C.6)$$

$$F_3^* = -i\rho \frac{2}{3\pi} \omega_0 A C_D \int a(x) e^{k(-d_1 + ix \cos\beta)} \left(e^{ikS_D \sin\beta} |\dot{z}_{1s}| + e^{-ikS_D \sin\beta} |\dot{z}_{1p}| \right) dx$$

$$- i \frac{\rho}{2} \omega_0 A a_0 U \int a(x) e^{k(-d_1 + ix \cos\beta)} \cos(kS_D \sin\beta) dx \quad (C.7)$$

$$F_5^* = i\rho \frac{2}{3\pi} \omega_0 A C_D \int xa(x) e^{k(-d_1 + ix \cos\beta)} \left(e^{ikS_D \sin\beta} |\dot{z}_{1s}| + e^{-ikS_D \sin\beta} |\dot{z}_{1p}| \right) dx$$

$$+ i \frac{\rho}{2} \omega_0 A a_0 U \int xa(x) e^{k(-d_1 + ix \cos\beta)} \cos(kS_D \sin\beta) dx \quad (C.8)$$

where the integrals are along both hulls.

$$\dot{z}_{1s} = \dot{\xi}_3 - x\dot{\xi}_5 - \dot{z}_v(x, -S_D(x), -d_1(x))$$

$$\dot{z}_{1p} = \dot{\xi}_3 - x\dot{\xi}_5 - \dot{z}_v(x, S_D(x), -d_1(x))$$

$$\dot{z}_{10} = |\dot{z}_{1s}| + |\dot{z}_{1p}|$$

Two types of terms are present: ones which include C_D , a cross flow drag coefficient, and ones which include a_o , a body lift coefficient.

CROSS FLOW DRAG

In investigating the force F acting on fixed cylinders in oscillatory flow, the Morison equation has been applied

$$F = C_m \rho A_o \frac{dU_o}{dt} + \frac{\rho}{2} dU|U| \quad (C.9)$$

C_m is an inertia term, A_o is the characteristic body area normal to the velocity vector, U is the fluid velocity, and d is the width of the body transverse to the flow. Note that the second terms in Equation (C.9) and Equation (C.1) are equivalent. In an experimental investigation of two-dimensional cylinders and flat plates in sinusoidal flow, Keulegan and Carpenter²³ showed that C_m and C_D can be represented as functions of the parameter $U_m T/d$ where U_m is the amplitude of the harmonically varying velocity and T is the period of oscillation. This parameter, K_c , is referred to as the Keulegan-Carpenter Number. Additional experimental work on circular cylinders has been reported by Sarpkaya.⁵ He introduced an additional parameter, β_k , which is defined as $d^2/\nu T$ where ν is the kinematic viscosity of water.

The potential for applying this data to SWATH ships is evident, since the lower hulls of SWATH configurations are typically circular. Experimental data for the zero speed heave added mass and damping coefficients for eight configurations* is available. Utilizing one circular lower hull, three strut variations, and two draft variations for one strut were constructed. Three elliptical sections

*Reported by Stahl in an NSRDC Test and Evaluation Report of limited distribution.

with the middle strut and the middle draft were constructed. The results from the oscillation experiments showed strong dependence of damping on wave amplitude and some dependence of added mass on wave amplitude.

In applying Sarpkaya's data to SWATH ships, results for C_D are linearly interpolated as a function of both K_c and β_k . In addition, for each β_k , results are linearly extrapolated to a zero value of K_c . For large K_c , results are assumed to be equal to the value for the largest K_c . However, the values of K_c encountered for the experimental conditions are small. For small K_c the value of C_m is 2.0 which corresponds to the potential flow case. Consequently, Sarpkaya's data do not alter the added mass results.

In Figure 11 typical correlation is shown for the case where Sarpkaya's data are applied directly. The open symbols represent experimental results and the solid symbols represent predicted results. A different symbol is used for each amplitude of oscillation. Heave damping nondimensionalized by mass times frequency is plotted versus wave number nondimensionalized by $2/(\text{strut beam})$. Clearly, the damping is overpredicted.

It is reasonable that a circular section with strut will have less viscous damping than a circular section without strut. Based on the correlation for the eight configurations, a modification factor was developed to alter C_D for application to SWATH sections. There are certain limiting conditions: for a circular section without strut, C_D should equal Sarpkaya's C_D ; for a section where the strut thickness is the same as the major axis, C_D should be close to zero. An expression which satisfies these conditions and which includes a factor to alter results for ellipses is

$$C_D = \left(1.0 - \frac{B}{a} \frac{b}{a}\right) C_{D \text{ SARP KAYA}} \quad (C.10)$$

where B is the beam.

Predicted results for the eight configurations in Stahl's investigation are given in Figure 12. For elliptical sections, C_D is evaluated using Sarpkaya's data for a section with the diameter equal to the major axis. The predicted potential flow contribution also is given on each figure. Although the experimental and predicted results do not agree precisely, the results are generally encouraging.

BODY LIFT

In Equations (C.2) through (C.8) terms of the form

$$\frac{\rho}{2} a_0 U \int_{\ell} x^i a(x) dx, \quad i = 0, 1, 2$$

appear. These terms are due to lift on the body, and follow from Equation (C.1). In other nomenclature commonly used for hydrodynamic coefficients, B_{33} , B_{53} , B_{35} , and B_{55} can be related to

$$-\frac{\rho}{2} UL^2 Z'_w, \quad -\frac{\rho}{2} UL^3 M'_w, \quad -\frac{\rho}{2} UL^3 Z'_q, \quad \text{and} \quad -\frac{\rho}{2} UL^4 M'_q$$

respectively. That is, B_{33}^* , B_{53}^* , B_{35}^* , and B_{55}^* can be equated to $-Z'_w$, $-M'_w$, $-Z'_q$, and $-M'_q$, respectively. In Reference 24 it is suggested that submarine data be used to define the body lift expressions for SWATH. This approach was not pursued by Lee² but is pursued here. The body lift components in Equations (C.2) through (C.6) will be replaced by expressions related to the submarine hydrodynamic coefficients and an expression for a_0 will be developed for use in Equations (C.7) and (C.8).

Dempsey* developed semiempirical expressions for vertical plane hydrodynamic coefficients for submarines. For a bare hull submarine the expressions are:

$$Z'_w = 2.439[(k_2 - k_1)m']^{4/3} - m' \quad (C.11)$$

$$M'_w = 0.793(k_2 - k_1)m' \quad (C.12)$$

$$Z'_q = -0.207(k_2 - k_1)m' \quad (C.13)$$

$$M'_q = (Z'_q)^2 / Z'_w \quad (C.14)$$

where $m' = 2V/L^3$ with V equal to the bare hull volume and L equal to the ship length. Lamb's hydrodynamic coefficients, k_1 and k_2 , are given by:

*Given in a DTNSRDC report of higher classification.

$$k_1 = \frac{\alpha_o}{2 - \alpha_o}$$

$$k_2 = \frac{\beta_o}{2 - \beta_o}$$

$$\alpha_o = 2 \frac{(1 - \epsilon^2)}{\epsilon^3} \left(\frac{1}{2} \ln \frac{(1 + \epsilon)}{(1 - \epsilon)} - \epsilon \right)$$

$$\beta_o = \frac{1}{\epsilon^2} - \frac{1 - \epsilon^2}{2\epsilon^3} \ln \frac{(1 + \epsilon)}{(1 - \epsilon)}$$

$$\epsilon = \left(1 - \left(\frac{a_{\max}}{L} \right)^2 \right)^{1/2}$$

where a_{\max} is the maximum of the horizontal axis of the lower body.

In applying these equations to SWATH configurations, the obvious approach is to evaluate the submarine expressions for one SWATH lower hull and double the value. For the SWATH 6A, comparison between predicted and experimental results showed that the calculated results were lower than the experimental results. Consequently, in evaluating Dempsey's expressions for SWATH, the volume is taken to include the volume of the strut as well as that of the submarine-like lower hull.

Dempsey's expressions could not be applied directly for B_{53}^* . When it was taken to be $-2M_w$, where the factor of 2 is used to include the effect of both hulls, it differed in sign and significantly in magnitude from the results for the experiment documented in Reference 12. However, the difference between the experimental results and the sum of the potential flow and cross flow drag components is approximately equal to $-2Z_q$. Therefore, B_{53}^* is taken to be equal to $-2Z_q$. That is, B_{35}^* is taken to be equal to B_{53}^* . This is consistent with Equation (C.3) in the theoretical development.

Appropriate body lift components for C_{35} and C_{55} must be determined. Reference to Equations (C.2), (C.3), (C.5), and (C.6) indicates that B_{33}^* and C_{35}^* as well as B_{53}^* and C_{55}^* are similar in form. Analysis of data taken for the SWATH 6A during the experiment documented in Reference 12 indicates that for that

configuration, at least, C_{35}^* can be approximated by $-2UZ_w$ and that C_{55}^* can be approximated by $-0.278 UM_w$.

In order to evaluate the excitation components, some value for a_o must be chosen. Several possible relationships follow from Equations (C.2) through (C.4) and the corresponding Equations (C.11), (C.13), and (C.14). For the SWATH 6A, Equations (C.2) and (C.11) yield

$$a_o = - \frac{L^2 Z'_w}{\int a(x)dx} = 0.068 \quad (C.15)$$

Equations (C.3) and (C.13) yield

$$a_o = \frac{L^2 Z'_q}{\int xa(x)dx} = 3.98 \quad (C.16)$$

Equations (C.4) and (C.14) yield

$$a_o = - \frac{L^3 M'_q}{\int x^2 a(x)dx} = 0.127 \quad (C.17)$$

The value which is given in Equation (C.15) is close to the value of 0.07 suggested in Reference 22 and used by Lee². In Reference 22 the experimental data which produced this value was for the heave force. Thus it is reasonable that it should agree with the value from Equation (C.15). The other values differ substantially and are a measure of the difference between using Equations (C.2) through (C.8) with a constant value of a_o to represent the body lift, and using the above relationships derived from the submarine hydrodynamic coefficients to represent the body lift component.

These three values for a_o were substituted in Equations (C.7) and (C.8). Correlation with experimental results for heave exciting force and pitch exciting moment for the 6D and the SSP KAIMALINO¹² indicates that the best correlation results from using Equation (C.15) to evaluate a_o .

FIN CONTRIBUTIONS

Contributions to the added mass due to the presence of stabilizing fins are given in Lee's development. In addition, a development similar to that for the

body results in fin contributions due to cross flow drag and lift in the damping coefficients. The resulting equations require evaluation of a cross flow drag coefficient, C_{D1} , and the lift curve slope, $C_{L\alpha}$, for the i^{th} fin. Lee suggests using 1.2 for C_{D1} and uses a technique for evaluating $C_{L\alpha}$ which includes the effect of the body on the fin and the fin on the body.²⁵ Alternate approaches for evaluating these coefficients are possible.

Data in Reference 6 are used to evaluate C_{D1} . These data are given as a function of K_c , the Keulegan-Carpenter number, $U_m T/d$. They are presented in Figure 10, in which C_{D1} values for a flat plate range from 2.5 to 6.0. K_c is evaluated using a value of twice the span for d with U_m as the amplitude of the harmonically varying velocity. T is the encounter period as for the C_D values of the body.

As noted by Dempsey,¹⁰ work by Whicker and Fehlner⁷ showed that for low aspect ratio control surfaces in the free stream, experimental results agreed with this expression

$$C_{L\alpha} = \frac{1.8\pi AR}{1.8 + (AR^2 + 4.0)^{1/2}}$$

where $C_{L\alpha}$ is the slope of the lift coefficient with respect to angle of attack α in radians and a rectangular planform has been assumed. AR is the effective aspect ratio which for the SWATH case is given by

$$AR = \frac{a + 2s}{c}$$

where s is the span and c is the chord of the lifting surface.

A source of interference on lift is the effect of the hull on the stern foil. Dempsey¹⁰ developed a semiempirical expression for a correction to $C_{L\alpha}$ for sternplanes

$$C_{Lz} = \left[1.0 - \frac{0.2556}{(a + 2s)/a} \left(\left(\frac{a + 2s}{a} \right)^2 - 0.1612 \right)^{1/2} - 0.6366 \sin^{-1} \frac{0.4015}{(a + 2s)/a} \right] C_{L\alpha}$$

Application of her expression to the SWATH 6A forced oscillation results in Reference 12 for one and two fins yielded poor correlation. Analysis of the respective geometries suggests why this correlation generally will not be appropriate for SWATH hulls. The sternplanes of a submarine are very near the stern so

that the wake of the submarine will mask the fin and reduce lift. For SWATH configurations with the aft fins set near the parallel mid-body the effect of hull outreach will be insignificant. The correction is included when the ratio of the maximum transverse axis to the transverse axis at the quarter chord is at least 2.

Fin-fin interference also is a source of change in lift. Experimental work by Lloyd⁸ investigated the frequency dependent interference effects on lift due to the presence of more than one appendage. In this experiment two identical fins with an aspect ratio of 2.0 were attached to a board. For separations of 10, 20, and 30 times the span, the fins were oscillated at several frequencies at amplitudes of oscillation of 10 to 20 degrees. Cox and Lloyd⁹ corrected this data for boundary layer effects and tabulated the data in terms of the ratio of the lift on the aft fin to the lift on the forward fin. In tabular data, chord was used as a nondimensionalization factor. For application here, the outreach is of importance and consequently parameters given in Reference 9 have been nondimensionalized using span. Reference to Table 4 shows that over the range of values tested the effect of interference ranged from a 59% reduction to a 15% increase in comparison with the lift of a single fin.

These experimental data apply to the case where both fins are the same size. This is not the usual case for SWATH configurations. In the absence of data for various fin size ratios, the interference factor associated with the span of the forward fin was used to modify the free-stream lift curve slope of the aft fin.

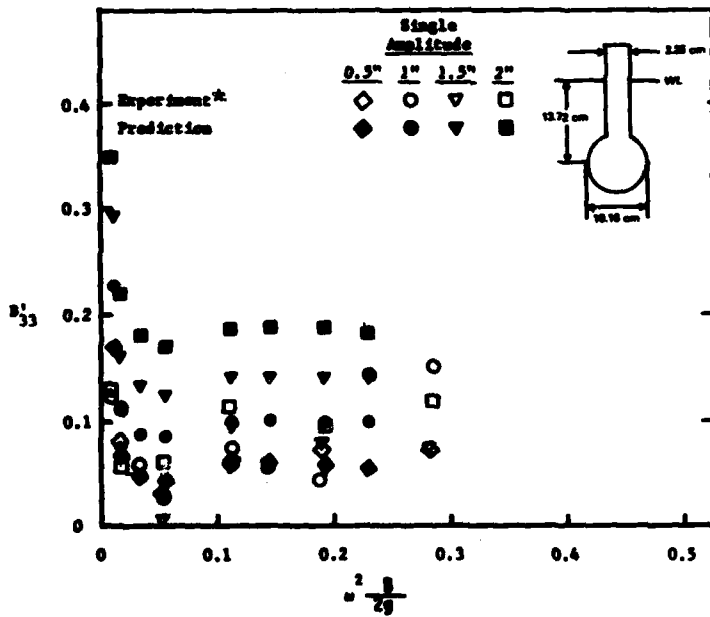
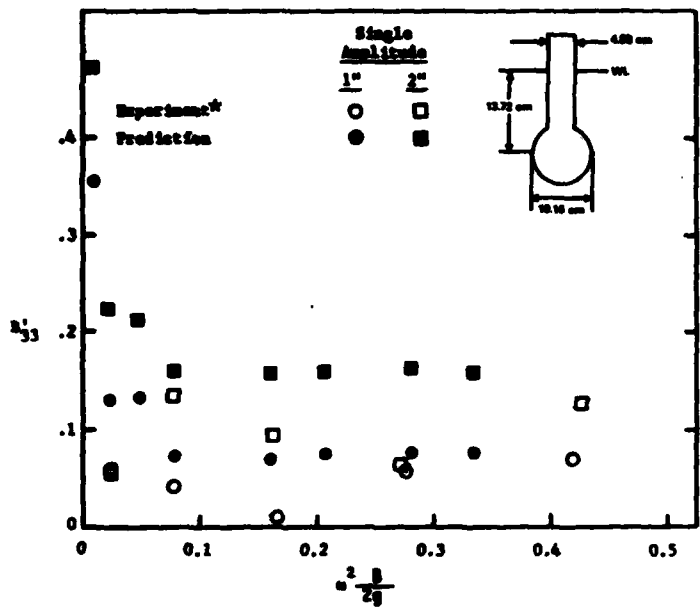


Figure 11 - Experiment-Prediction Comparison for Damping Coefficient with No Correction for C_D

* Reported by Stahl in a report of limited distribution.

Figure 12 - Experiment-Prediction Comparison for Damping Coefficient for Two-Dimensional Cylinders

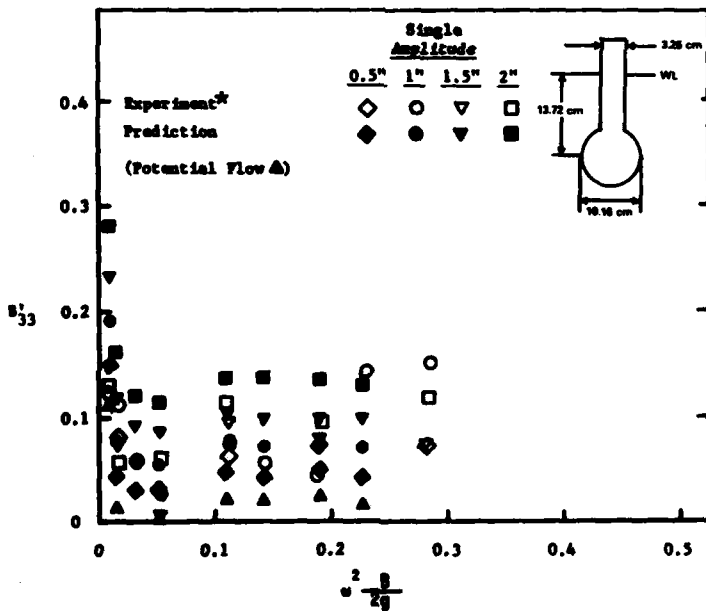
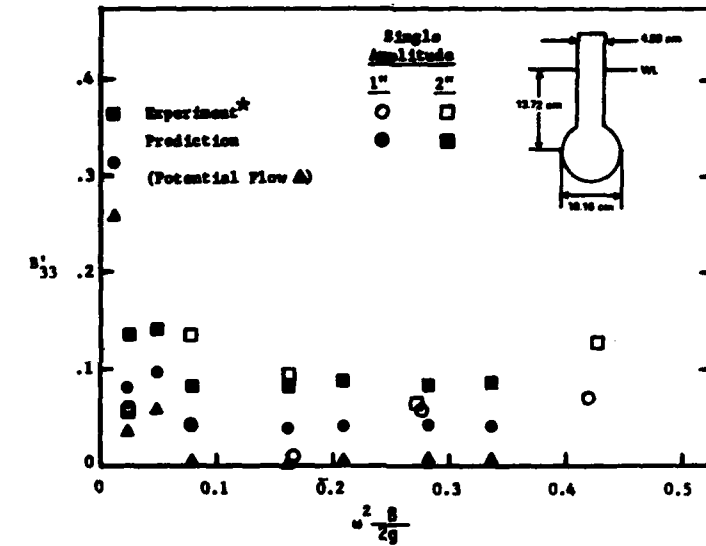


Figure 12a - Coefficients for Configurations with Strut Variations

* Reported by Stahl in a report of limited distribution.

Figure 12 (Continued)

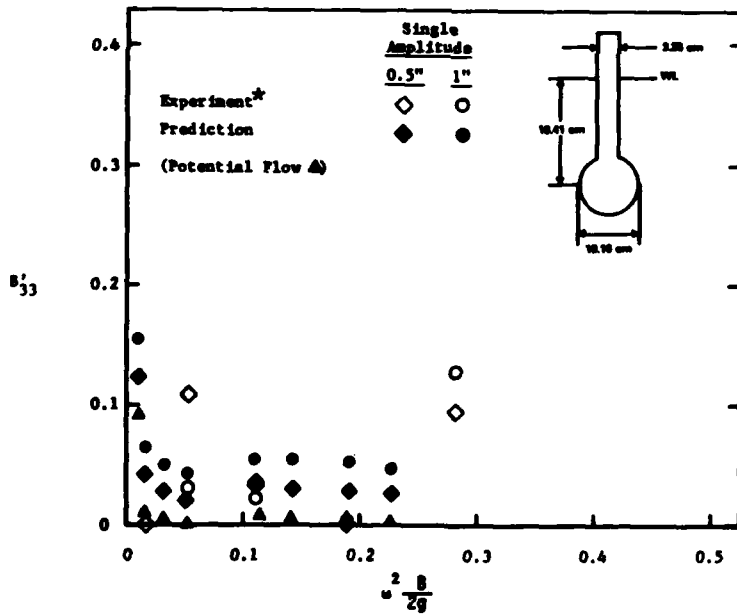
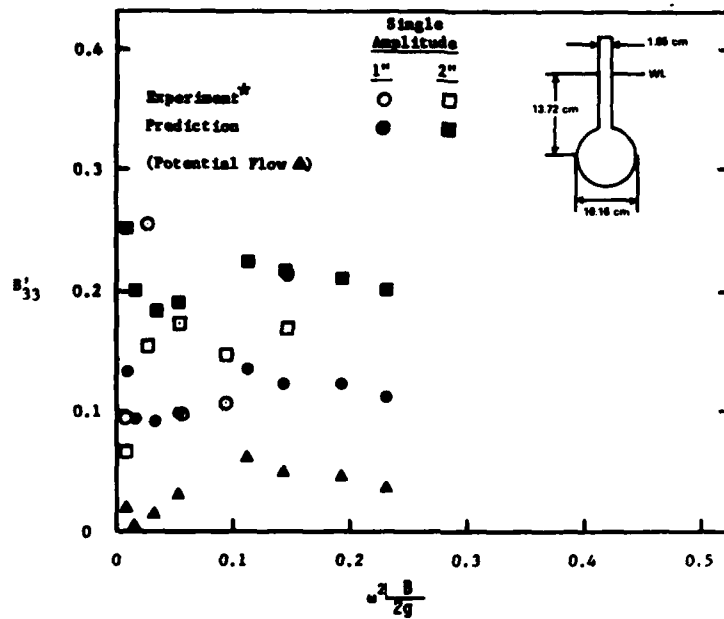


Figure 12b - Coefficients for Configurations with Strut Thickness and Draft Variations

* Reported by Stahl in a report of limited distribution.

Figure 12 (Continued)

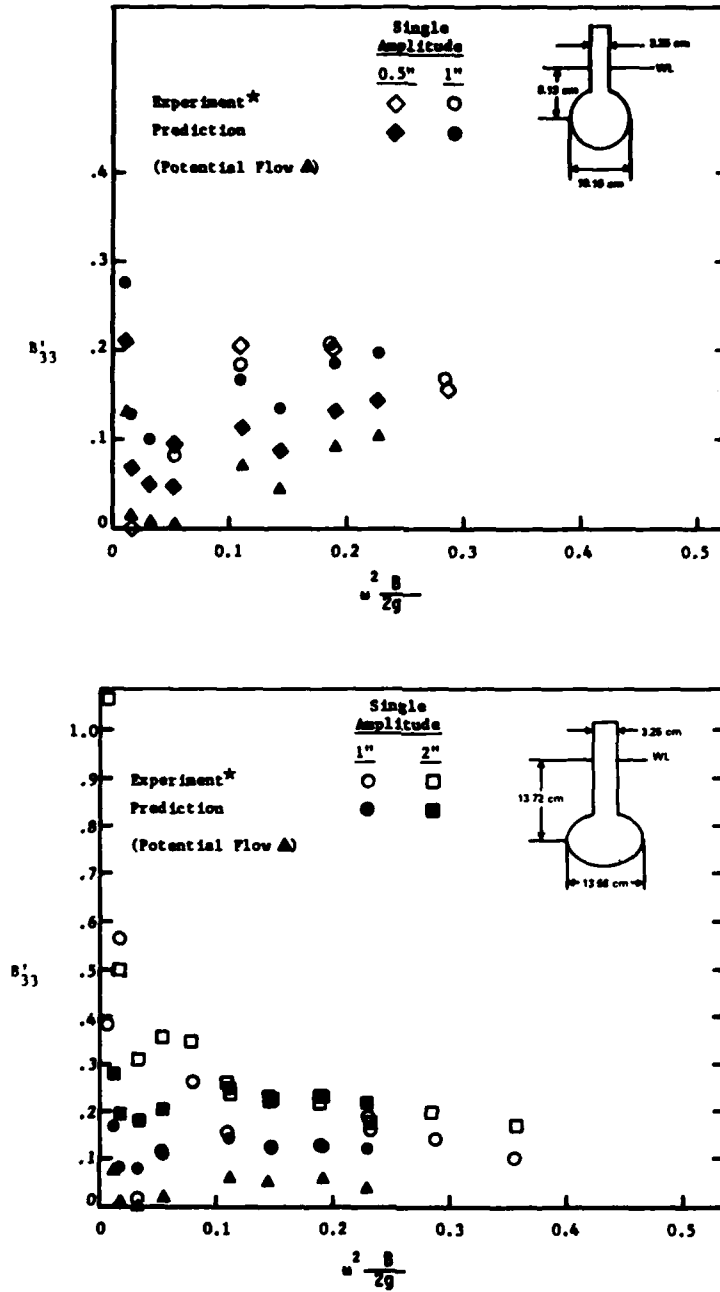


Figure 12c - Coefficients for Configurations with Draft Variations and Elliptical Lower Hull

* Reported by Stahl in a report of limited distribution

Figure 12 (Continued)

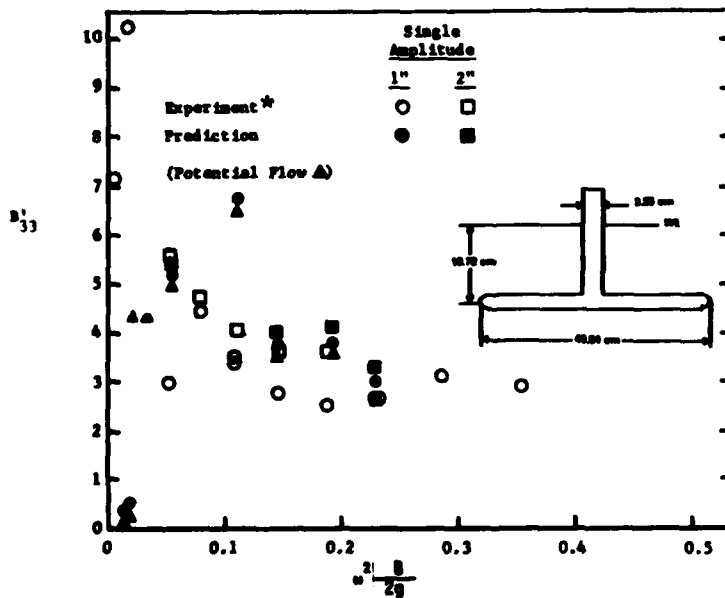
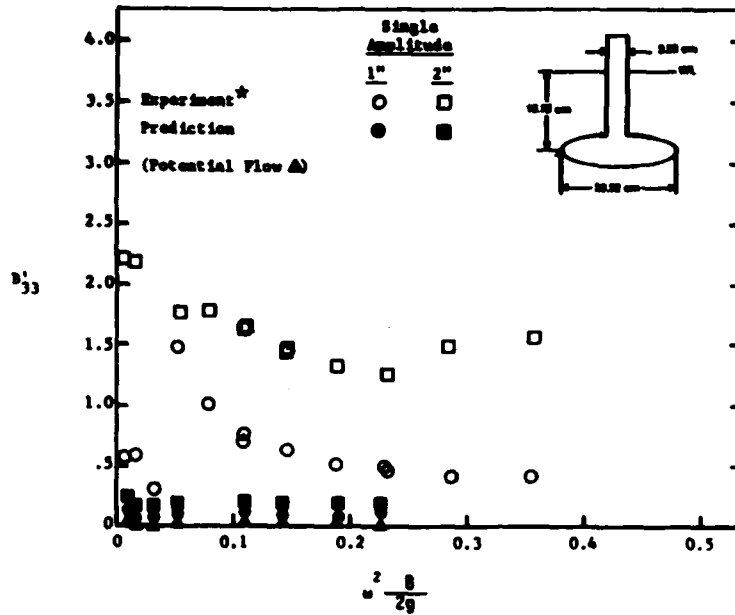


Figure 12d - Coefficients for Configurations with Elliptical Lower Hulls

* Reported by Stahl in a report of limited distribution.

DTNSRDC ISSUES THREE TYPES OF REPORTS

1. DTNSRDC REPORTS, A FORMAL SERIES, CONTAIN INFORMATION OF PERMANENT TECHNICAL VALUE. THEY CARRY A CONSECUTIVE NUMERICAL IDENTIFICATION REGARDLESS OF THEIR CLASSIFICATION OR THE ORIGINATING DEPARTMENT.

2. DEPARTMENTAL REPORTS, A SEMIFORMAL SERIES, CONTAIN INFORMATION OF A PRELIMINARY, TEMPORARY, OR PROPRIETARY NATURE OR OF LIMITED INTEREST OR SIGNIFICANCE. THEY CARRY A DEPARTMENTAL ALPHANUMERICAL IDENTIFICATION.

3. TECHNICAL MEMORANDA, AN INFORMAL SERIES, CONTAIN TECHNICAL DOCUMENTATION OF LIMITED USE AND INTEREST. THEY ARE PRIMARILY WORKING PAPERS INTENDED FOR INTERNAL USE. THEY CARRY AN IDENTIFYING NUMBER WHICH INDICATES THEIR TYPE AND THE NUMERICAL CODE OF THE ORIGINATING DEPARTMENT. ANY DISTRIBUTION OUTSIDE DTNSRDC MUST BE APPROVED BY THE HEAD OF THE ORIGINATING DEPARTMENT ON A CASE-BY-CASE BASIS.